Interactions of 1 um latex microbeads with biofilms
by William Joseph Drury

A thesis submitted in partial fulfillment of the requirements for the degree of Doctor of Philosophy in Civil Engineering
Montana State University

Abstract:
Fluorescently-labelled latex microbeads were used to study the interaction of particles with Pseudomonas aeruginosa biofilms in a continuous flow annular reactor. Microbeads could be readily identified and distinguished from bacteria under the microscope in both plan and cross-section views. Microbeads concentrations were quantifiable. The fraction of beads that attached to biofilm during a 24 h period ranged from 0.001 to 0.01 and was proportional to biofilm cell carbon and standard deviation in biofilm thickness. Microbeads formed aggregates on the biofilm, but not in the associated bulk water. Microbeads added to biofilm of steady state thickness (30 μm) were observed to be located throughout the entire biofilm depth in 24 hours. It was hypothesized that pores in biofilm permitted beads to enter the biofilm interior. Bacterial growth filled in the pores, trapping beads beneath them. Many of the microbeads that attached to biofilm shortly after bacterial inoculation (thickness of 2 μm) remained near the substratum as cells grew past and covered them. Whether added to mature or nascent biofilms, microbeads were observed near the biofilm-substratum interface for up to five days after bead addition. Microbeads were retained by biofilm for longer periods (120 hours) than the average retention experienced by suspended beads in the reactor (0.25 hours), suggesting differences between biofilm and suspended cell ecology. Microbeads located at or near the substratum were released more slowly than were beads nearer to the biofilm-bulk water interface. The bead release rate (0.028 h^-1) was lower than the average cellular growth rate (0.15 h^-1). Model predictions of particle locations and detachment rates by a onedimensional model (BIOSIM) were poor. It was hypothesized that the roughness of the biofilm surface directed particle advection parallel as well as perpendicular to the substratum. This could have been responsible for the inaccuracy of the one-dimensional model. Collectively, these results point to an important role of biofilm roughness in determining particle capture and retention by biofilms.

INTERACTIONS OF 1 μm LATEX MICROBEADS WITH BIOFILMS

by

William Joseph Drury

A thesis submitted in partial fulfillment
of the requirements for the degree

of

Doctor of Philosophy

in

Civil Engineering

MONTANA STATE UNIVERSITY
Bozeman, Montana

August 1992

APPROVAL

of a thesis submitted by

William Joseph Drury

This thesis has been read by each member of the thesis committee and has been found to be satisfactory regarding content, English usage, format, citations, bibliographic style, and consistency, and is ready for submission to the College of Graduate Studies.

August 11, 1992 — Date

Philip A. Stewart — Chairperson, Graduate Committee

Approved for the Major Department

11 August 1992 — Date

Leedan E. Long — Head, Major Department

Approved for the College of Graduate Studies

8/28/92 — Date

R K Brown — Graduate Dean

STATEMENT OF PERMISSION TO USE

In presenting this thesis in partial fulfillment of the requirements for a doctoral degree at Montana State University, I agree that the Library shall make it available to borrowers under rules of the Library. I further agree that copying is allowable only for scholarly purposes, consistent with "fair use" as prescribed in the U.S. Copyright Law. Requests for extensive copying or reproduction of this thesis should be referred to University Microfilms International, 300 North Zeeb Road, Ann Arbor, Michigan 48106, to whom I have granted "the exclusive right to reproduce and distribute copies of the dissertation in and from microfilm and the right to reproduce and distribute by abstract in any format."

Signature William J. Drury

Date September 6, 1992

ACKNOWLEDGEMENTS

It would be misleading to present this research as totally the effort of one individual. Therefore, I wish to thank those who participated and helped me complete this goal in my life.

The late Bill Characklis deserves the most thanks for his guidance and patience. I dedicate this thesis to his memory. Phil Stewart is thanked for the advice and ideas given to me. Al Cunningham, Zbigniew Lewandowski, Gordon McFeters, and Ron Larsen are my other committee members who are thanked for their contributions.

I especially thank Paul Stoodley, Anne Camper, Gary Harkin, and Shawn Handran for their assistance. Additional faculty and staff who made contributions are Warren, Gill, Paul, Marty, John, Dave, Bryan, Frank, Whon Chee, Peg, Sandy, Diane, Wendy, Jamie, Cheryl, Susan, Lynda, Cheryl, Nick, Kim, Jordan, Phil, Brian, Jason, Bill, Ralf, and Mary. I also thank Gayle Callis, Gordon Williamson, and Oskar Wanner.

The students who helped me are almost too numerous to mention. I am most thankful to Brent Peyton and Ewout van der Wende. I also thank Satoshi, Robert, Vivek, Gabi, Feisal, Paul, Ross, Thomas, Ernie, Kirk, Leora, Wendy, Sandor, Rick, Barbara, and Rick.

I thank the National Science Foundation for financial support.

TABLE OF CONTENTS

TABLE OF CONTENTS - Continued

LIST OF TABLES

LIST OF TABLES - continued

LIST OF TABLES - continued

LIST OF FIGURES

LIST OF FIGURES - Continued

Figure

Page

LIST OF FIGURES - Continued

ABSTRACT

Fluorescently-labelled latex microbeads were used to study the interaction of particles with *Pseudomonas aeruginosa* biofilms in a continuous flow annular reactor. Microbeads could be readily identified and distinguished from bacteria under the microscope in both plan and cross-section views. Microbeads concentrations were quantifiable. The fraction of beads that attached to biofilm during a 24 h period ranged from 0.001 to 0.01 and was proportional to biofilm cell carbon and standard deviation in biofilm thickness. Microbeads formed aggregates on the biofilm, but not in the associated bulk water. Microbeads added to biofilm of steady state thickness (30 μm) were observed to be located throughout the entire biofilm depth in 24 hours. It was hypothesized that pores in biofilm permitted beads to enter the biofilm interior. Bacterial growth filled in the pores, trapping beads beneath them. Many of the microbeads that attached to biofilm shortly after bacterial inoculation (thickness of 2 μm) remained near the substratum as cells grew past and covered them. Whether added to mature or nascent biofilms, microbeads were observed near the biofilm-substratum interface for up to five days after bead addition. Microbeads were retained by biofilm for longer periods (120 hours) than the average retention experienced by suspended beads in the reactor (0.25 hours), suggesting differences between biofilm and suspended cell ecology. Microbeads located at or near the substratum were released more slowly than were beads nearer to the biofilm-bulk water interface. The bead release rate (0.028 h^{-1}) was lower than the average cellular growth rate (0.15 h^{-1}). Model predictions of particle locations and detachment rates by a one-dimensional model (BIOSIM) were poor. It was hypothesized that the roughness of the biofilm surface directed particle advection parallel as well as perpendicular to the substratum. This could have been responsible for the inaccuracy of the one-dimensional model. Collectively, these results point to an important role of biofilm roughness in determining particle capture and retention by biofilms.

INTRODUCTION

A biofilm has been defined as a film consisting of cells immobilized at a substratum and frequently embedded in an extracellular organic polymer (EPS) matrix of microbial origin (Characklis and Marshall, 1990). Biofilms may contain inorganic particles, such as clays, silts, corrosion products, or organic colloids, all of which are retained by the EPS matrix. Microorganisms and EPS may themselves be viewed as particulate constituents of biofilms. Interactions between particles and biofilms represent processes that affect biofilm structure, chemistry, and ecology significantly.

One important particle-biofilm interaction is the capture of particles from the bulk liquid. For example, the filamentous surface of a rotating biological contactor (RBC) biofilm entrapped particles such as organic solids (Alleman *et al.*, 1982). Reactor geometry influences particle capture by biofilms because it affects the surface area available for deposition of solids by gravity or interception of particles in the bulk flow (Bouwer, 1987). Biofilm grown on granular activated carbon (GAC) improved the capture of colloidal particles over clean GAC (Sprouse and Rittman, 1990). Many substrates in natural systems exist as colloidal particles (Levine *et al.*, 1985). Capture of such substrates could increase biofilm growth over that

produced by soluble substrates alone. Capture of suspended microorganisms could introduce new species to a biofilm.

Inorganic particles may be captured by or formed in biofilms. Corrosion products are examples of particles produced within a biofilm by microbially influenced corrosion. Inorganic corrosion products include FeS, $Fe(OH)_2$, $CaCO_3$, and elemental sulfur (Starkey, 1985). $Fe(OH)_2$ and sulfur are corrosive to steel, and FeS is cathodic to metallic iron and increases corrosion (Starkey, 1985; Tiller, 1985). Iron tubercles form in aerobic systems due to the dissolution of iron by iron oxidizing bacteria (Tiller, 1985). Since particulate corrosion products affect the corrosion process, knowledge of their location and rate of movement is an important aspect of understanding microbially influenced corrosion.

Inorganic particles can also be formed by chemical precipitation. Such particles were found in biofilms grown on swine wastes after 4 to 12 months of growth (Harvey *et al.*, 1984; Robinson *et al.*, 1984). Energy dispersive X-ray analyses revealed the precipitates to be composed mostly of calcium and phosphorus. It was assumed that the precipitates formed in the biofilms and were not captured from the bulk liquid because of their presence on the substratum and surrounding some bacterial cells.

Particle movement due to advection has a direct effect on the population dynamics of the biofilm community. Particle advection in biofilms is due to the expansion of particulate volume as cells grow and EPS is

formed. Advective velocity is most heavily influenced by the fastest growing microbial species, because this species creates the most particulate volume. Over time, a biofilm should become composed of greater concentrations of the fastest growing species, as the concentrations of slower growing species declines because of a limitation of space. Eventually, slowly growing microorganisms are pushed out the biofilm by faster growing cells. If population dynamics were determined by advection alone, only the fastest growing species would remain in a biofilm at steady state conditions. In a one-dimensional biofilm with only cell growth influencing particle transport, this species would be the one with the highest growth rate at the substratum (Gujer and Wanner, 1990).

Experimentation on biofilm population dynamics is difficult because significant spatial gradients exist in the chemical composition and population structure. Analysis of the interactions between the components of biofilm structure, and the processes occuring in a biofilm, requires maintenance of the intact structure in order to preserve the various gradients involved. The cellular structure and composition in biofilms are troublesome to study because of the minuscule spatial separations (on the order of micrometers) and the high volumetric density (ca. 10^{10} cells ml^{-1}).

Goal and Objectives

The goal of this research was to investigate particle-biofilm interactions, and to apply the results to further the understanding of biofilm population dynamics.

One objective was to develop an experimental technique that allowed detailed analysis of particle-biofilm interactions. The technique had to be able to differentiate particles from bacterial cells, determine spatial and temporal distribution of particles in biofilms, and permit quantification of particle concentrations in biofilm and bulk water. A second objective was to demonstrate capture and retention of micron-sized particles by biofilm. A third objective was to evaluate the capability of an existing biofilm model to simulate bead concentrations and distributions in biofilm, and to suggest possible improvements to the model.

LITERATURE REVIEW

Gradients in Biofilm Structure

Within biofilms are microbiological, chemical, and physical gradients that represent significant changes over distances of a few micrometers. Microbiological gradients represent changes in species composition and cell density in any dimension. Microcolonies within sludge granules have been revealed with immunologic methods (Grotenhuis *et al.*, 1991; Visser *et al.*, 1991), and microcolonies of different phenotypes in close proximity to each other present steep microbiological gradients. Chemical gradients are changes in chemical concentration in the interstitial water of the biofilm matrix. Dissolved oxygen (Lewandowski *et al.*, 1991) and nitrous oxide (N_2O) (Revsbech *et al.*, 1989) gradients have been measured with microelectrodes in studies of oxygen and nitrate respiration in biofilms. Variation in thickness and density represent physical gradients; thickness variations occur on a small spatial scale (Bakke, 1986).

All three categories of gradients are interrelated. Pores or crevices in biofilm cause changes in chemical composition by creating pathways for diffusion in biofilms without reaction (Wanner, 1989). Differing species composition across the substratum can cause changes in biofilm thickness

(Siebel and Characklis, 1991). Microbial activity strongly influences chemical gradients, both in depletion of substrates and production of products (sulfide, for example). Chemical gradients, in turn, regulate the environment and define where certain microbes may grow - aerobes where oxygen is present, or strict anaerobes in zones where oxygen is exhausted. Anaerobic conditions in biofilm depths often occur due to aerobic respiration in the biofilm nearer to the oxygen source.

Interactions between biofilms and viable and inert particles affect the various structures. Biofilm has been shown to enhance the capture of colloidal particles (Sprouse and Rittman, 1987). Filamentous surface structure, representing changes in physical and perhaps microbiological structure, may improve capture of particles from the bulk liquid (Alleman *et al.*, 1982). Particles may be substrates for microbial growth (Levine *et al.*, 1985) and thereby change substrate gradients and, indirectly, population gradients. If the particles are microbial cells or spores, new species may be introduced into biofilm, changing the microbiological structure, and introducing different activities that change the chemical structure.

Growth of different species in biofilms may alter biofilm structure and function. Particle movement in biofilms reflects competition for space by microbes, which may be important in biofilms (Atlas and Bartha, 1981). Some locations, such as adjacent to the substratum, have a special significance in population dynamics (Wanner, 1989). Therefore, the

locations occupied by particles (cells) and the rate of change of the locations are indicative of shifts in population dynamics. However, making observations on processes such as particle movement in intact biofilm is difficult (Gujer and Wanner, 1990).

Mathematical Description of Biofilm Structure and Activity

Mathematical modelling is a necessary companion to experimentation in biofilm research because of the experimental difficulties inherent in taking measurements of gradients that exist on a scale of micrometers. Explicitly stating the conceptual model in mathematical terms aids in the separation of known facts from the assumptions required because of a lack of information. Because of difficulties in making observations on particle movement in biofilms, writing equations to describe particle movement does require some *a priori* assumptions about biofilm behavior.

Assumptions made to permit computation of particle movement include (Wanner, 1989):

- the volume fraction of solid phases is constant
- density (or, specific gravity) of the various solid phases to convert mass to volume units
- the displacement velocity for all particles located the same distance from the substratum is equal - that is, there is no variation across the substratum,

and no modelled attachment to the substratum

- movement occurs only in the dimension perpendicular to the substratum for one-dimensional models

An additional assumption commonly made in biofilm modelling is that all phenomena can be adequately described by a one-dimensional model of a uniformly thick biofilm.

Particle volume is created by the conversion of soluble substrates to cells and extracellular polymeric substances (EPS) during the growth of microbial cells. This conversion produces solid phase material (mass and volume). Space limitations in biofilm create an advection of particulates as new solid material is produced. Both the cell specific growth rate (μ) and the advective velocity (v) exist in gradients across the biofilm thickness (Figure 1). Advection is greatest near the biofilm-bulk water interface, because solid phase volume production between the substratum and the depth of interest must be included in the advection rate along with solid phase volume production at the depth of interest. The production of particulates normally causes a combination of film expansion and biofilm detachment. The rate of expansion (advection) equals the rate of biofilm volume produced per plan area of biofilm if advection is one-dimensional.

The change in concentration of solid components can be described by a one-dimensional mass balance (after Gujer and Wanner, 1990):

$$\frac{\partial \epsilon_s X_s}{\partial t} = - \frac{\partial J_s}{\partial z} + r_s \qquad (1)$$

where: X_s = particle concentration (M L^{-3})

ϵ_s = volume fraction occupied by a solid phase of the total biofilm volume (dimensionless)

J_s = flux of solid matter (M L^{-3} t^{-1})

r_s = reaction rate (production or degradation) (M L^{-3} t^{-1})

The change in soluble matter is described by a similar equation, which uses Fick's Law to predict the flux of material:

$$\frac{\partial \epsilon_l C}{\partial t} = D_f \frac{\partial^2 C}{\partial z^2} + r_{solute} \qquad (2)$$

where: C = concentration of solute (M L^{-3})

ϵ_l = volume fraction occupied by liquid of the total biofilm volume (dimensionless)

D_f = diffusion coefficient for solute in water in biofilm (L^2 t^{-1})

r_{solute} = reaction rate of solute (M L^{-3} t^{-1})

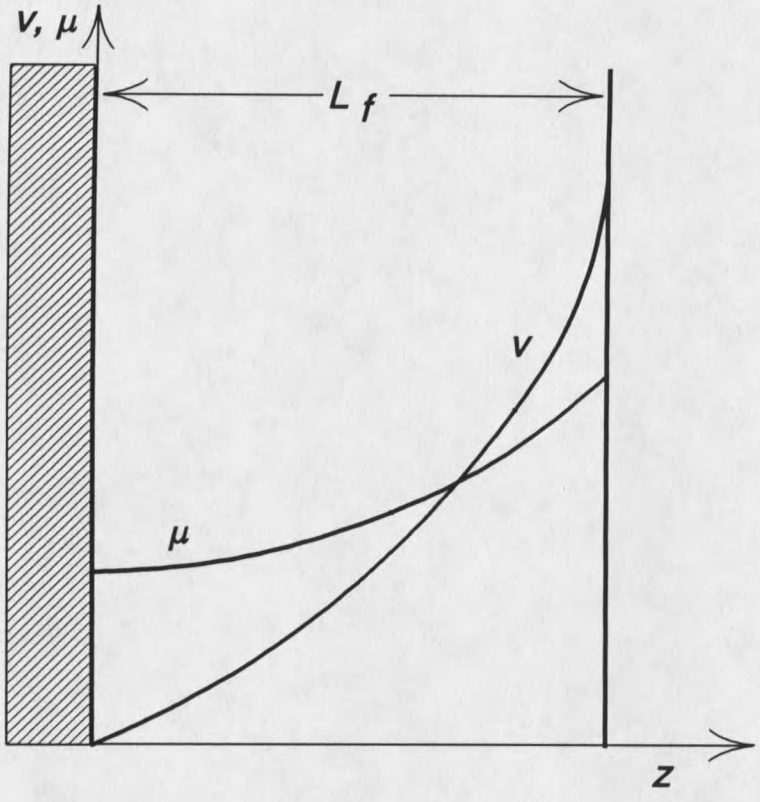

Figure 1. Typical gradients of specific cellular growth rate (μ) and advective velocity (v) over biofilm depth (L_f).

The creation of particle volume produces an advection of solid matter in the biofilm. A one-dimensional model such as BIOSIM (Reichert *et al.*, 1989) places all advection in the direction perpendicular to the substratum. However, the expansion of solids may fill in pores or the liquid occupied volume fraction of the biofilm as well as expanding the film away from the substratum. The advective flux is:

$$J_s = v_s X_s \qquad (3)$$

where: J_s = advective flux of solids relative to the substratum (M L^{-2} t^{-1})

v_s = velocity of particle relative to the substratum (L t^{-1})

While diffusive-like transport of particles may be possible, it is normally assumed to be negligible (Gujer and Wanner, 1990; Stewart *et al.*, 1991; Kissel *et al.*, 1984).

Substituting equation (3) into equation (1) produces:

$$\frac{\partial X_s}{\partial t} = - v_s \frac{\partial X_s}{\partial z} - X_s \frac{\partial v_s}{\partial z} + r_s \qquad (4)$$

Equation (4) may be solved with the following conditions (Gujer and Wanner, 1990):

- an initial condition that describes the profiles of the various particles over biofilm depth.
- a boundary condition of no flux at the biofilm-substratum interface:

$$\frac{\partial X_s}{\partial t}(z = 0, t) = 0 \qquad (5)$$

Equation (2) requires a second boundary condition of continuity of concentration at the biofilm-bulk water interface:

$$C(z = L_f, t) = C_{bulk\,liquid}(z = L_f, t) \qquad (6)$$

The advection of particulates (that is, cells) has been observed in immobilized cell reactors. Karel and Robertson (1989) used a radiotracer (^{35}S) to determine the location and rate of change of the bacterial growth

region. Stewart *et al.*, (1991) measured growth region dimensions and cell growth rates with the same radiotracer and liquid emulsion radiography. Their experimental system was not a true biofilm because it entailed the placement of *Escherichia coli* on a microporous membrane, thus precluding cell detachment. While particulate advection has not been observed in biofilm systems, advection caused by cell growth has been theorized (Bryers and Characklis, 1982; Gujer and Wanner, 1990).

Applicability of the One-Dimensional Model

The model listed above is in a one-dimensional form. Although the model can be expanded to two or three dimensions (Gujer and Wanner, 1990), it is normally employed in the one-dimensional form (Reichert *et al.*, 1989; Kissel *et al.*, 1984). One-dimensional modelling considers gradients that exist in the dimension perpendicular to the substratum, but neglects any gradients parallel to the substratum. It is uncertain as to when the gradients parallel to the substratum are significant. Soluble substrate utilization appears to be insensitive to them, because one-dimensional models predict this phenomenon with good accuracy (Fruhen *et al.*, 1990; Gujer and Boller, 1990; Siegrist and Gujer, 1987). Other phenomena, such as particle capture and retention and population dynamics, involve particles with dimensions on the order of 1 to 10 μm. Heterogeneities in biofilm thickness, such as pores and crevices, exist at these and greater magnitudes, and may affect particle

capture and retention.

The remainder of this thesis will show that variations in biofilm thickness across the substratum, such as pores, have a significant effect on particle capture and retention. Generalization of the results indicate that phenomena involving micron-sized particles, such as particle movement in biofilms, population dynamics, and particle detachment from biofilms, are poorly described by one-dimensional models because physical, microbiological, and chemical gradients exist across the substratum that determine the rates and magnitudes of changes in these phenomena.

EXPERIMENTAL SYSTEMS AND METHODS

Bacterial Characteristics

Pseudomonas aeruginosa, a rod-shaped chemoorganotroph, was used as the biofilm-forming species in all monopopulation biofilm experiments. It is motile by means of a polar flagella, and is obligately respiratory with oxygen or, in some circumstances, nitrate, as the terminal electron acceptor (Palleroni, 1984). A cell of this species is typically 1.5 to 4.0 μm long by 0.5 to 0.8 μm wide. *P. aeruginosa* have Gram negative cell walls. They form an extracellular polymer that consists mainly of mannuronic and guluronic acids (Evans and Linker, 1973). The optimum temperature range for this species is 35 to 37°C, with an optimal pH of 6.8.

Experimental System

Experiments were run in an annular reactor (RotoTorque) under turbulent flow conditions. A RotoTorque (RT) consists of a stationary vertical cylinder containing a co-axial rotating cylinder (Figure 2, Appendix A). Both cylinders are made of polycarbonate. The inner cylinder has four tubes at an angle from the axis so that the centripetal acceleration caused by rotation forces liquid up the angled tubes and thereby creates vertical

mixing. The RT is a completely mixed reactor (Trulear 1980). Twelve removable slides for sampling of biofilm are set in dove-tailed vertical grooves in the outer cylinder, and are accessed through the top of the reactor through rubber-stoppered holes. The inner surface area of the reactor upon which biofilm can grow is 0.19 m^2.

The outer cylinder experiences a uniform shear stress since the annular gap is constant over the height of the reactor. Because the shear stress is uniform and the RT is a completely mixed reactor, it can be assumed that the biofilm growing on the outer cylinder is uniform in thickness and density, and that a biofilm specimen from any of the twelve slides (or, a portion of one of the slides) is a representative sample. The RT effluent is representative of the bulk fluid because the system is completely mixed.

Shear stress is dependent on the rotational speed of the inner cylinder, but is independent of the fluid flow rate. Shear stress and the hydraulic retention time can be controlled separately. The high surface area to volume ratio (Appendix A) provides adequate space for twelve slides while providing a short hydraulic retention time at relatively low flow rates. The rotational speed of the inner cylinder of the RT was 200 rpm in all experiments. The volume occupied by liquid at this rotational speed was 5.75×10^{-4} m^3.

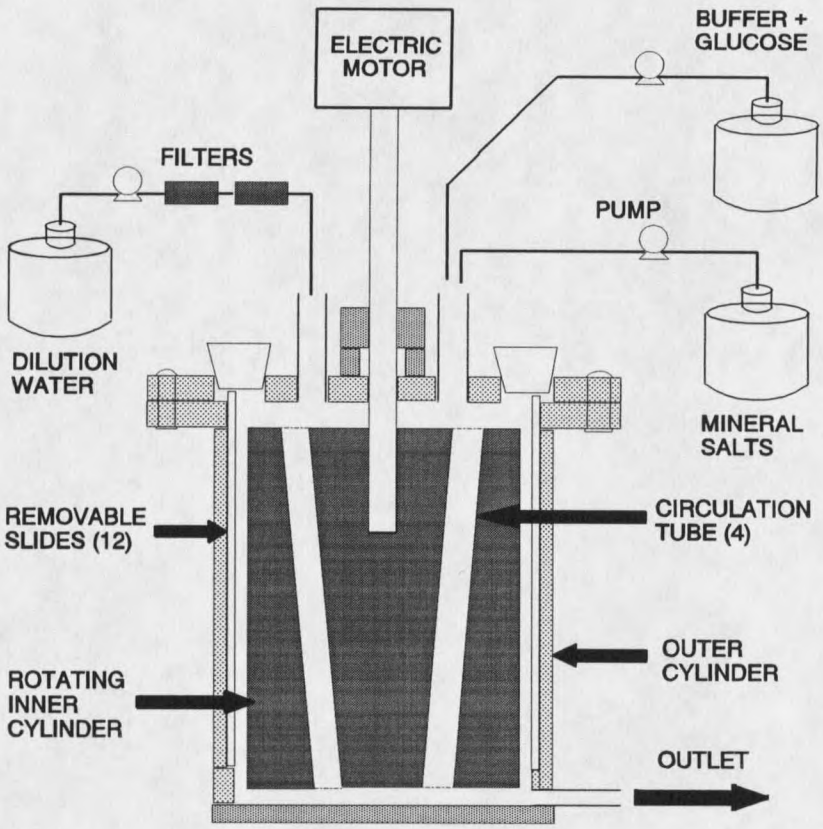

Figure 2. The RotoTorque reactor.

Experimental Procedures

Three separate flows were added to the RT. These summed to a flow rate of 0.0023 $m^3 h^{-1}$ (38 ml min^{-1}), producing a hydraulic retention time of 0.25 h. At this retention time suspended bacteria are quickly washed from the RT and their activity can be neglected. The three component flows were mineral salts ($5.8x10^{-5}$ $m^3 h^{-1}$, or 1 ml min^{-1}), phosphate buffer ($5.8x10^{-5}$ $m^3 h^{-1}$, or 1 ml min^{-1}), and dilution water (0.0022 $m^3 h^{-1}$, or 36 ml min^{-1}). Glucose was included with the phosphate buffer. Flow rates were measured with in-line flow meters (Gilmont Instrument Co., nos. 11 and 12). In addition, the total flow rate was determined once per day by measurement of the effluent volume in a graduated cylinder over a predetermined time, with the dilution flow rate adjusted to bring the total flow rate to 0.0023 $m^3 h^{-1}$. Peristaltic pumps (Masterflex #7553-30, Cole-Parmer Instrument Co., with pump heads 7013 and 7014) were used to supply the dilution water, mineral salts, and buffer solutions.

Dilution water was taken from the Cobleigh Hall distilled water system. Three 0.02 m^3 (20 l) containers were filled daily. Water was transferred from container to container by siphons. The dilution water was aerated to ensure oxygen saturation before it was supplied to the RT. Sterilization of the dilution water was obtained by filtration through two 0.2 μm capsule filters (Gelman Sciences, Inc., #12122) in series.

The compositions of the mineral salts solution and the phosphate buffer solution are listed in Table 1. The medium was carbon limited according to the stoichiometry for *P. aeruginosa* growth on glucose (Characklis 1990a) and the dissolved oxygen concentration for water in equilibrium with the atmosphere at the elevation of Montana State University (Appendix B). Concentrated solutions (38x) were prepared in 0.011 m^3 (11 l) containers and autoclaved. In Experiments A-1, B-1, and A-2, the containers were autoclaved together for 50 min. After Experiment A-2, it was determined that this time period was inadequate for killing spores when such large liquid volumes were autoclaved. Thereafter, the two containers were autoclaved for a conditioning period of 0.17 h, a sterilization period of 3.3 h, and a slow exhaust period (variable). Glucose was added to a container by injecting 30 ml of concentrated glucose solution through a septum into the container. The glucose solution was filter-sterilized at the time of addition by passage through a 0.22 μm, 25 mm diameter nylon filter (Cameo IIS, Micron Separations, Inc.).

All experiments were run at 25 ± 1°C. The RT was immersed in a water bath to a depth of 0.14 m. Approximately 0.75 m of the dilution water tubing was immersed in the water bath to adjust the dilution water temperature. The water bath temperature was controlled by a Yellow Springs Instrument Co., Inc. temperature controller (Model 74), or by a Fisher Scientific Co. Immersion Circulator (Model 730).

Table 1. Substrate solution compositions for the RotoTorque and chemostat reactors. All concentrations in g m^{-3}. The final pH is 6.8.

	RotoTorque	Chemostat
Glucose (Glucose - C)	15 (6)	100 (40)
NH_4Cl	7.2	36
$MgSO_4.7H_2O$	2.0	10
$(NH_4)_6Mo_7O_{24}.4H_2O$	0.001	0.005
$ZnSO_4.7H_2O$	0.1	0.5
$MnSO_4.H_2O$	0.008	0.04
$CuSO_4.5H_2O$	0.002	0.01
$Na_2B_4O_7.10H_2O$	0.001	0.005
$FeSO_4.7H_2O$	0.112	0.56
$(HOCOCH_2)_3N$	0.4	2.0
$CaCO_3$	-	1.0
$CaCl_2.2H_2O$	11.0	-
Na_2HPO_4	213	568
KH_2PO_4	204	544

Reactor Start-up

The RT assembly (including connecting tubing, with silicone tubing used exclusively, flowmeters, flow breaks, and dilution water filters) was autoclaved for 0.33 h. All open tube ends were covered by aluminum foil. Water (about 20 ml) was placed inside the RT before autoclaving in order to provide moist heat for the sterilization.

Connections were made to the mineral salts and phosphate buffer

containers by heating a borosilicate glass tube connector with a propane torch until its end was red hot, then pushing the glass connector into the silicone tubing attached to a container. The RT was filled with the nutrient and buffer solutions and dilution water in the correct proportion. Adequate care was necessary to release trapped air from the RT. The inner cylinder rotation was initiated. Chemostat effluent (5.8×10^{-5} m^3 h^{-1} (1 ml min^{-1}), cell concentration was 5 to 7 x 10^7 cells ml^{-1} for a *P. aeruginosa* flow rate of 4 x 10^9 cells h^{-1}) was added to provide an inoculum of the desired species. This inoculation period lasted 12 h (total flow rate of 0.0023 m^3 h^{-1} (38 ml min^{-1}), dilution water flow rate of 0.0021 m^3 h^{-1} (35 ml min^{-1})), at which time the chemostat was disconnected from the RT.

One experiment was run with an undefined, mixed population biofilm. Non-sterile, unfiltered water from the Engineering Research Center's reverse osmosis treatment system (cell concentration of 1.1 x 10^6 ml^{-1}) was the inoculum source. This water was used in place of dilution water for 48 h during the RT inoculation. At that time, filtered, sterile distilled water replaced the unfiltered reverse osmosis system water as dilution water, and bead addition was begun. Bead addition took place for 24 h. The system was monitored for 144 h after the end of bead addition. A homogenized biofilm sample taken at 24.3 h after the end of bacteria inoculation was streaked onto R2A agar supplemented with glucose, and bacteria from the three predominant colony morphologies were characterized (Table 2).

Table 2. Bacteria characteristics of the three predominant colony morphologies (yellow, white, and small colonies) in experiment MP-1.

	Colony Morphology		
Characteristic	yellow	white	small
Gram stain	-	-	-
cell morphology	rod	short rod	short rod
motility	-	+	+
oxidase test	+	-	+
colony diameter (mm)	7-8	7-8	2-3
colony shape	round	round	round

Sampling

Effluent was grab sampled daily. Approximately 75 ml of effluent was collected in a sterile 250 ml beaker. A subsample was taken for glucose analysis; it was filtered through a 0.2 μm membrane filter to remove cells and then frozen. The remaining sample was homogenized with a Tekmar Tissuemizer for 90 sec at 90% power. A subsample was removed for cell enumeration and was preserved in 2% formaldehyde and refrigerated until analysis. Another subsample for TOC analysis was acidified with concentrated phosphoric acid to a pH less than 2 and frozen until analysis. Subsamples for bead counts were refrigerated.

Biofilm samples were obtained from the removable slides in the RT. Before slide removal, the area around the stopper to be pulled was dosed with 70% ethanol. After approximately 2 min, the ethanol was ignited, and after the flame was extinguished, the stopper was removed and stored in 70% ethanol. The slide was pulled out with a needle nose pliers which had been disinfected with 70% ethanol (residual ethanol burned off before sampling). Residual ethanol was burned off of the stopper before its replacement in the top of the RT. On some samples, biofilm thickness was measured. Biofilm was scraped off of a measured area on a slide into sterile 3 mM phosphate buffer (variable volume, from 5×10^{-5} to 1×10^{-4} m^3 (50 to 100 ml)). This mixture was homogenized with the Tissuemizer for 5 min at 90% power. Subsamples for cell counts, bead counts, and TOC were handled as described for effluent samples.

Microbead Characteristics

Latex microbeads used in these experiments (Polysciences, Inc., #15702) were chosen to simulate the physical characteristics of a bacterial cell. Their properties include (1) a nominal diameter of 1 μm, (2) a specific gravity of 1.05, and (3) a negative surface charge due to the incorporation of carboxyl groups during bead manufacture. The microbeads contained a fluorescent dye which made them easy to distinguish and enumerate under the microscope. The beads were suspended in distilled water or 0.85%

NaCl solutions and autoclaved (20 min) before their addition to the annular reactor, with the exception of Experiment A-2, where the beads were sterilized by glutaraldehyde (1%, 1 h contact time), and separated from the glutaraldehyde through centrifugation. Microbeads were added to the RT at a flow rate of 5.8×10^{-5} m^3 h^{-1} (1 ml min^{-1}) for 24 h. The point in the experiment when the microbeads were added varied (Table 3).

Table 3. Experimental protocols.

Experiment	initiation of bead addition[1]	length of bead addition period (h)	total experiment duration (h)	bulk liquid bead concentration during bead addition (# m^{-3})	fraction of beads which attached
A-1 (nascent)	0	24	144	3.9×10^{13}	0.0013
A-2 (nascent)	0	24	144	8.9×10^{12}	0.0038
B-1 (mature)	120	24	264	3.9×10^{12}	0.012
B-2 (mature)	120	24	264	2.9×10^{12}	0.010
B-3 (mature)	120	0.14	216	7.2×10^{14}	0.100
MP-1 (nascent)	0	24	168	-	-

[1] Hours after the end of bacterial inoculation.

According to the manufacturer (personal communication), latex microbeads are composed of polystyrene, with trace amounts of carboxylate groups, a fluorescent dye, and a surfactant to allow the dye to be incorporated in the non-water soluble matrix. The polymers are not cross-

linked. Carboxylate groups are at a concentration of 1 to 10 parts per million. A monomer containing these groups is added after the beads are made but some groups do diffuse into the polystyrene matrix. Therefore, the negative charges are not located solely on a bead surface. The carboxylate groups are tightly bound to the polystyrene; fluctuation of charges over time does not occur. Polystyrene and attached carboxylate groups are not biodegradable in the time periods covered by the experiments. Also, the beads are not affected by glutaraldehyde or formaldehyde.

Chemostat Reactor

A chemostat is a continuously flowing stirred tank reactor in which bacteria are grown. A chemostat was used in these experiments to inoculate the RT. This was done to standardize, as much as possible, the initial conditions in order to aid modelling and improve comparisons between duplicated experiments.

The composition of the chemostat influent solution is given in Table 1. Since the solution was oxygen limited, filtered air was sparged into the chemostat to increase the bacterial concentration.

The chemostat, accessory tubing, flowmeter, air filter, and 0.006 m^3 (6 l) of chemostat medium were autoclaved together for 0.83 h. After the problem with the spores was discovered, the autoclave time was increased

to 1.5 h. Glucose and calcium carbonate were added to the medium by injection through a septum with filter sterilization after autoclaving. The chemostat was inoculated with approximately 0.5 ml of a frozen cell suspension of *P. aeruginosa*. The broth was run in a batch mode (zero flow rate) for 8-12 h, by which time it had become turbid. The chemostat was then run at a dilution rate (flow rate divided by reactor volume) of 0.125 h^{-1} (5.8×10^{-5} m^3 h^{-1}) for 24 h (3 retention times) to produce a steady state cell concentration before the RT inoculation began.

The chemostat temperature was not controlled. Ambient temperatures ranged from 20-26°C.

Analytical Methods

Cell counts. All cell counts were total direct counts (Hobbie *et al.*, 1977). Samples (variable volumes) were added to an equal volume of Hoechst 33342 stain (100 μM), vortexed, and stored in the dark for 1 to 24 h. The samples, or an aliquot, were filtered through a 0.2 μm black membrane filter and observed under an Olympus BH-2 microscope using epifluorescent light. Cells were counted by an image analysis computer program using either a Cambridge/Olympus hardware and software package or an American Innovision package. The image analysis systems also provided average cell area. Cell concentrations and cell area were converted to cell carbon equivalents (Bakke *et al.*, 1984).

Microbead counts. The fluorescent microbeads were counted with a procedure similar to that used for cells. The samples were not fixed in formaldehyde, and no fluorescent stain was necessary.

Total Organic Carbon (TOC). TOC was determined on a Dohrmann DC-80 Carbon Analyzer according to the directions of the manufacturer.

Soluble Organic Carbon (SOC). The sample was centrifuged for 0.25 h at 20,000 rpm. The tubes had been washed in Micro™ soap and hot water, and then rinsed three times each in tap, distilled, and ultrapure water. The supernatant was analyzed for total carbon as described above.

Dry density. A measured area of biofilm was scraped into a pre-weighed aluminum dish. The sample was dried at 96°C for at least 3 h,

cooled in a dessicator, and weighed. Areal density was calculated as the quantity of dried solids divided by the area scraped. Volumetric density was calculated as the areal density divided by the biofilm thickness.

Glucose. Glucose was determined by a colormetric enzymatic method (Sigma Diagnostic, #510-A). The method employed was similar to the Sigma method, with the exception being that 2.5 ml of sample was used instead of 0.5 ml because of the relatively low glucose concentrations.

Biofilm thickness. Two methods were used to measure biofilm thickness. The more frequently used method was observation by light microscopy at 400x. The difference in the vernier on the fine focus knob between focusing on the biofilm surface and on the biofilm-substratum interface was noted, with the difference being read directly in μm (Trulear and Characklis, 1982). Optical thickness was multiplied by 1.33 to determine mechanical thickness (Bakke and Ollsen, 1986). For two samples in Experiment B-1, thickness was measured by a displacement of water method (van der Wende, 1991). This technique gave average film thickness in one measurement, and did not give any information on variation in film thickness.

Microscopy of cross-sections. In experiments where samples for sectioning were taken, polycarbonate membranes were taped to RT slides. After the slides were removed from the RT, the biofilm-membrane specimens were fixed in glutaraldehyde (2.5% glutaraldehyde in phosphate buffered

saline), dehydrated in ethanol, and embedded in JB-4 plastic (Polysciences, Inc., #18570). Other fixatives were tried besides glutaraldehyde (paraformaldehyde, formaldehyde, and cationic ferritin in combination with each of the three aldehydes), but the procedure described above worked the best. Thin sections (2.5 μm) were cut from the plastic blocks with a microtome using a glass knife, and the sections stained with Giemsa stain to highlight the bacteria.

The thin sections were examined and photographed with an Olympus BH-2 microscope using simultaneous transmitted white and epifluorescent light. Distance measurements from the thin cross-sections were made with the Olympus microscope and an American Innovision Videometric 150 image analysis system. Microbead profiles were constructed from distances measured on thin cross-sections with the American Innovision Videometric 150 image analysis system. Distances were measured along a normal to the substratum to beads (z) and to the biofilm-bulk water interface (L_f) where beads were located (Figure 3). Ratios of distance to beads over distance to the biofilm-bulk water interface were normalized to an average biofilm thickness (z^*):

$$z^* = \frac{z}{L_f} * L_f^* \qquad (7)$$

where L_f^* is a biofilm thickness averaged over space and time for the period covered by the profiles. Absolute and normalized bead locations were grouped into 1 μm intervals, and the frequencies converted to

concentrations using the independently-measured areal bead concentrations.

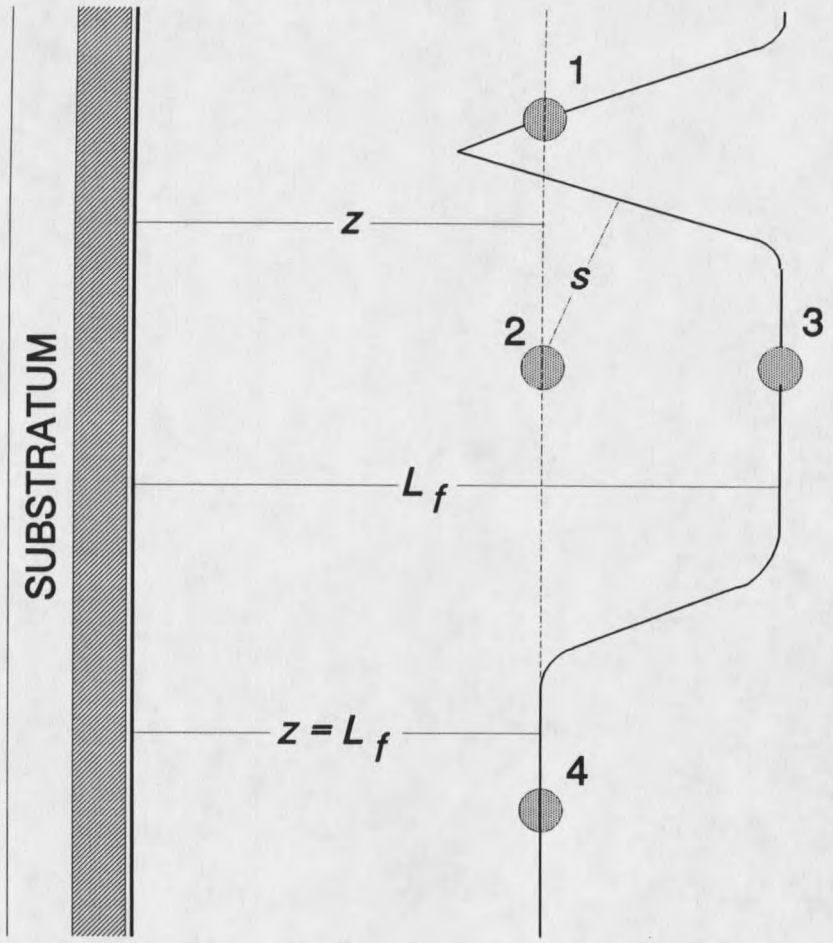

Figure 3. Schematic of bead position measurements. The substratum is on the left; the biofilm surface on the right. The distance between the substratum and beads (z) is less than or equal to the distance between the substratum and the biofilm surface (L_f). All measurements (except s) are perpendicular to the substratum.

Microbead aggregation studies. Microbead aggregation in biofilm and bulk water was assessed using the Hopkins statistic nearest-neighbor analysis for clustering (Jain and Dubes, 1988). Clean microbeads were

mixed with RotoTorque effluent for 0.25 h (one residence time in the reactor), then filtered on to a 0.2 μm black membrane filter. The filters were observed microscopically with ultraviolet light, and bead locations were determined in a Cartesian coordinate frame with the American Innovision image analysis system. Hopkins statistics were determined for ten fields per filter, with the ten values from each filter being averaged. Four treated samples and one no-treatment control (beads without reactor effluent) were analyzed. Hopkins statistics were similarly determined for two biofilm samples. These samples were observed by phase contrast microscopy, with coordinates determined for a total of three fields.

RESULTS

The interaction of microbeads with biofilm was studied in two experimental designs. Microbeads were added to either nascent (Type A experiments) or mature (Type B experiments) *P. aeruginosa* biofilms, or a nascent undefined mixed population (MP-1) biofilm. Nascent biofilms were thin (approximately 2 μm for *P. aeruginosa*, an average of 17 μm for the mixed population biofilm) with only partial surface coverage, while a mature *P. aeruginosa* biofilm had reached its maximum average thickness (approximately 35 μm) with complete surface coverage. The biofilm reactor was operated for 96 to 144 hours after the end of bead addition, during which time the biofilm was sampled to determine the number and distribution of beads in the biofilm. Experimental protocols are summarized in Table 3. Data on areal biofilm concentrations (microbeads, cells, TOC, EPS, biofilm thickness) and reactor effluent concentrations (microbeads, cells, EPS, TOC, and glucose) are listed in Appendix C. Microbead profile data are in Appendix D.

Microbeads added in aqueous suspension to the reactor attached to the biofilm. The fractions of attaching microbeads ranged from 10^{-3} to 10^{-1} and are reported in Table 3. The fractions were calculated as the number of microbeads attached to biofilm at the end of the bead addition period divided

by the number of beads delivered to the reactor.

Individual microbeads attached to biofilm were readily identified and distinguished from bacteria. Section views indicated that beads were located within the biofilm (Figure 4). Beads were also observed in the biofilm interior by phase contrast microscopy and scanning confocal laser microscopy. Beads can be identified at relatively low magnification (125x) when fluorescing, giving sensitivity to the identification and counting process. Counting of individual beads directly on the slides (plan view) was not always possible because of the presence of some bead aggregates.

Biofilm microbead concentrations decreased over time. The progression of microbead concentrations in experiments A-1, A-2, B-1, and B-2 is presented in Figure 5. Data for Experiment B-3 are not shown, since those concentrations are an order of magnitude greater than the concentrations for the other experiments. Areal bead concentrations in the mixed population biofilm experiment remained constant throughout the experiment (Appendix C).

Microscopic examination of thin cross-sections from the nascent biofilm experiment A-1 indicated that microbeads were located near the substratum at 48 h after the end of bacterial inoculation and were still near the substratum at 144 h (Figure 6). Quantitative measurements of bead positions from cross-sections also revealed skewed distributions, with bead concentrations decreasing toward the biofilm-bulk water interface (Figure 7).

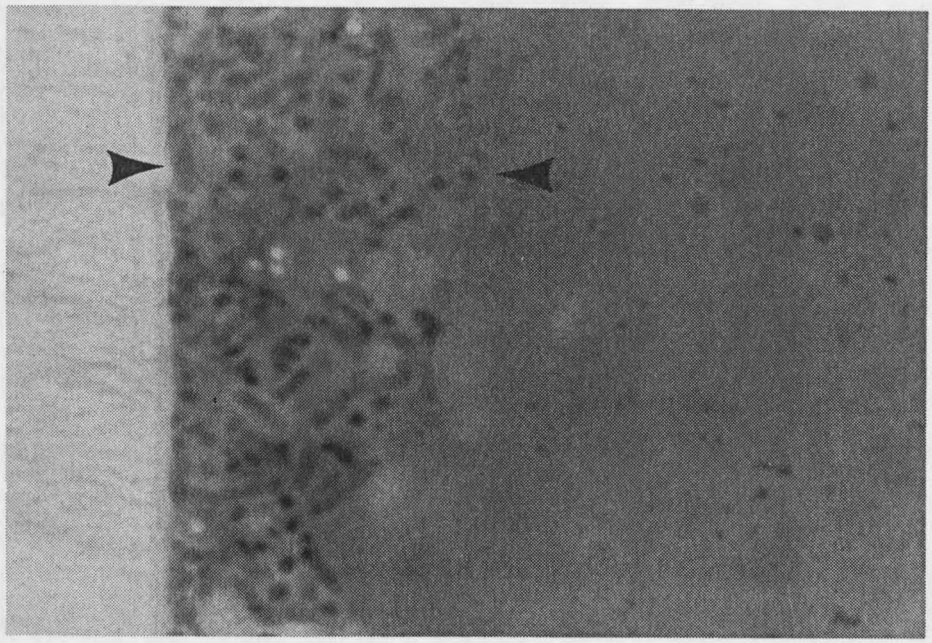

Figure 4. Biofilm cross-section from 144.75 h in Experiment B-2. The sample was taken 45 minutes after the cessation of microbead addition. Microbeads had effectively penetrated the entire biofilm thickness.

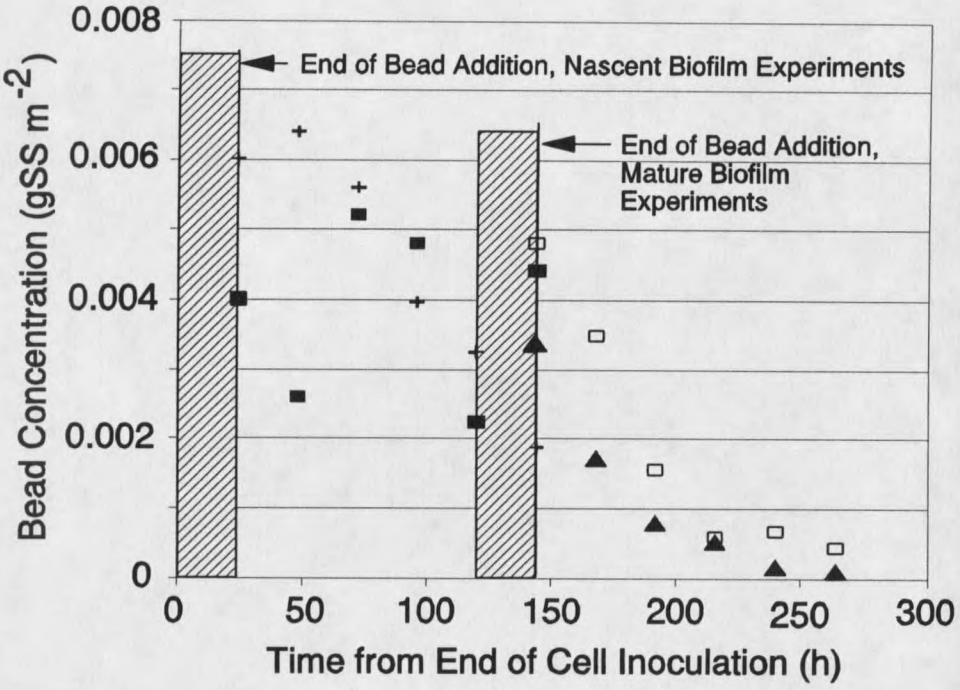

Figure 5. Biofilm microbead concentrations versus time for the nascent and mature biofilm experiments. The shaded regions indicates the bead addition periods. Experiment A-1 (+); A-2 (■); B-1 (□); and B-2 (▲).

The profiles also indicate that bead concentrations decreased over time. The change in bead concentration near the substratum was equal to the rate of dilution by cell growth and EPS production. The growth rate is given by:

$$\mu = \frac{-\ln \frac{X_{f,2}}{X_{f,1}}}{t_2 - t_1} \qquad (8)$$

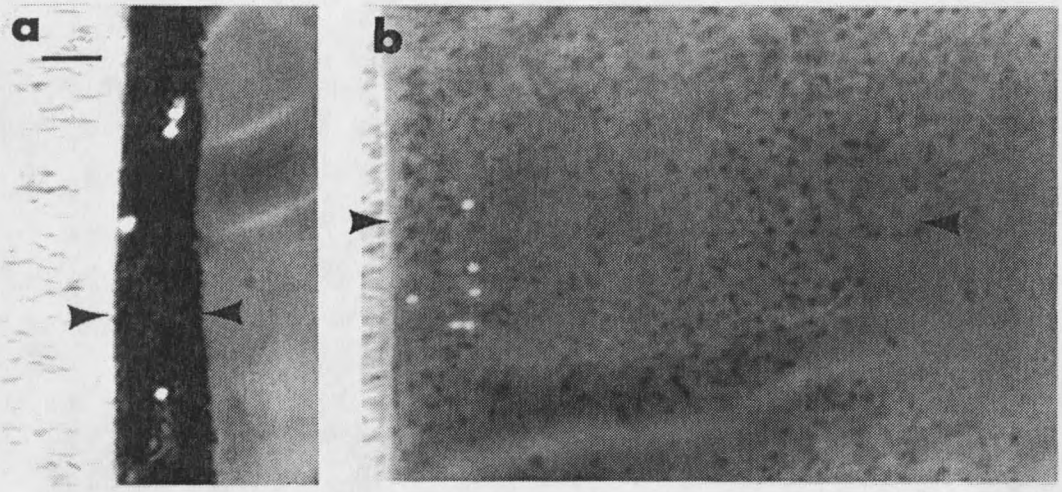

Figure 6. Biofilm cross-sections from Experiment A-1. The microbeads are approximately 1 μm in diameter. (a) Section from 48 h after the end of bacteria inoculation. The bacteria (dark particles) have grown over and entrapped the microbeads (light particles). Bar = 5 μm. (b) Section from 144 h. The remaining microbeads were generally located near the substratum. The dark areas in (a) and (b) are wrinkles produced during manufacture of the cross sections.

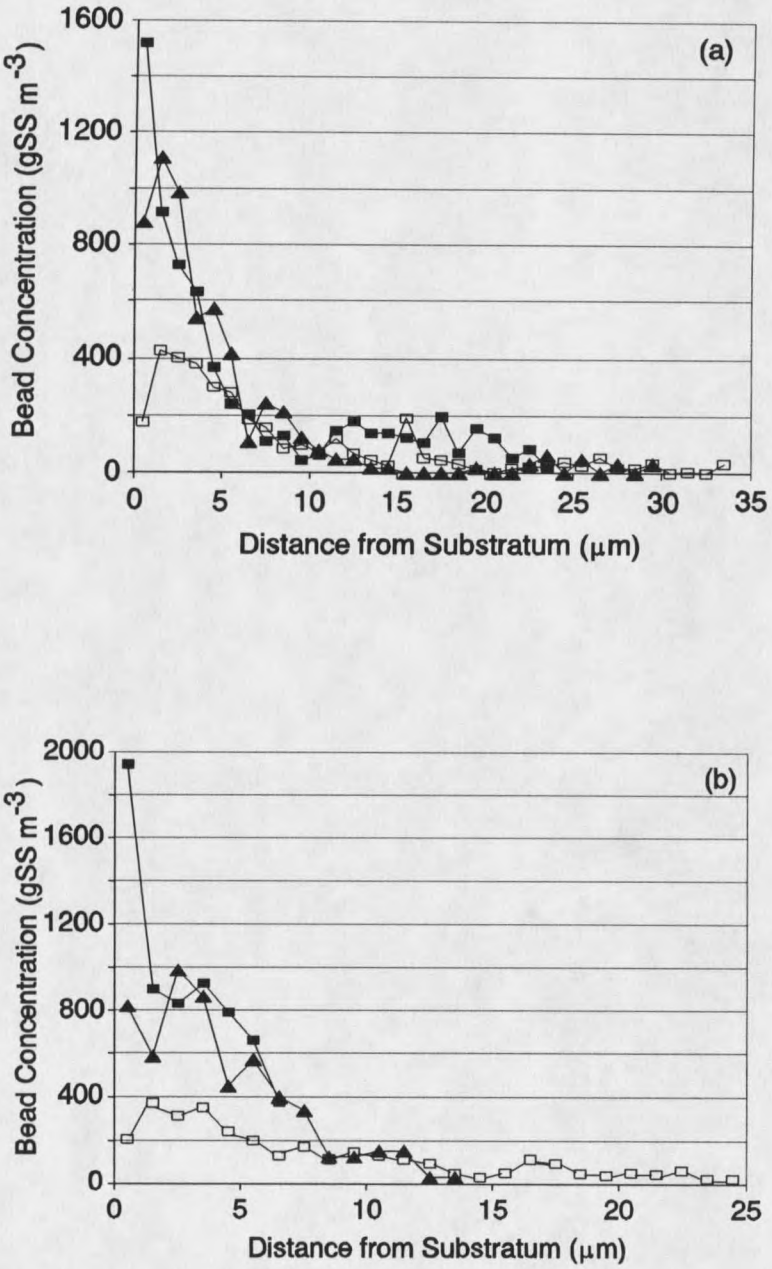

Figure 7. Bead profiles in the biofilm at 48 (■), 72 (▲), and 120 (□) h after cell inoculation in experiment A-1. The end of bead addition was at 24 h. (a) Unaltered profiles of bead concentrations. (b) Bead profiles normalized to the local biofilm thickness and then scaled to average film thicknesses of 7, 14, and 25 μm, respectively.

where: μ = biomass growth rate measured from bead dilution rate (t^{-1})

X_f = volumetric bead concentration ($M\ L^{-3}$)

1,2 = subscripts denoting consecutive times

The calculated rate (μ) was 0.028 h^{-1} for the beads in the first micrometer next to the substratum over the 72 hour period covered by the profiles.

Thin sections from the mature biofilm experiment B-2 show microbeads located throughout the depth of the biofilm 0.75 h after the end of microbead inoculation (t = 144.75 h) (Figure 4). The 168.6 h profile has concentrations similar to the 144.75 h profile at the substratum (Figure 8a). Most of the microbeads were located near the biofilm-bulk water interface at the earlier time, but later in the experiment (24.6 h after bead addition, or t = 168.6 h) a larger fraction of the beads was nearer to the substratum (Figure 8b).

In the mature biofilm experiment B-3 (pulse bead addition), beads were associated primarily with the biofilm-bulk water interface immediately after bead addition. The biofilm surface was irregular, with pores or crevices. The pores usually contained beads (Figures 9a, 9b). Therefore, beads were located at different distances from the substratum. At 8.9 h after bead addition (t = 128.9 h), several layers of bacteria covered most of the beads (Figure 9c). Beads were located even farther away from the biofilm-bulk water interface as time progressed (Figure 9d). Absolute-distance bead profiles show little change between 120.05 and 128.9 h, with

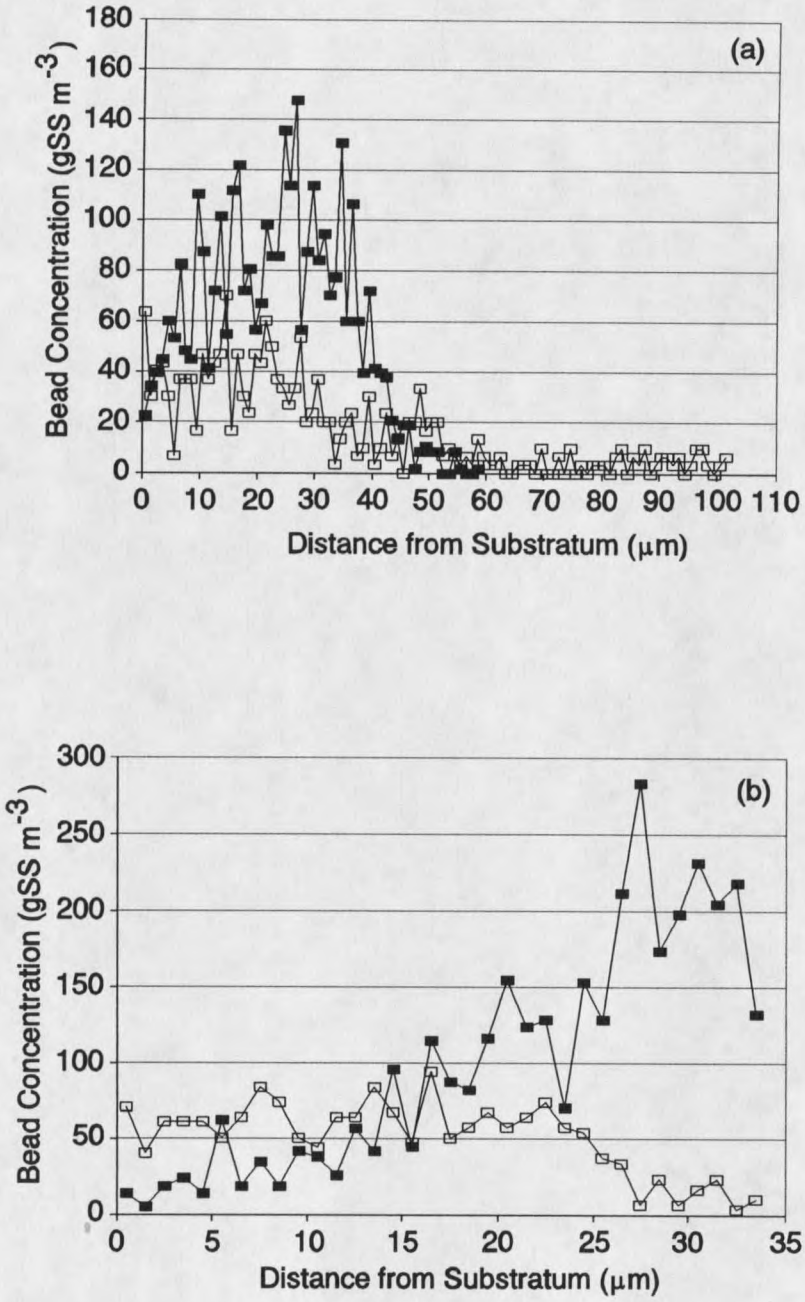

Figure 8. Bead profiles in the biofilm at 144.75 (■) and 168.6 (□) h after cell inoculation in experiment B-2. The end of bead addition was at 144 h. (a) Unaltered profiles of bead concentrations. (b) Bead profiles normalized to the local biofilm thickness and then scaled to an average thickness of 34 μm.

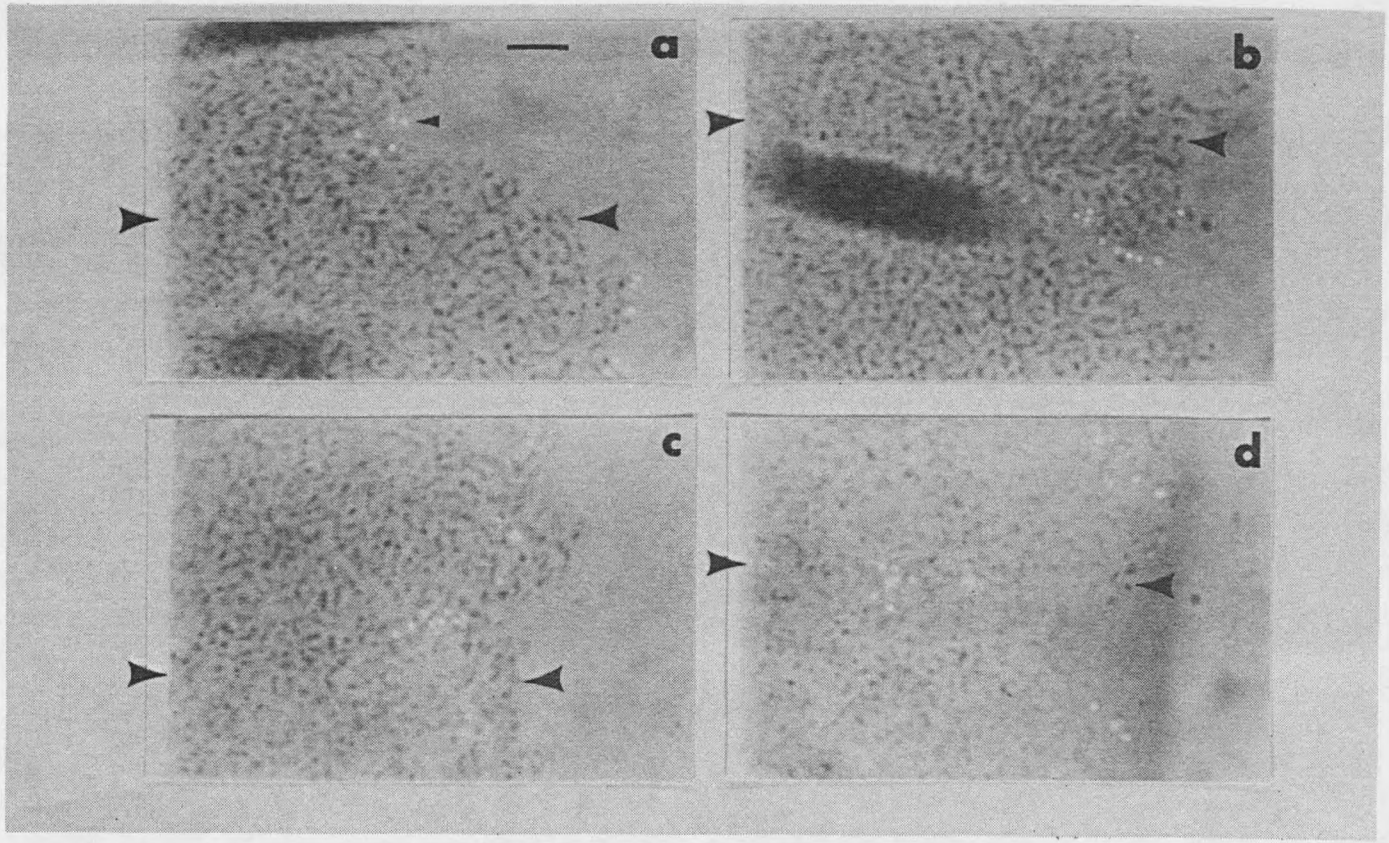

Figure 9. Biofilm cross-sections from Experiment B-3. (a) At 120.05 h, microbeads are at the biofilm-bulk water interface, including pore interfaces. Small arrowhead = bead; large arrowhead = biofilm surface. Bar = 5 μm. (b) Also at 120.05 h, another view of how pores provide a conduit for particle movement into a biofilm. (c) Microbeads are in the interior of the biofilm and not associated with an interface at 128.9 h. (d) Much of the biofilm thickness contains microbeads at 143.9 h.

higher bead concentrations near the substratum at 143.9 and 191.9 h (Figures 10a and 11a). Profiles normalized to a thickness of 37 μm indicate that bead concentrations near the biofilm-bulk water interface decreased over time, but increased over time near the substratum (Figures 10b and 11b).

A bead profile was constructed from scanning confocal laser microscope (SCLM) images. This profile, from four scans of a biofilm sample from experiment B-3, has a mode in approximately the same location as profiles made from cross-sections from the experiment (Figure 12). However, the peak bead fraction in the SCLM profile is twice that of the cross-section profiles, and the distribution is narrower. Artifacts due to sample handling should be less in the SCLM profile, because that sample was not fixed, dehydrated, sliced, or stained. A difficulty encountered in preparation of the SCLM profile was overlapping "halos" around the beads prevented counting of individual beads in the SCLM images, and caused transference of bead images to neighboring horizontal sections. Beads were quantified by the area they illuminated. Determination of the area due to beads truly in a horizontal section, and not from bead halos in other sections, required judgement. Also, vertical movement of the microscope stage had not been calibrated at the time the SCLM scans were made, and it is possible that the biofilm thickness reported to be scanned was not accurate. Therefore, the SCLM profile was normalized to the maximum

thickness obtained from the cross sections (41 μm). Uncertainty exists in the profiles from both the SCLM images and the cross-section samples, due to unfamiliarity with SCLM optimization and sample preparation and handling for the cross-sections. Similarity in the profiles indicates that artifacts in the profiles from cross-sections are not pronounced.

In experiment MP-1, beads were generally near the substratum at 80.6 h after the end of bacteria inoculation (Figure 13a). However, at 142.4 h, the beads were dispersed throughout the thick biofilm (Figure 13b).

The percentage of beads at the biofilm-bulk water interface decreased rapidly in the first 3 hours after bead addition in experiment B-3 (Figure 14). This decrease continued at a lesser rate for the next 21 hours. The numbers of beads within 3 μm of the biofilm-bulk water interface decreased in a similar pattern.

Bead aggregation was evaluated using the Hopkins statistic. With this measure, a value of 0.5 represents a random distribution of points, whereas values near 1.0 indicate that aggregation has occurred. The Hopkins statistic values for all bulk liquid samples, including the control, ranged from 0.60 to 0.63, with standard deviations in the ten analyses per filter ranging from 0.059 to 0.14 (Appendix E). Because the statistics are near 0.5 and the values for the treated samples equal that of the control, no bead aggregation occurred in these tests. The small amount of aggregation indicated by the values of 0.6 was most likely an artifact created during

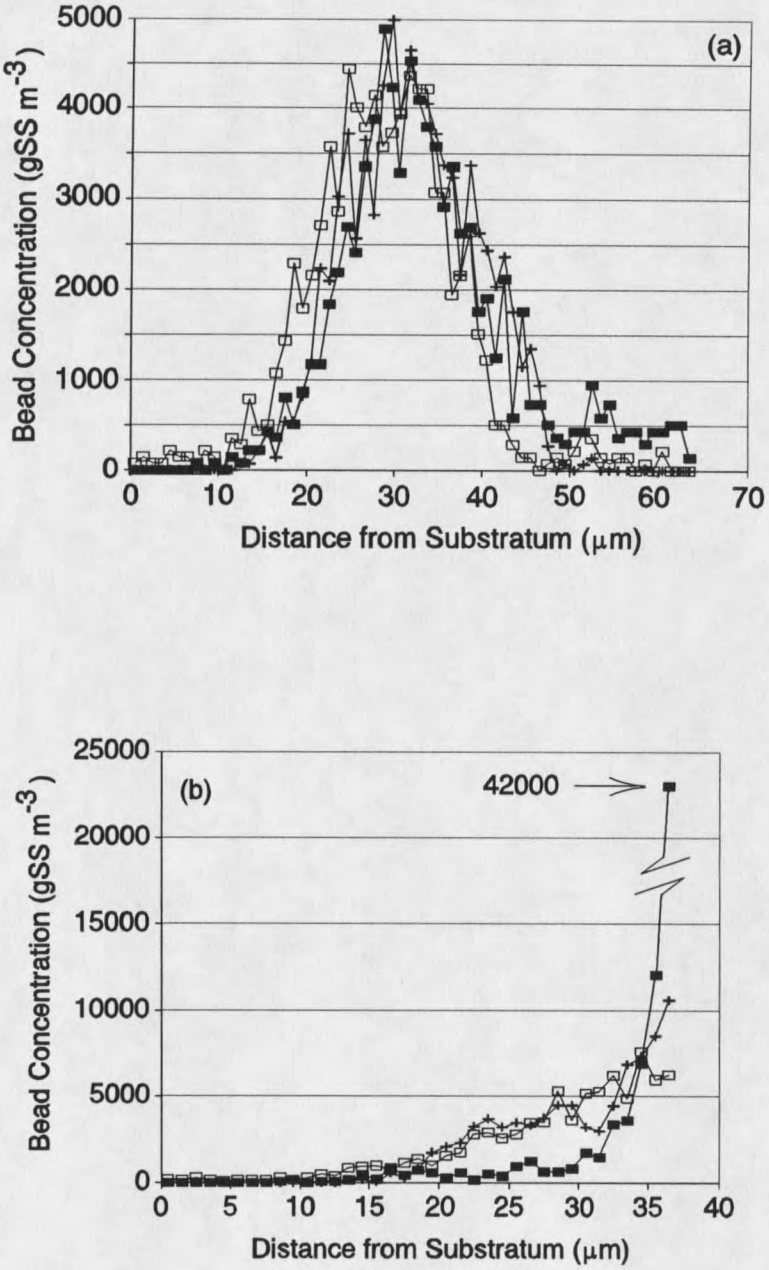

Figure 10. Bead profiles in the biofilm at 120.05 (▪), 122.9 (+), and 128.9 (▫) h after cell inoculation in experiment B-3 (pulse bead addition). The end of bead addition was at 120 h. (a) Unaltered profiles of bead concentrations. (b) Bead profiles normalized to the local biofilm thickness and then scaled to an average film thickness of 37 μm.

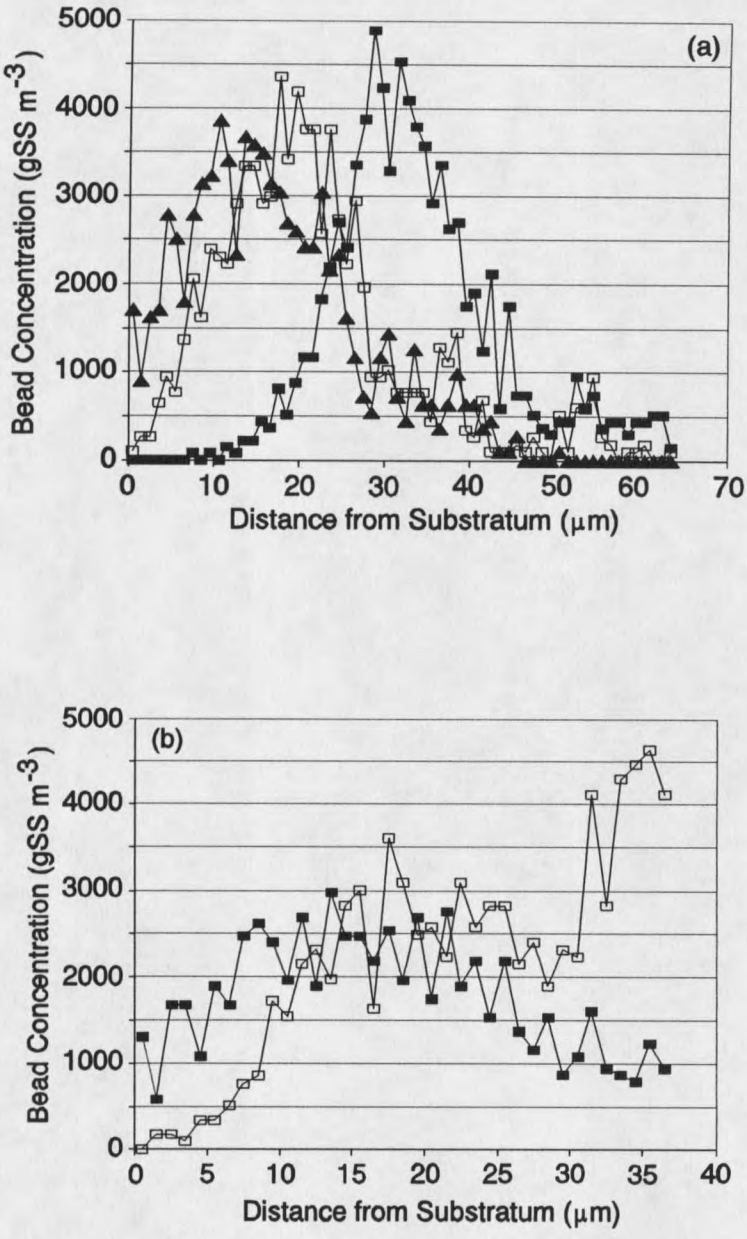

Figure 11. Bead profiles in the biofilm at 120.05 (■), 143.9 (□), and 191.9 (▲) h after cell inoculation in experiment B-3 (pulse bead addition). The end of bead addition was 120 h. (a) Unaltered profiles of bead concentrations. (b) Bead profiles normalized to the local biofilm thickness and then scaled to an average film thickness of 37 μm. The normalized profile at 120.05 h is not shown in (b).

filtration by imperfections in the filters. Biofilm samples, in contrast, had Hopkins statistic values ranging from 0.93 to 0.98. Therefore, beads did aggregate in or on the biofilm.

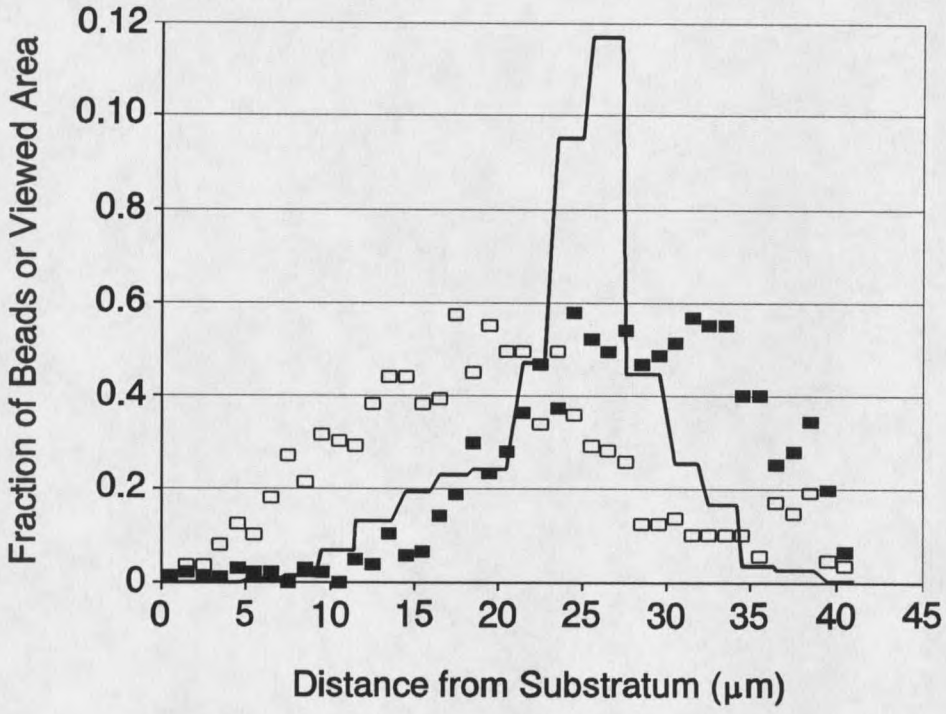

Figure 12. Bead profiles by scanning confocal laser microscope at 136.9 h (———) and from embedded, sliced cross-sections at 128.9 (■) and 143.9 (□) h. Both the peak locations and shapes of the profiles are similar.

Biofilm thicknesses for the nascent and mature *P. aeruginosa* biofilm experiments are shown in Figure 15. The mixed population biofilm had a large variation in thickness (Figure 16), with an average thickness an order of magnitude greater than the *P. aeruginosa* biofilms. Biofilm thicknesses measured at distinct points on a given sample vary significantly, suggesting

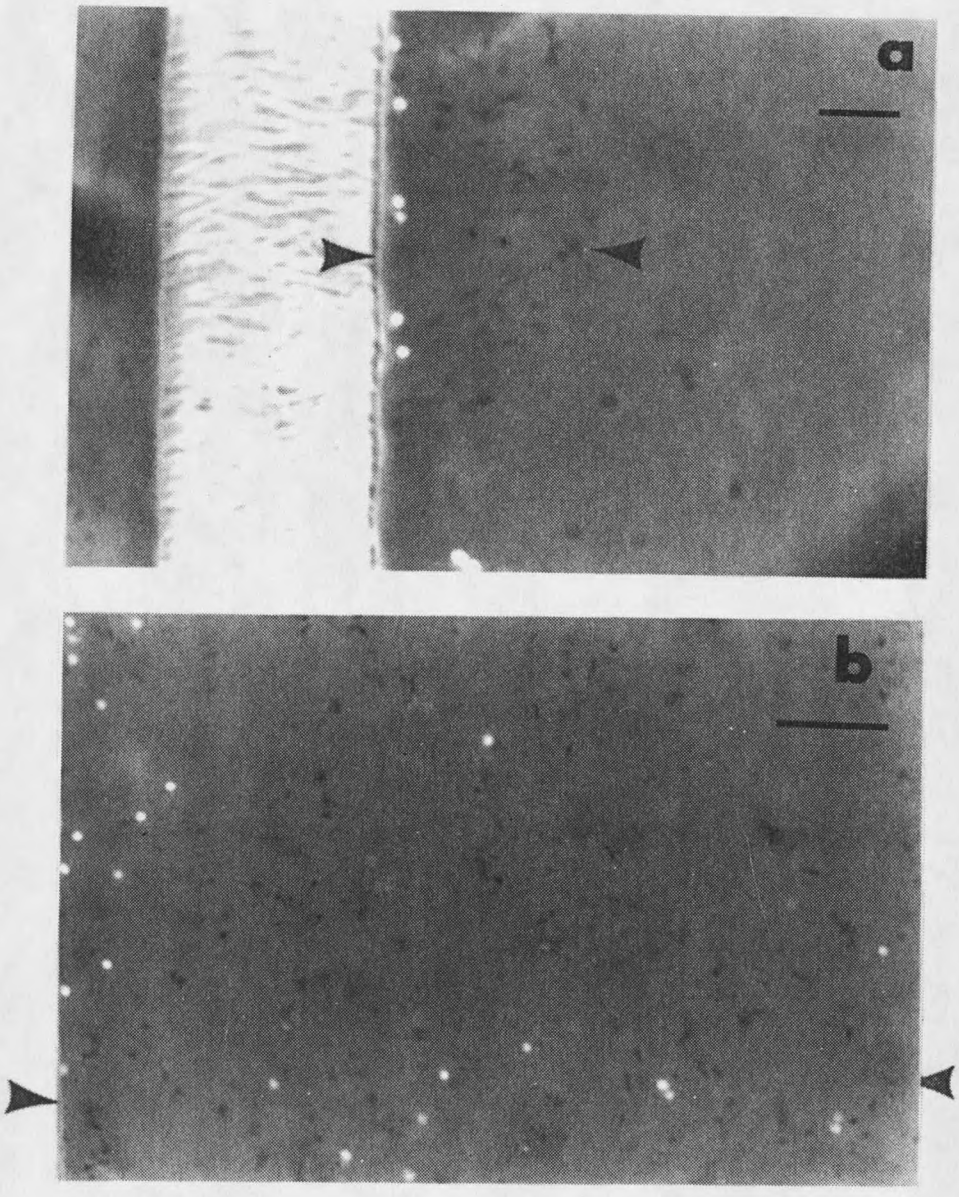

Figure 13. Biofilm cross-sections from experiment MP-1. The substratum (at left) and biofilm surface (at right) are marked by arrowheads. (a) Cross-section at 80.6 h. The film is 13 μm thick. Bar = 5 μm. (b) Cross-section at 142.4 h. The film is thick (approximately 78 μm) and beads are distributed throughout the depth. Bar = 10 μm.

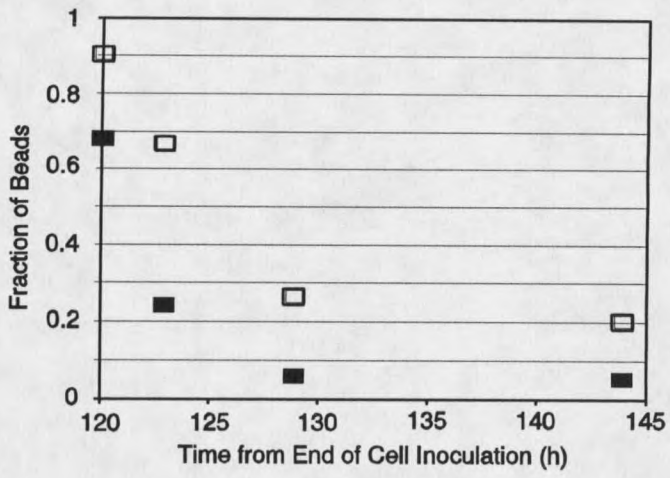

Figure 14. Fractions of microbeads located at (▪) and within 3 μm (▫) of the biofilm-bulk water interface over the first 24 h after bead addition in experiment B-3.

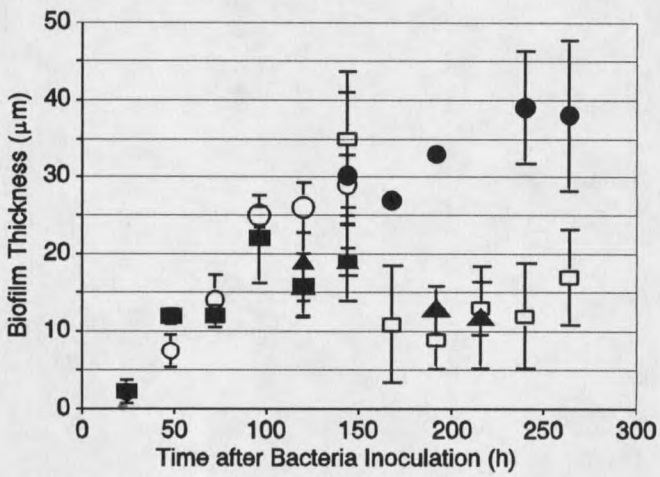

Figure 15. Biofilm thickness over time in the nascent and mature biofilm experiments. The thicknesses are the mean of several measurements, and the error bars are one standard deviation of the measurements. The two points with no standard deviations reported represent measurements by the volumetric displacement method. Experiment A-1 (○); A-2 (▪); B-1 (●); B-2 (▫); and B-3 (▲).

a three-dimensional biofilm structure that includes pores or ridges. A putative pore is shown in a scanning confocal laser microscope image of a specimen from Experiment A-2 (Figure 17). The pore is approximately 50 μm in diameter.

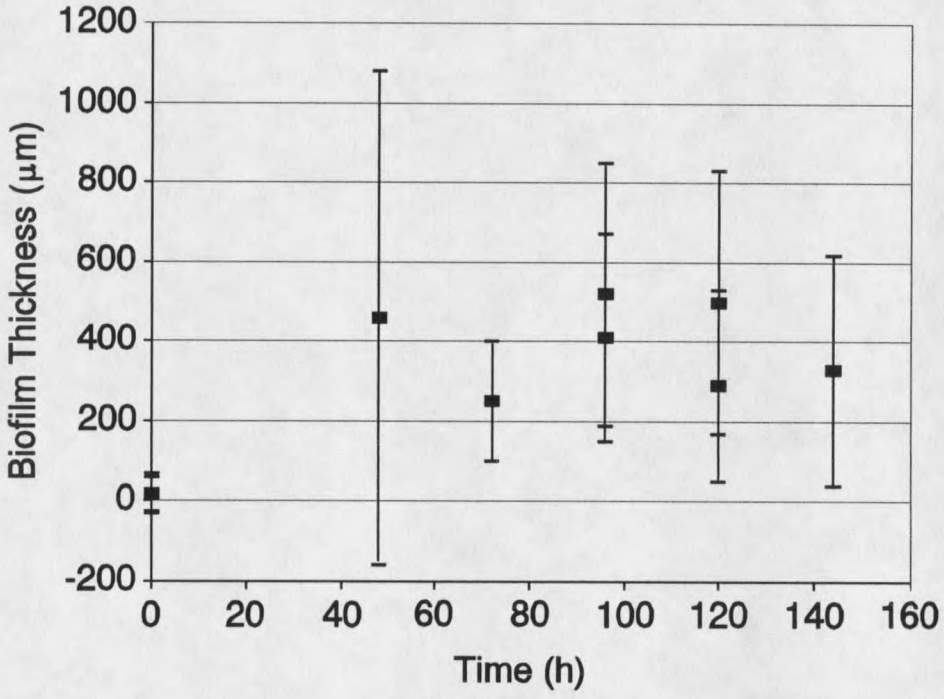

Figure 16. Biofilm thickness over time in experiment MP-1. Error bars are one standard deviation in the thickness measurements.

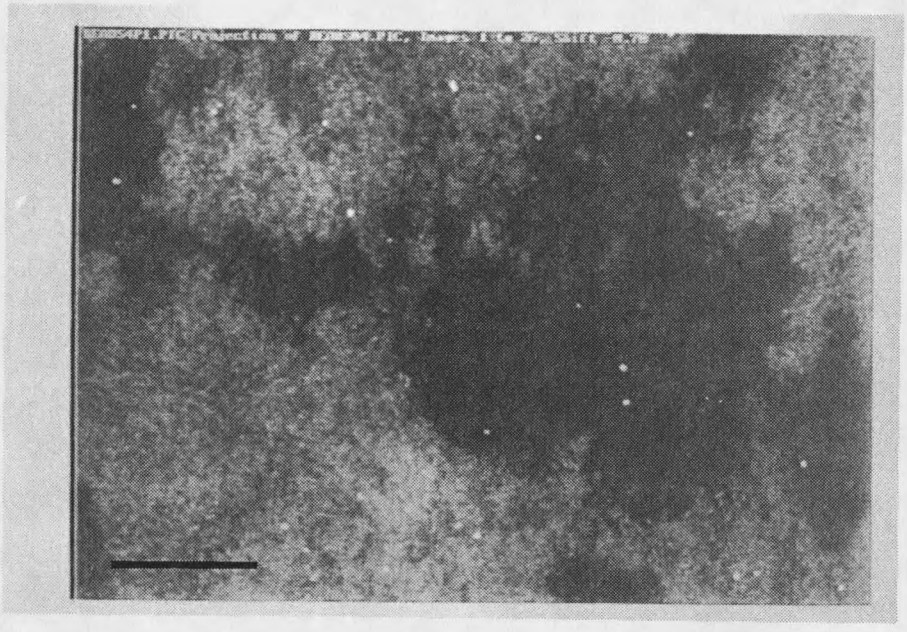

Figure 17. A photomicrograph taken by a scanning confocal laser microscope of a biofilm sample taken at 142 h in Experiment A-2. A putative pore, representing an area of relatively thin biofilm, is evident in the center of the image. Microbeads were located in areas of thick and thin biofilm. Bar = 20 μm.

DISCUSSION

Fluorescent latex microbeads have been shown to be effective tracers for particle movement in biofilms. They are easily differentiated from bacterial cells when viewed under a microscope, whether or not the beads are fluorescing. The locations occupied by microbeads can be determined in both plan and section views. Microbead concentrations in biofilm were quantifiable.

Microbead Attachment

Microbeads added to the RT in the bulk liquid attached to biofilm in the reactor. The fraction of attaching microbeads was proportional to the quantity of biofilm present during the attachment period. Both the amount of biofilm present at the ends of the 24 h attachment periods and the fractions of attaching microbeads in the nascent biofilm experiments were approximately one order of magnitude less than in the mature biofilm experiments (Figure 18). This result is consistent with the observations that microbeads (J. Bryers, personal communication) and bacterial cells (Banks and Bryers, 1992) attach to biofilm at higher rates than to a clean glass surface. It agrees with the observations of Rittman and Wirtel (1991), who reported the removal of 1 μm diameter milk colloids in a fluidized bed,

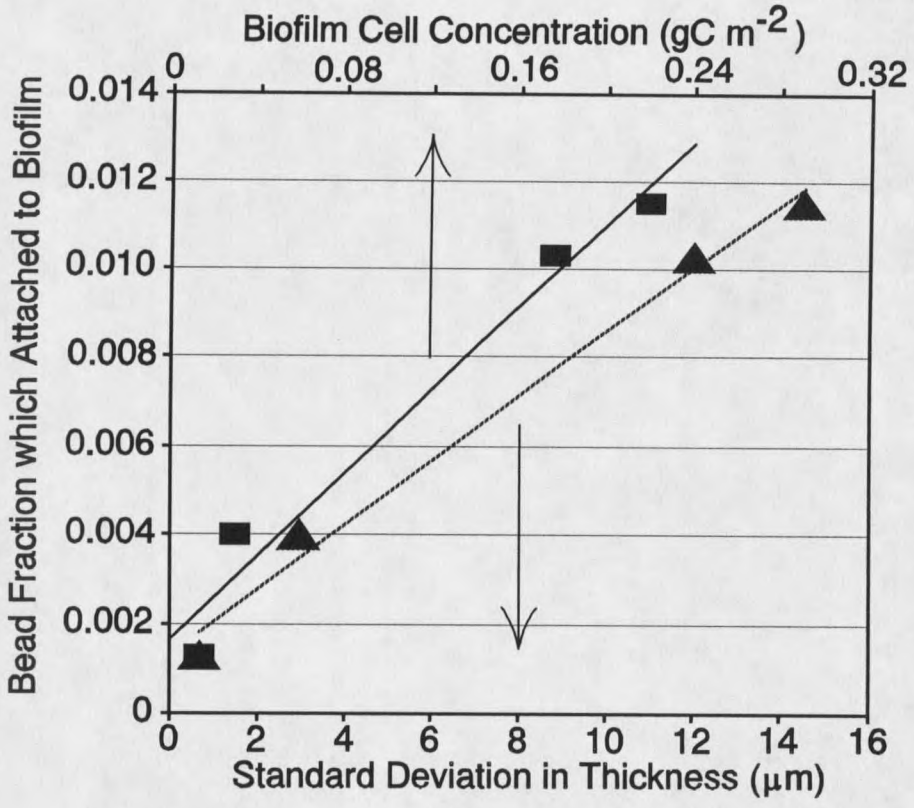

Figure 18. Fraction of microbeads attached to the biofilm versus biofilm cell carbon (■) and standard deviation in thickness (▲). The fraction which attached was directly proportional to the amount of biomass and the variation in thickness. r^2 = 0.990 for cell carbon; r^2 = 0.969 for standard deviation.

granular activated carbon biofilm reactor to increase from 87.4% to 91.5% when the amount of biofilm increased from 0.134 to 1.74 mg cellular carbohydrate per gram of dry carbon. The attachment fractions for beads were comparable to the 0.03 to 0.06 measured for *P. aeruginosa* cells attaching to a *P. aeruginosa* biofilm in a RotoTorque (Gunawan, 1991). The attachment fraction in Experiment B-3 (0.100) was higher than in the other mature biofilm experiments. This could have occurred due to attached

microbeads detaching before quantification in Experiments B-1 and B-2. Another possibility for this difference is that the higher bead concentration in the bulk water during bead addition in Experiment B-3 (200 times, Table 3) resulted in greater attachment or retention than occurred in the other mature biofilm experiments.

The fraction of microbeads that attached to biofilm was also proportional to the standard deviation in biofilm thickness measurements (Figure 18). The standard deviations in the mature biofilm experiments were greater than for the nascent biofilm experiments (Figure 15). The increase in thickness standard deviation with biofilm age is consistent with research by Bakke (1986), who found that the standard deviation of thickness measurements doubled between 50 and 300 hours of growth for a *P. aeruginosa* film. Biofilms consisting of other bacterial species can have standard deviations in thickness larger than the standard deviations measured in this research (Siebel and Characklis, 1991; Eighmy *et al.*, 1983; Mack *et al.*, 1975). A larger variation in thickness could represent more or deeper pores, crevices and ridges. Beads attached in pores may be retained for longer periods than beads at the exposed biofilm-bulk water interface. Beads attached in pores may be relatively protected from hydrodynamic shear stress, and less likely to detach than beads not in pores. Also, cell growth or re-attachment of detached cells can fill in the pores and bury the beads, increasing their retention in the biofilm. The mixed population biofilm

developed an average steady state thickness that was an order of magnitude greater than that achieved by the *P. aeruginosa* biofilms, and had standard deviations in thickness measurements that were greater than an order of magnitude larger than for the *P. aeruginosa* biofilms (Figures 13 and 14). Therefore, mixed population biofilms may capture and retain particles to a greater extent than the *P. aeruginosa* biofilms used here because of their large variation in biofilm thickness.

Microbead Movement into Biofilm

Particulate tracers have shown two distinct phases of particle movement in biofilms. The first phase, particle movement into biofilm during particle addition, is discussed in this section. The second phase, particle movement after entrapment within biofilm is discussed in the "Particle Transport within Biofilm" section.

The existence of pores in biofilms provides a possible mechanism for biofilms to envelop cells and particles. Pores were observed in the biofilms grown in these experiments (for example, Figure 9). Electron microscopic observations of biofilms and sludge granules have shown their rough surfaces and their interiors to be penetrated by pores. Switzenbaum and Eimstad (1987) examined anaerobic biofilms from biological filters and fluidized beds, and reported the films to be uneven, containing ridges, holes and channels. Eighmy *et al.* (1983) reported the existence of channels in

biofilms which markedly increased the biofilm surface area. The bacteria in the films appeared to be aggregated and did not reside in contiguous layers. Robinson *et al.* (1984b) observed biofilms from anaerobic fixed film reactors, which contained rough and uneven surfaces, with "volcano-like" structures penetrating the films. Openings and channels throughout the films were common. Mack *et al.* (1975) observed "slit-like" openings in trickling filter biofilms. Cavities in bacterial aggregates have been reported (Beeftink and Staugaard, 1986; MacLeod *et al.*, 1990; Bochem *et al.*, 1982).

Beads that attached in pores were likely to become buried within the biofilm. Deposition of particles in a random manner would place some beads in pores. Observations of the thin cross-sections (for example, Figure 9) indicated that pores appeared to fill in with bacteria, burying any particles residing in the pores. Therefore, pores in the biofilms were relatively short-lived with their creation causing a biofilm to capture particles and their disappearance leading to particle retention. The presence of beads in pores immediately after bead addition (Figure 9) and the decreasing fraction of beads at the biofilm-bulk water interface over time (Figure 14) indicated that bacteria covered the beads, which would have happened as the bacterial population increased. Surface films have pores such as these biofilms did, as opposed to a base films which do not (Gujer and Wanner, 1990). Since *P. aeruginosa* forms biofilms of relatively uniform thickness and would seem to be an optimum example of a base film (Siebel and Characklis, 1991), the

concept of a base biofilm may have no value in terms of modelling particle capture and retention.

The "penetration" of a mature biofilm by microbeads indicates that there was a mechanism for transport of beads toward the substratum. This mechanism is not considered in models which have growth-driven advection as the only means of particle transport (Gujer and Wanner, 1990, Stewart *et al.*, 1991). This mechanism (or mechanisms) may act during bead addition to the biofilm (Figures 6b and 8b).

Two hypotheses exist to explain particle movement in the direction opposite to growth-driven advection in a biofilm of steady-state thickness. The existence of pores in biofilms provides a means for particles to diffuse into the depths of biofilms without being retarded by contact with the particles (EPS and cells) composing the biofilm. This can include transport of previously attached beads, because detached beads may re-attach into pores. Because of the long retention time experienced by attached beads (Figure 5), open pores could permit diffusion of beads into biofilm depths throughout an experiment. The microbeads have a diffusion coefficient of 1.75×10^{-9} m^2 h^{-1} according to the Stokes-Einstein equation. Therefore, they could traverse the 35 μm thickness of a mature biofilm in approximately 0.7 h if suspended in the pore space. The penetration of the entire biofilm thickness by beads in 8.9 to 24 hours (Figures 6 and 8) represent a conservative rate of transport when compared to that possible by diffusion.

The second hypothesized mechanism of bead penetration into biofilm is inertial transport by momentum obtained from bulk water movement. The momentum may be derived from centripetal acceleration associated with the annular flow or from turbulent motion perpendicular to the average fluid flow. The relative importance of inertial forces in bead transport can be determined from the Reynolds number for particle movement in water. The velocity perpendicular to the rotation at the outer wall of the RT is approximately 0.018 m h^{-1}, producing a particle Reynolds number of 5.5 x 10^{-6} (Appendix F). Velocity perpendicular to the reactor wall due to turbulence is 0.112 m h^{-1}, giving a particle Reynolds number of 3.5 x 10^{-5}. In both cases, the very small Reynolds numbers indicate that viscous forces strongly dominate over inertial forces. The momentum imparted to beads by movement of the bulk water is insufficient to explain penetration of the biofilm.

Particle penetration into biofilm should be enhanced by more and larger pores, but such an increase in porosity may not be described by measurement of biofilm density. For example, *Pseudomonas putida* cells added to a 70 μm thick monopopulation *Hyphomicrobium* biofilm showed little movement toward the substratum - only 10 μm in 72 h (Bryers and Banks, 1990). The density of this biofilm was 10,000 g m^{-3}. The *P. aeruginosa* biofilms used in the bead experiments had an average volumetric density of 60,000 to 140,000 g m^{-3} (Experiment B-3, Appendix C), and

were totally penetrated (about 35 μm) by bacterially-sized particles in less than 24 h. Bryers and Banks grew their biofilm in a laminar flow environment, unlike the *P. aeruginosa* biofilms, which existed in a turbulent flow environment. More pores and surface roughness may have existed in the biofilm grown in turbulent flow, because biofilm surface roughness can increase with an increasing amount of turbulence as the Reynolds number was changed from 9700 to 32,000 in the bulk water (Santos *et al.*, 1991).

Bead locations relative to the biofilm-bulk water interface change due to cells covering the beads. The profiles at 120.05, 122.9, and 128.9 h in experiment B-3 indicate that the beads did not move significantly with respect to the substratum over that interval (Figure 10a). However, bead concentration changed dramatically at the biofilm-bulk water interface (Figure 10b). The interface has moved away from the beads over time, filling in pores and expanding film thickness in areas where there were beads. Since the average film thickness was constant, the local film thickness had to be decreasing in areas without beads - the beads having detached along with cells and EPS. Also, Figure 10b may indicate that this biofilm expanded from growth near its surface. The beads were relatively stationary with respect to the substratum and their concentrations nearly uniform (Figure 10a), so z was constant, yet the ratio of z/L_f was decreasing. Therefore, the distance from the substratum to the biofilm surface (L_f) must have increased from growth between the beads and the

biofilm surface.

Particle Transport within Biofilms

When a pore containing microbeads closes, the transport of beads out of the film changes to a mechanism and time scale different from diffusion down a pore. Electron micrographs of biofilm reveal polymers to be spaced at intervals smaller than the 1 μm microbeads (Jones *et al.*, 1969; Beeftink and Staugaard, 1986; MacLeod *et al.*, 1990). Bead contact with the polymers would make diffusion in a polymer matrix retarded compared to diffusion in clean water, if diffusion occurred at all. Beads trapped within pores will remain in biofilm for a longer period than the time needed for diffusion into a pore.

The decrease in areal bead concentration in experiments A-1, B-1, and B-2 may be described by the empirical equation:

$$X_f' = X_{f,o}' e^{-kt} \qquad (10)$$

where: X_f' = areal microbead concentration (M L^{-2})

k = bead release rate coefficient (t^{-1})

t = time (t)

Microbead release coefficients were computed using linear regression of the natural logarithm of X'_f against t (Table 4, Figure 19). The bead release coefficient for experiment A-1 is less than the values obtained in the Type B experiments and is different at the two standard error level. The initial bead

profile in experiment A-1 was skewed so that the highest bead concentrations were near the substratum (Figure 7), while in the mature biofilm experiments, the initial profile had the highest concentrations at the biofilm surface (Figures 8 and 10). The high bead release coefficient from the Type B experiments indicates that beads near the biofilm surface detach relatively quickly. In contrast, beads near the substratum detach slowly, as demonstrated by the low bead release coefficient in experiment A-1. Therefore, detachment was a surface phenomenon in these experiments, with the majority of detachment occurring at or near the biofilm surface.

The average retention time in biofilm for microbeads was greater than for cells. The cellular growth rate measured in the *P. aeruginosa* experiments averaged 0.15 h^{-1}, based on net overall biomass production (Table 4). Therefore, the time scale for growth-driven advection (μ^{-1}) in the biofilm was approximately 7 h. The time scale for bead release (k^{-1}, 33 to 100 h) was significantly greater than the time scale for advection (μ^{-1}, 5 to 12 h).

Table 4. Bead release coefficients and average cell growth rates for the *Pseudomonas aeruginosa* experiments.

Experiment	$k \pm$ *standard error* (h^{-1})	μ (h^{-1})
A-1	0.0097 ±0.0019	0.19
A-2	6.0×10^{-5} ±0.0038	0.20
B-1	0.0212 ±0.0030	0.083
B-2	0.0306 ±0.0016	0.11
B-3	-0.0011 ±0.0025	-

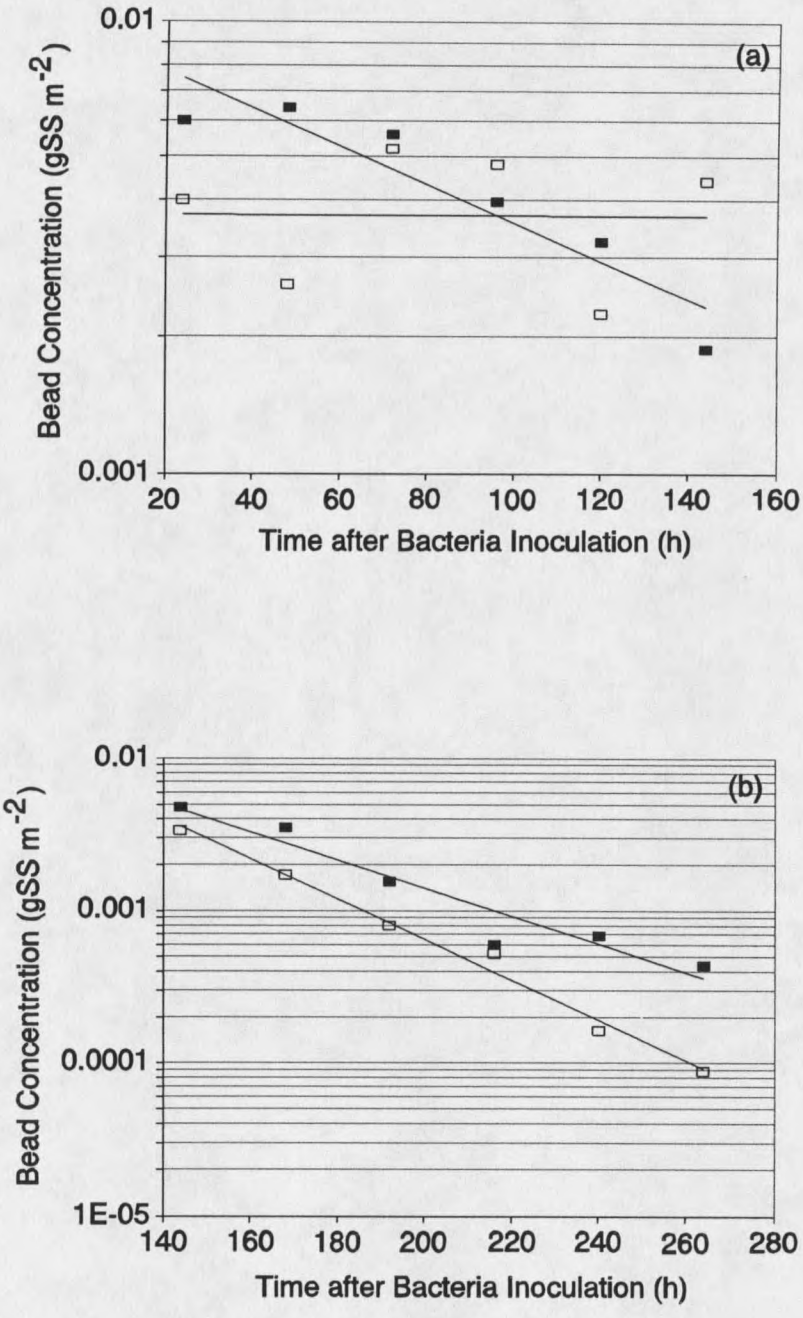

Figure 19. Biofilm microbead concentrations over time for the nascent (a) and mature (b) biofilm experiments compared to a first order rate of detachment. Symbols: A-1 (■, ———); A-2 (□, ---); B-1 (■, ———); B-2 (□, ---). Values for r^2: A-1, 0.87; A-2, 0.39; B-1, 0.92; B-2, 0.99.

Determination of the probability of detachment for individual beads depends upon the location of the bead relative to the biofilm-bulk water interface, assuming that detachment is a surface phenomenon (for example, erosion) as demonstrated above. Referring to the illustration in Figure 3, beads 1, 2, and 4 would plot at the same z in a graph of absolute bead locations. Their probable fate, however, is different. Bead 4 will quickly detach because it is at the biofilm surface in the zone of rapid detachment. Bead 2, however, will remain in the biofilm for an extended period because it is covered by cells. Bead 1 will remain in the biofilm as well if the pore it is in becomes filled with cells before the bead detaches. In a plot of normalized bead distances (z^*), beads 1 and 2 would be placed at the same position because they have the same values for z and L_f, while beads 3 and 4 would be at a different $z^* = L_f^*$. Bead 4 will probably detach rapidly, but is grouped with the slowly-detaching beads 1 and 2 in a plot of absolute bead distance from the substratum. Beads 3 and 4 would not be at the same depth in a plot of absolute z values, although both are likely to detach rapidly. If the biofilm thickness at bead 4 increases to L_f and bead 4 does not move, the bead will appear to be transported toward the substratum in a normalized bead location graph. Beads 1, 3 and 4 are all at the interface and would be plotted together on a graph of bead distance from the biofilm-bulk water interface, while bead 2 is the lesser of (L_f - z) or s from the interface and would not be grouped with the other three beads.

Biofilm Ecology

The fate of quiescent microorganisms is simulated by the microbeads in these experiments and demonstrates the ecological difference between biofilm and the bulk water associated with the biofilm. Quiescent microorganisms are microbes subsisting in a nonreproducing state brought on by nutrient starvation or other conditions (Lewis and Gattie, 1991; Lewis, 1991). Suspended particles do not remain in the reactor environment for more than an hour (4 hydraulic residence times). At least 10 to 30 per cent of those beads that were attached when the bead concentrations were first quantified remained in the biofilms for 120 hours. The large difference in particle retention times between biofilm and the bulk water means that particles in the biofilm have a better chance of being subjected to differing time-variable environmental conditions. The long retention times that can be experienced by quiescent microorganisms in biofilms provide a greater possibility that these microbes attain significant activity if the environment changes so that conditions are conducive for their replication.

Particle movement into biofilms has two other implications for biofilm dynamics. It indicates how anaerobic bacteria may move from oxygenated bulk water to the lower anaerobic layer of an oxygen-limited biofilm. For example, while sulfate reducing bacteria cannot grow under aerobic conditions, they can be found in biofilms on the walls of pipes carrying aerated water. They could be transported to the anaerobic depths

of the biofilm through pores in the biofilm. Also, particle transport into biofilms provides a mechanism for colloidal substrates to move deep into a biofilm and provide substrate directly to microorganisms there.

Biofilm Modelling

Modelling of biofilm structure and activity is an important part of biofilm research. Modelling permits the testing of hypotheses about biofilm structure, often without the need for analysis of the microscale gradients within biofilms. To do this, the model must be able to predict population dynamics so that the cells of different species are placed in the proper locations. Cell populations must also be predicted with accuracy. If the cells are not in the correct concentrations in the proper microenvironments, their predicted activity and biofilm structure will be inaccurate.

A commercially available computer program (BIOSIM; Reichert *et al.*, 1989) was employed to test the state-of-the-art in the ability of a model to predict microbead concentrations and locations. Coefficients used with the model to describe *P. aeruginosa* growth and activity are listed in Table 5.

Areal microbead concentrations were predicted by the model to test the accuracy of population predictions. With this model, beads added to a biofilm cannot move through biofilm toward the substratum as long as the advection velocity is positive. All of the beads which attached to biofilm would be at the biofilm-bulk water interface, in which case detachment is

rapid (Figure 20). Since BIOSIM cannot accomodate the initial movement of beads into the biofilm, a bead profile from a time after this transport (Figure 8b, 144.75 h profile) was put into BIOSIM as the initial bead distribution in order to test the ability of the model to predict particle movement away from the substratum. When experiments B-1 and B-2 were simulated, BIOSIM predicted bead concentrations that were lower than the data (Figure 20). Therefore, BIOSIM predicted a greater advection rate than experienced by the beads.

Table 5. Kinetic and yield coefficients for growth of *Pseudomonas aeruginosa* on glucose and oxygen.

Coefficient	Value	Reference
μ_{max}	0.37 h^{-1}	Characklis, 1990b
K_S	1.6 $gS_c\ m^{-3}$	Characklis, 1990b
K_{O2}	0.1 g m^{-3}	Lewandowski *et al.*, 1991
$Y_{x/s}$	0.24 $gX_c(gS_c)^{-1}$	Siebel, 1987
$Y_{p/s}$	0.41 $gP_c(gS_c)^{-1}$	Siebel, 1987
$Y_{x/o}$	0.21 $gX_c(gO_2)^{-1}$	Robinson *et al.*, 1984a; Turakhia and Characklis, 1989
k_p	0.36 $gP_c(gX_c)^{-1}$	Siebel and Characklis, 1991
k_p'	2.40 $gP_c(gX_c)^{-1}d^{-1}$	Siebel and Characklis, 1991
ϵ_l	0.90	Appendix G
D_f/D	0.90	Westrin and Axelsson, 1991
ρ_{cells}	118,000 gC m^{-3}	Robinson *et al.*, 1984a
ρ_{EPS}	110,000 gC m^{-3}	assumed less than ρ_{cells}
L_L	1 μm	Appendix H

A hypothesis that addresses this discrepancy is that advection in the dimensions parallel to the substratum is significant compared to advection perpendicular to the substratum because the film thickness is nonuniform

and cells and EPS move laterally into pores, detaching from the biofilm without adding to the advection perpendicular to the substratum. If this was true, BIOSIM would overestimate the advection rate because it would have all advection occurring in the dimension perpendicular to the substratum while some advection is actually directed parallel to the substratum. BIOSIM did predict the bead concentrations well when μ_{max} and the non-growth associated polymer formation coefficient were divided by 20 (Figure 20). At this reduced growth rate, the sum of the cell and polymer growth rates (0.013 h^{-1} and 0.014 h^{-1}, respectively) is 0.027 h^{-1}. This is equal to the bead dilution rate near the substratum in experiment A-1, and equal to the bead release rate in the mature biofilm experiments. There is experimental justification, therefore, for modelling bead transport with the low growth rate.

BIOSIM does not predict particle spatial distributions within the biofilm well (Figure 21). Experimentally measured profiles from mature biofilms have modes which move toward the substratum, if at all, and maintain significant slopes throughout the experiments. In BIOSIM-generated profiles, the mode of the distribution moves toward the the biofilm surface, and progressively flattens, tending toward a zero slope. The mathematical model predicts monotonically decreasing bead concentrations (toward the biofilm surface) as a steady state profile is approached, because, from equation (4), the partial derivative of X_s with respect to z is negative for inert particles (r_s

= 0) and when the cell growth rate is positive through the film. The experimental profiles do not decrease monotonically (Figures 10 and 11). Decreasing the growth rates by a factor of twenty still pushes the mode of the profile toward the biofilm surface in a manner not shown in the data (Figure 21).

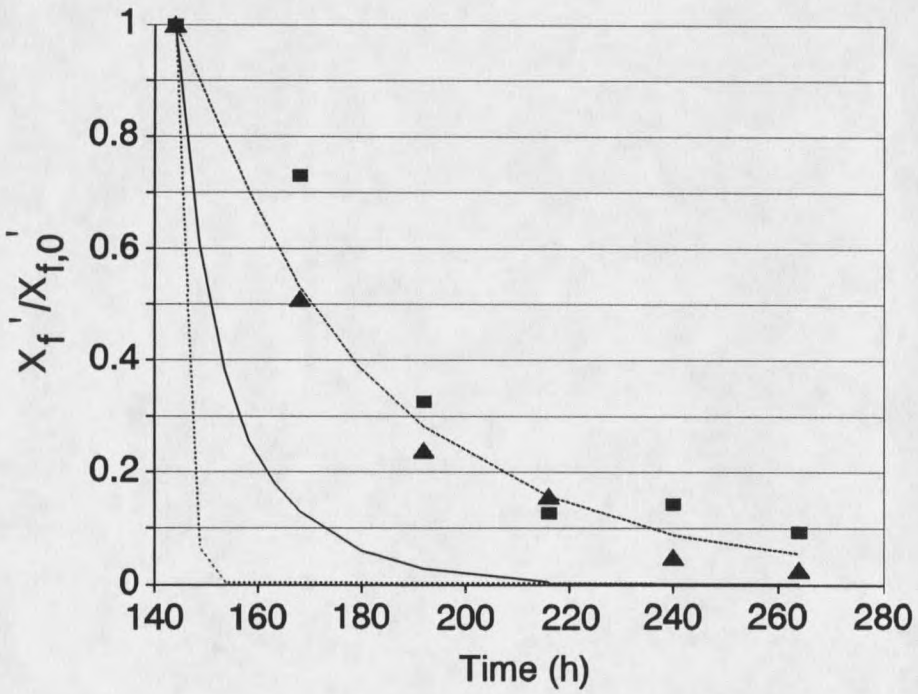

Figure 20. Effect of the initial microbead placement and cellular growth rate on the biofilm microbead concentration over time for the *P. aeruginosa* mature biofilm experiments. Data: B-1 = ■; B-2 = ▲. BIOSIM simulations: (1) normal growth rates (——); (2) 1/20 normal growth rates (---), (3) normal growth rates and all beads at the biofilm surface for an initial condition (• • •).

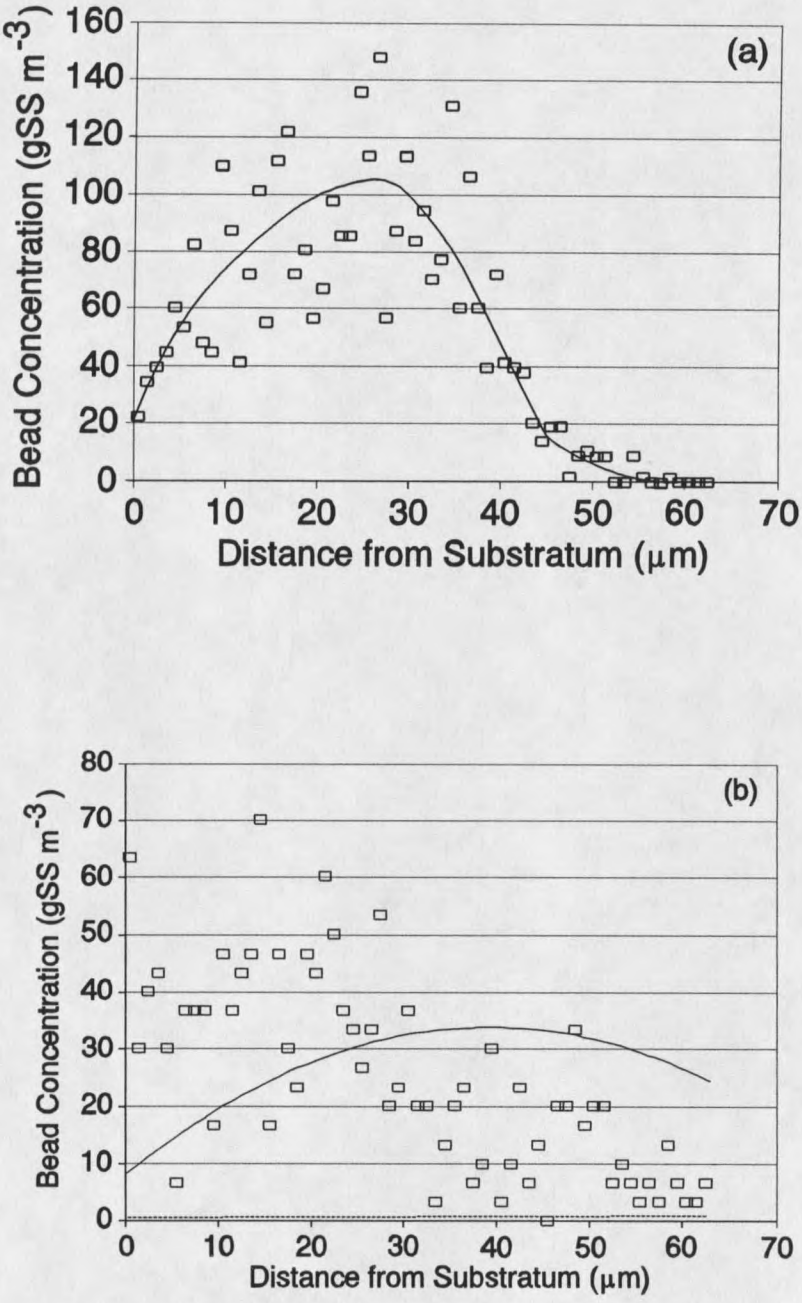

Figure 21. Bead profiles from Experiment B-2 at 144.75 (a) and 168.6 (b) h after cell inoculation. Data (□); the line (———) indicates the assumed initial condition in (a) and the predictive distribution for $\mu = 0.025\ h^{-1}$ in (b). (----) is the simulated profile in (b) for $\mu = 0.15\ h^{-1}$.

Much growth may occur in the rough upper layer of biofilm. BIOSIM, with its one-dimensional view, may overestimate growth in the depth of the biofilm. Figure 22 represents a conceptual view of how a rough biofilm surface might increase the cellular growth rate in the rough biofilm surface. The large amount of surface area of a rough biofilm may increase substrate flux. Substrate transfer into the biofilm would be multi-dimensional, because the pores probably have substrate concentrations higher than in the biofilm surrounding them (Wanner, 1989). Substrate transport parallel to the substratum would primarily benefit cells in biofilm ridges. The higher substrate concentration in the ridges around the pores would increase cellular growth. Even though the cells are growing relatively quickly at the biofilm surface, they are below their maximum specific growth rate. The Monod equation predicts that their highest specific growth rate is one-fourth of the maximum (0.37 h^{-1}). Each cell has a large capacity for additional growth and substrate utilization, which is demonstrated in the early stages of the nascent biofilm experiments where the bulk liquid substrate concentrations reached steady state values when the biofilm was only 7 to 12 μm thick (Appendix C). The additional growth in the surface layer would utilize more substrate than predicted by a one-dimensional model, decreasing the substrate available to the deeper portion of the biofilm. The reduction in cell growth rates deep in the film would decrease advection in the biofilm depths.

It is worth considering whether the results on bead transport in biofilm could be explained by changes in surface charge of the microbeads. According to the manufacturer of the beads, the negative charge on the beads is stable and the carboxylate groups are not excised from the beads by bacteria. If bacteria did remove the carboxylate groups, the surface charge of the beads would become neutral. Carboxylate groups attached to organic polymers are unlikely to possess a neutral charge above a pH of 5.0 (Hart, 1983). The charge on the beads would never become positive at the pH of the buffered medium (6.8). Also, the structure of polystyrene ($(-C_8H_8-)_n$) is unlikely to accept a proton and obtain a positive charge in this manner. It is most probable, therefore, that the beads maintain their negative surface charge. The worst case is that they would have no charge.

Should the beads lose their negative charge and become neutral, it is doubtful that this would impact retention in the biofilm significantly. The loss of the charges would eliminate ionic bonding of the negatively-charged carboxylate groups to positively charged sites on the EPS, which could hasten bead detachment. Bryers (personal communication), however, found that neutral microbeads attached to biofilm at only slightly lower rates than did negatively-charged microbeads. Therefore, the loss of the bonds should have only a small influence on biofilm-microbead interactions. It would be difficult for bacterial cells to move past the beads without their attached polymers dragging the beads along because the closely-spaced polymers in

biofilm lattices would enmesh the polymers in a "sweep floc" manner. The conclusion that the advective velocity of the beads was low compared to that predicted by conventional theory is valid regardless of the possible loss of the surface charge.

At this time, BIOSIM does not re-attach previously detached beads. Since 10% of the added beads in experiment B-3 attached to biofilm, bead re-attachment may be of the same order of magnitude and therefore significant, especially since some beads may re-attach in pores. Bead re-attachment would explain some of the discrepancy between observed and modelled bead detachment rates if the re-attachment occurred in pores so that the beads went directly into the biofilm depths. Much re-attachment would have to occur in the biofilm depths for simulated bead concentrations to reasonably match experimentally determined bead concentrations (Figure 21).

Simulation of the nascent biofilm experiments again predicted lower bead concentrations than were experimentally measured (Figure 23). The beads were initially close to the biofilm surface because the film was thin. Therefore, the model pushed them out of the film quickly because of the locally equal displacement velocity for all particles. BIOSIM also overpredicted bead detachment in the mixed population biofilm experiment (Appendix I). The rapid expansion of this film (Figure 16) left very few beads near the top of the film where they would detach through erosion.

The BIOSIM simulation pushed many more beads to the rapid detachment zone than occurred in the experiment, where they were distributed throughout the biofilm (Figure 13b). The low volume fraction of solids (0.01, compared to 0.1 for the *P. aeruginosa* biofilms) caused advection of inert particles in the model to be relatively high, because more water became incorporated in the film for each unit mass of solid particles produced.

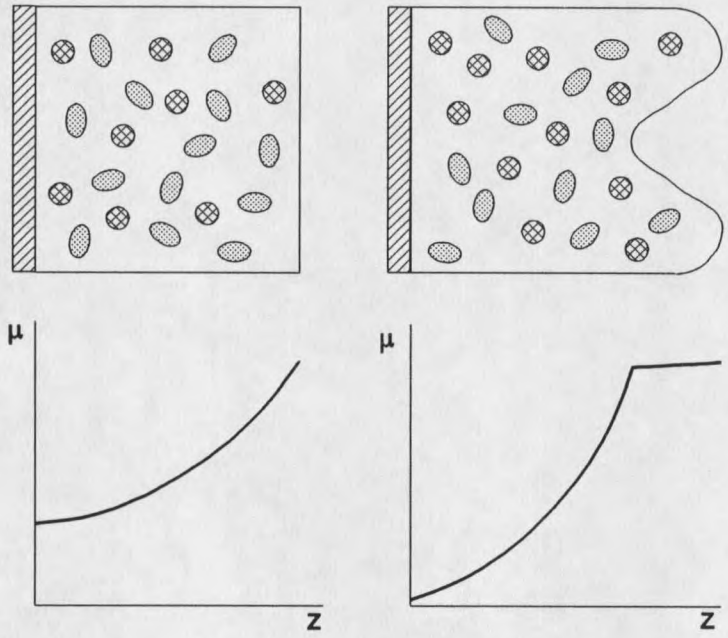

Figure 22. Conceptual cellular growth rate profiles for a smooth (left) and rough (right) biofilm. The profile for a smooth biofilm was proportioned to a BIOSIM growth rate profile. The areas under the two curves are equal.

The population dynamics of a binary population biofilm consisting of *P. aeruginosa* and *K. pneumoniae* was also modelled with BIOSIM (Appendix J). The model predicted concentration of *P. aeruginosa* cells to decrease to

40% of the initial value over the course of the experiment while *K. pneumoniae* increased by 180 times (Figure 24). This was because the higher μ_{max} (2.0 h^{-1}) and lower K_S (1.4 gC m^{-3}) of *K. pneumoniae* gave that microorganism a competitive advantage in growth on the same substrate. Instead, not only did *P. aeruginosa* remain in the biofilm, but grew to a greater concentration than did *K. pneumoniae*. These results are related to the bead dynamics results because they reinforce the importance of the consideration of spatial heterogeneities in modelling particle locations in biofilms. The binary population biofilm consisted of microcolonies of the two species and was not a homogenous mixture (Siebel and Characklis, 1991). Over any point on the substratum, there was likely to be cells of only one species, while BIOSIM, initially, would have cells of both species over the entire substratum because of its one-dimensional nature. Thus, the two species do not compete with each other for substrate, as is assumed by BIOSIM, but for space over the substratum. The slower-growing *P. aeruginosa* "won" the competition over the length of the experiment because its motility enabled it to colonize a larger amount of the substratum (Siebel and Characklis, 1991).

BIOSIM predicted *P. aeruginosa* activity and accumulation well. The model was calibrated to average biofilm thickness (approximately 35 μm) by empirically adjusting the detachment equation. Biofilm cell carbon, EPS carbon, and substrate (glucose) concentrations were simulated well by the

model (Figures 25, 26, and 27). Simulation of substrate utilization was robust with respect to biofilm characteristics (cell concentration, density, D_f/D, etc.) but was sensitive to the mesoscale reactor characteristics such as the thickness of the mass transfer boundary layer (Appendix H) and the hydraulic retention time. Bulk liquid cell (Figure 28) and EPS (Figure 29) concentrations were overpredicted by the model. This discrepancy is probably due to the use of lower yield coefficients in the model than occurred in the experimental biofilms.

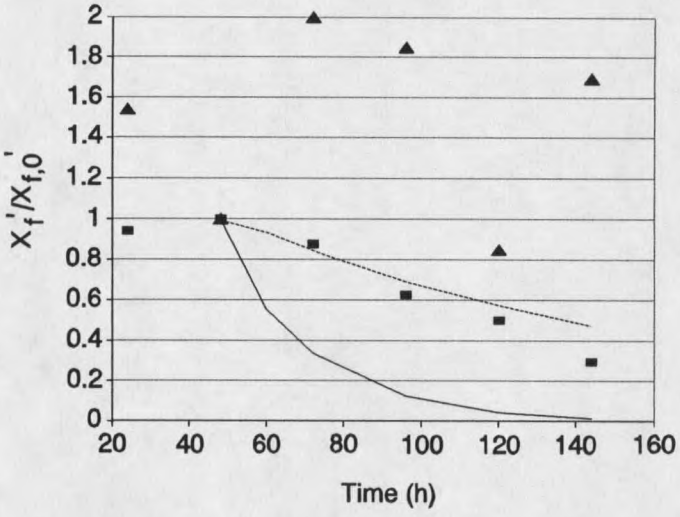

Figure 23. Effect of cell growth rate on the biofilm microbead concentration over time for the *P. aeruginosa* nascent biofilm experiments. Data: A-1 = ■; A-2 = ▲. BIOSIM simulations: (1) normal growth rates (———); (2) 1/20 normal growth rates (---).

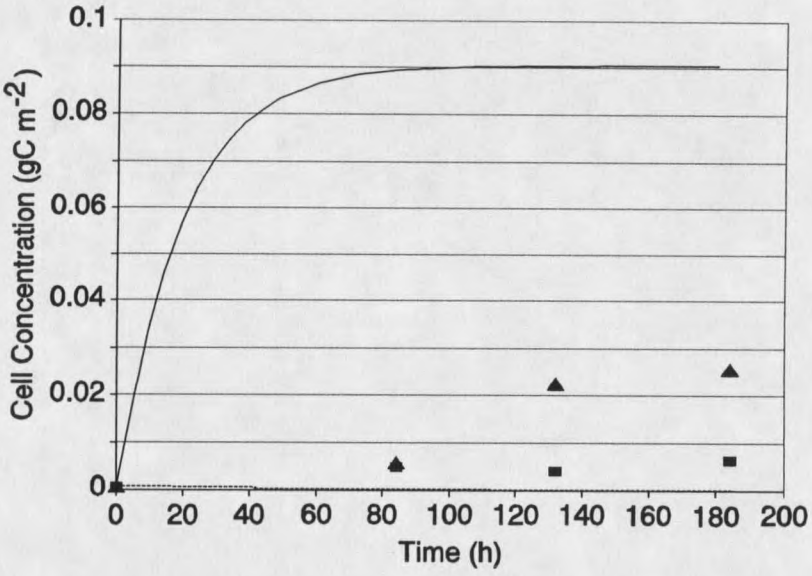

Figure 24. Biofilm cell concentrations over time for the binary population biofilm experiment. Data and BIOSIM simulation: *P. aeruginosa* (▲, ---); *K. pneumoniae* (■, ———).

Adjusting the coefficients to close the discrepancy would have little effect on the bead advective velocities. The model, as utilized, conservatively estimates advection velocities because higher yield coefficients would produce more biomass, higher advection velocities, and, therefore, lower bead concentrations. There is no evidence that the inability of the model to predict concentrations and profiles occurred because of the use of incorrect *P. aeruginosa* kinetic or stoichiometric coefficients, or the use of incorrect biofilm characteristics (ϵ_l, for example).

A monopopulation biofilm would seem to be a good case for simulation with a one-dimensional model, because the model need not

predict particle locations and detachment rates specific to each particulate phase. The simplicity of the experimental system (excluding the beads) permitted accurate predictions of cell concentrations and substrate utilization because these quantities are not sensitive to particle movement to the degree of bead concentrations and profiles.

The undefined mixed population biofilm was simulated with BIOSIM. Areal cell and EPS concentrations were modelled with reasonable accuracy, if the film was considered to be a pseudo-monopopulation biofilm (Appendix I).

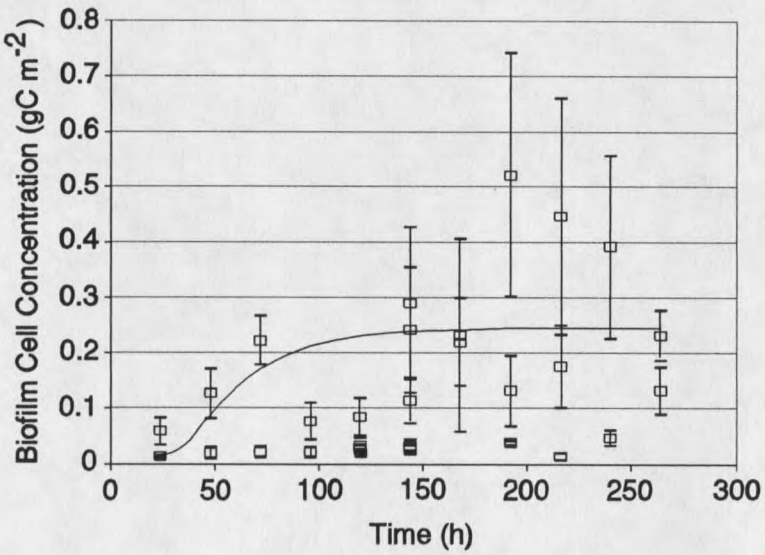

Figure 25. BIOSIM predictions and data for biofilm cell concentrations in the *P. aeruginosa* experiments. Error bars are one standard deviation in the counts of filtered cells.

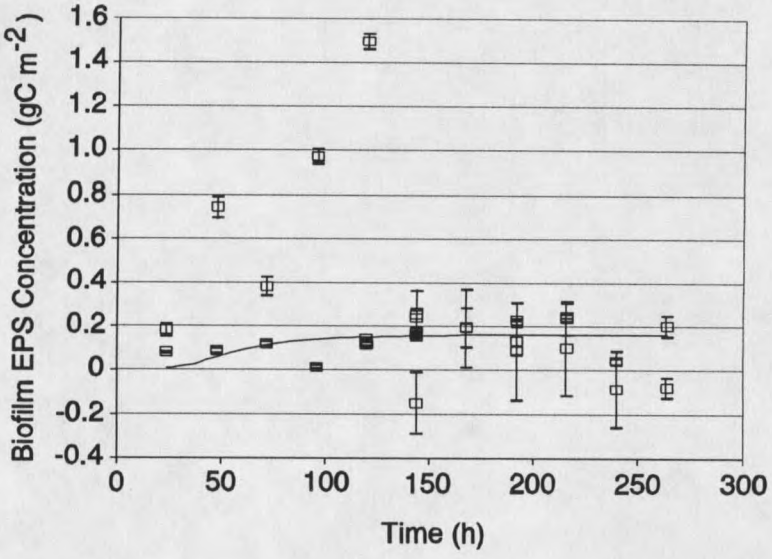

Figure 26. BIOSIM predictions and data for biofilm EPS concentrations in the *P. aeruginosa* experiments. Error bars are one standard deviation.

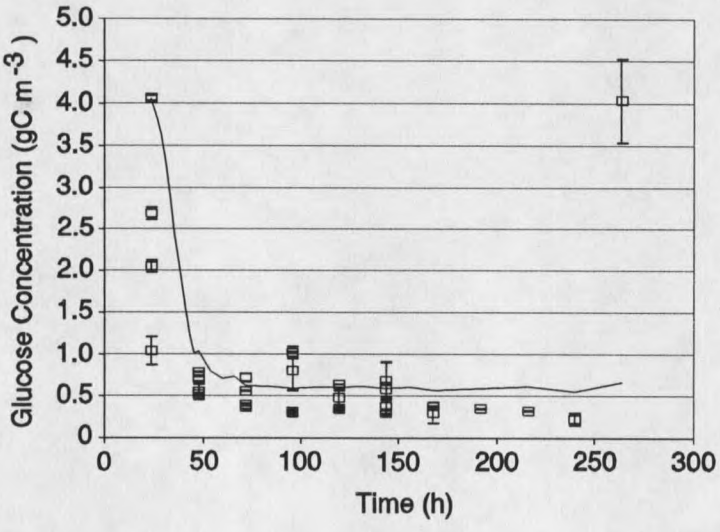

Figure 27. BIOSIM predictions and data for glucose concentrations in the *P. aeruginosa* experiments. Error bars are one standard deviation between the duplicated analyses. The high data point at t = 264 h is due to massive sloughing caused by experimenter error.

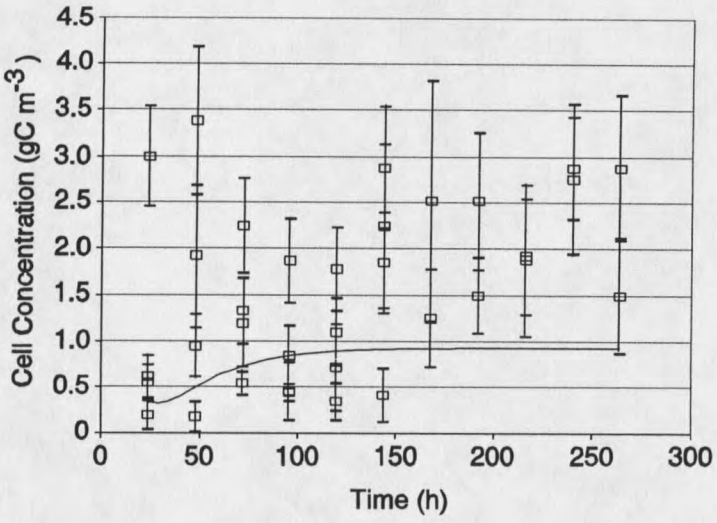

Figure 28. BIOSIM predictions and data for bulk liquid cell concentrations in the *P. aeruginosa* experiments. Error bars are one standard deviation in the counts of filtered cells.

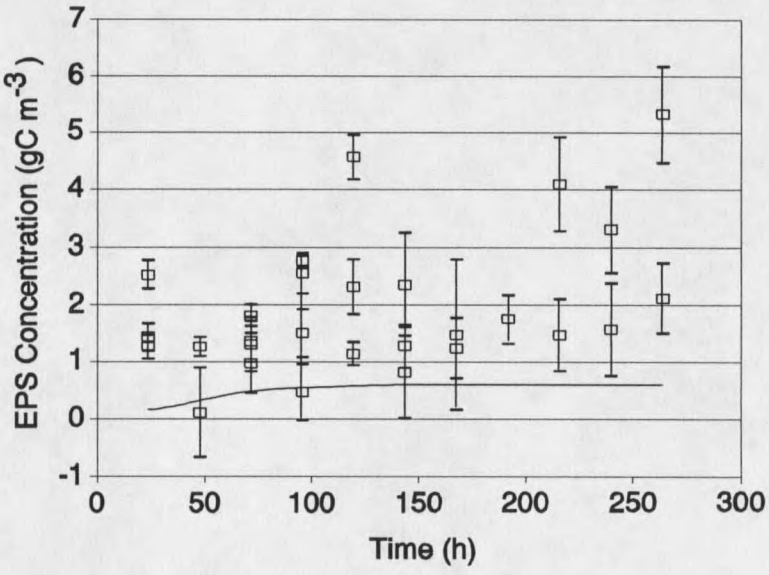

Figure 29. BIOSIM predictions and data for bulk liquid EPS concentrations in the *P. aeruginosa* experiments. Error bars are one standard deviation.

Spatial heterogeities in biofilms play a key role in particle capture and retention. Heterogeneities in thickness (that is, pores or crevices) allow particles to enter the interior of biofilms. When the pores close, the particles become trapped within the biofilm. Surface roughness appears to direct particle advection into the dimensions parallel to the substratum. If so, the particle velocity perpendicular to the substratum would be lower than that predicted by conventional theory which has all advection directed perpendicular to the substratum. The rough biofilm surface may influence the pattern of mass transfer so that cell growth and polymer formation are enhanced in the surface layer, decreasing the advection velocity away from the substratum in the lower portion of the biofilm. Spatial heterogeneity in cell location affects population dynamics because it impacts competition for space among microbes - a competition that is as important as the one for substrate.

To improve the ability of the model to simulate particle capture and retention and population dynamics, additional capabilities should be added. Two-dimensional or three-dimensional modelling would permit consideration of spatial heterogeneities with high dispersivities that would allow particles to enter the interior of biofilm. Multi-dimensional modelling has advantages in mixed population biofilms because surface roughness, microcolonies, filamentous growth, and sloughing can be described (Gujer, 1987; Gujer and Wanner, 1990). Substrate diffusion into pores and then laterally into the

biofilm may cause the high cellular growth rates in ridges as envisioned in Figure 22. Particle (bead) re-attachment should be included. Ability to direct some attaching particles into the biofilm interior would simulate the transport mechanism that works in the opposite direction of advection. To do this accurately, pore distribution over the plane parallel to the substratum, pore size (depth and width), and the time distribution over which pores are open would have to be known. Little data exists that quantify pore size and lifetimes, and would have to be collected. Also, consideration should be given to biofilm rheology and the potential energy available for deformation of the biofilm matrix (Gujer and Wanner, 1990). Little information has been gathered on this subject as well.

CONCLUSIONS

1. Fluorescent latex microbeads attached to biofilm and were easily identified and enumerated separately from bacteria.
2. Biofilms are sufficiently porous for bacterial-sized particles to become entrapped in them.
3. The retention time of microbeads in biofilm was much longer than the retention time of suspended particles in the biofilm reactor.
4. Microbead capture by biofilm was proportional to the biofilm cell carbon concentration and to the standard deviation in biofilm thickness measurements.
5. Microbeads formed aggregates on biofilms, but not in the associated bulk water.
6. The difference between the bead release rates for the nascent and mature biofilm experiments reveals that detachment is weighted toward the biofilm surface in *P. aeruginosa* biofilms.
7. Areal cell, EPS, and bulk liquid substrate concentrations for *P. aeruginosa* and mixed population (as a pseudo-monopopulation film) biofilms were modelled accurately as long as biofilm thickness and the volume fraction of water were determined experimentally and were included in the model.

8. Predictions made by a one-dimensional model of locations and detachment rates for specific particulate species were poor.

RECOMMENDATIONS FOR FUTURE RESEARCH

1. Examine biofilm grown in a flow cell with the SCLM. The flow cell is to permit observation of the same areas over time. Measure pore diameter, depth, and lifespan. Use fluorescently labelled latex microbeads to determine the direction and velocity of particle transport once the beads become buried in the biofilm. Try to determine if pores are filled in by bacterial growth adjacent to the pore, or if they are filled in by re-attachment of cells detached from elsewhere on the biofilm.
2. Add bacteria of one species to a monopopulation biofilm of a second species. Apply fluorescent antibodies for the invasive species, and observe the biofilm with the SCLM to determine the depth of penetration over time of the invading species.
3. Use a two- or three-dimensional computer model to simulate particle capture by and transport in biofilm.

NOMENCLATURE

NOMENCLATURE

A	area (L^2)
a	centripetal acceleration ($L\ t^{-2}$)
C	solute concentration ($M\ L^{-3}$)
C_D	drag coefficient (dimensionless)
D	diffusion coefficient in bulk water ($L^2\ t^{-1}$)
D_f	diffusion coefficient for solute in water fraction of biofilm ($L^2\ t^{-1}$)
d	diameter (L)
f	friction factor (dimensionless)
g	acceleration due to gravity ($L\ t^{-2}$)
H	height of inner cylinder (L)
h	one-half of annular gap distance (L)
J	flux ($M\ L^{-2}\ t^{-1}$)
K_S	half-saturation coefficient for bacterial growth ($M\ L^{-3}$)
k	bead release rate coefficient (t^{-1})
k_p	growth associated polymer formation coefficient ($M_P\ M_X^{-1}$)
k_p'	non-growth associated polymer formation coefficient ($M_P\ M_X^{-1}\ t^{-1}$)
L	length of bacterial cell (L)
L_f	biofilm thickness (L)
L_L	mass transfer boundary layer thickness (L)

P atmospheric pressure ($M\ L^{-1}\ t^{-2}$)

Q liquid flow rate ($L^3\ t^{-1}$)

R radius of curvature at ends of a bacterial cell (L)

Re Reynolds number (dimensionless)

r reaction rate (t^{-1})

r_i radius of inner cylinder (L)

Sc Schmidt number (dimensionless)

s distance from a bead to the biofilm-bulk water interface

T temperature (T)

t time (t)

U average bulk liquid velocity ($L\ t^{-1}$)

V volume (L^3)

V_* characteristic velocity ($L\ t^{-1}$)

v velocity ($L\ t^{-1}$)

v_m velocity of bulk fluid normal to wall due to fluid motion ($L\ t^{-1}$)

X particle concentration ($M\ L^{-3}$)

X' areal particle concentration ($M\ L^{-2}$)

$Y_{X/S}$ yield of cell carbon per substrate carbon utilized ($M_X\ M_S^{-1}$)

$Y_{P/S}$ yield of EPS carbon per substrate carbon utilized ($M_P\ M_S^{-1}$)

z dimension perpendicular to the substratum (L)

Greek letters

ϵ_l volume fraction of liquid to total biofilm volume (dimensionless)

ϵ_s volume fraction of solid phase to total biofilm volume (dimensionless)

η absolute viscosity (M L^{-1} t^{-1})

κ von Karman constant = 0.4 (dimensionless)

μ specific growth rate of bacteria (t^{-1})

μ_{max} maximum specific growth rate of bacteria (t^{-1})

ν kinematic viscosity (L^2 t^{-1})

ρ density (M L^{-3})

τ_o shear stress at reactor wall (M L^{-1} t^{-2})

ω angular velocity (radians t^{-1})

subscripts

c as carbon

eff in effluent

f in biofilm

l liquid

o for time = 0

P polymer

S substrate

s solid particulate

T total

w water

X cells

superscript

(t) in turbulent flow

\+ dimensionless variable

^ predicted value, using regression coefficients

REFERENCES

REFERENCES

Alleman, J. E., Veil, J. A. and Canaday, J. T. 1982. Scanning electron microscope evaluation of rotating biological contactor biofilm. Water Res. **16,** 543-550.

Atlas, R. M. and Bartha, R. 1981. Microbial Ecology: Fundamentals and Applications. Addison-Wesley, Reading, MA.

Bakke, R. 1986. Biofilm Detachment. Unpublished doctoral thesis, Montana State University, Bozeman, MT.

Bakke, R. and Ollsen, P. Q. 1986. Biofilm thickness measurements by light microscopy. J. Microb. Meth. **5,** 1-6.

Bakke, R., Trulear, M. G., Robertson, J. H. and Characklis, W. G. 1984. Activity of *Pseudomonas aeruginosa* biofilms: steady state. Biotechnol. Bioeng. **26,** 1409-1417.

Banks, M. K. and Bryers, J. D. 1992. Deposition of suspended bacterial cells onto glass and biofilm surfaces. Biofouling, in press.

Beal, S. K. 1970. Deposition of particles in turbulent flow on channel or pipe walls. Nuclear Science and Engineering. **40,** 1-11.

Beeftink, H. H. and Staugaard, P. 1986. Structure and dynamics of anaerobic bacterial aggregates in a gas lift reactor. Appl. Environ. Microbiol. **52,** 1139-1146.

Bird, R. B., Stewart, W. E., and Lightfoot, E. N. 1960. Transport Phenomena. Wiley, New York.

Bochem, H. P., Schoberth, S. M., Sprey, B. and Wengler, P. 1982. Thermophilic biomethanation of acetic acid: morphology and ultrastructure of a granular consortium. Can. J. Microbiol. **28,** 500-510.

Bouwer, E. J. 1987. Theoretical investigation of particle deposition in biofilm systems. Water Res. **21,** 1489-1498.

Bryers, J. D. Personal communication. Center for Biochemical Engineering, Duke University, Durham, NC.

Bryers, J. D. and Banks, M.K. 1990. Assessment of biofilm ecodynamics. In: Physiology of immobilized cells. Proceedings of an International Symposium held at Wageningen, The Netherlands, 10-13 December 1989. Ed. J.A.M. de Bont, J. Visser, B. Mattiasson, and J. Tramper. Elsevier Science Publishers B.V., Amsterdam, 49-61.

Bryers, J. D. and Characklis, W. G. 1982. Processes governing primary biofilm formation. Biotechnol. Bioeng. **24**, 2451-2476.

Characklis, W.G. 1990a. Energetics and Stoichiometry. In: Biofilms. Ed. W.G. Characklis and K.C. Marshall. John Wiley and Sons, New York, 161-192.

Characklis, W.G. 1990b. Kinetics of microbial transformations. In: Biofilms. Ed. W.G. Characklis and K.C. Marshall. John Wiley and Sons, New York, 233-264.

Characklis, W.G. and Marshall, K.C. 1990. Biofilms: a basis for an interdisciplinary approach. In: Biofilms. Ed. W.G. Characklis and K.C. Marshall. John Wiley and Sons, New York, 3-15.

Eighmy, T. T., Maratea, D. and Bishop, P. L. 1983. Electron microscopic examination of wastewater biofilm formation and structural components. Appl. Environ. Microbiol. **45**, 1921-1931.

Evans, L.R., and Linker, A. 1973. Production and characterization of the slime polysaccharide of *Pseudomonas aeruginosa*. J. Bacteriol. **116**, 915-924.

Fahien, R. W. 1983. Fundamentals of Transport Phenomena. McGraw-Hill, New York.

Fruhen, M., Christan, E., Gujer, W., and Wanner, O. 1990. Significance of spatial distribution of microbial species in mixed culture biofilms. Proceedings of IAWPC biannual meeting, Tokyo, Japan.

Grotenhuis, J.T.C., Smit, M., Plugge, C.M., Yuansheng, X., van Lammeren, A.A.M., Stams, A.J.M., and Zehnder, A.J.B. 1991. Bacteriological composition and structure of granular sludge adapted to different substrates. Appl. Environ. Microbiol. **57**, 1942-1949.

Gujer, W. 1987. The significance of segregation of biomass in biofilms. Wat. Sci. Tech. **19**, 495-503.

Gujer, W. and Boller, M. 1990. A mathematical model for rotating biological contactors. Wat. Sci. Tech. **22**, 53-73.

Gujer, W. and Wanner, O. 1990. Modelling mixed population biofilms. In: Biofilms. ed. W. G. Characklis and K. C. Marshall. John Wiley & Sons, New York, 397-444.

Gunawan, C. 1991. Rates of Cellular Attachment to an Established Biofilm. Unpublished Master of Science thesis, Montana State University, Bozeman, MT.

Hart, H. 1983. Organic Chemistry - A Short Course. Houghton_Mifflin, Boston.

Harvey, M., Forsberg, C. W., Beveridge, T. J., Pos, J., and Ogilvie, J. R. 1984. Methanogenic activity and structural characteristics of the microbial biofilm on a needle-punched polyester support. Appl. Environ. Microbiol. **48**, 633-638.

Hobbie, J. E., Dalen, R. J. and Jasper, S. 1977. Use of nucleopore filters for counting bacteria by fluorescence microscopy. Appl. Environ. Microbiol. **35**, 858-862.

Jain, A. K. and Dubes, R. C. 1988. Algorithms for Clustering Data. Prentice-Hall, Englewood Cliffs, NJ.

Jones, H.C., Roth, I.L. and Sanders, W.M. 1969. Electron microscopic study of a slime layer. J. Bacteriol. **99**, 316-325.

Karel, S. F. and Robertson, C. R. 1989. Autoradiographic determination of mass-transfer limitations in immobilized cell reactors. Biotechnol. Bioeng. **34**, 320-336.

Kissel, J.C., McCarty, P.L. and Street, R.L. 1984. Numerical simulation of mixed-culture biofilm. J. Env. Eng. **110**, 393-411.

Levine, A. D., Tchobanoglous, G. and Asano, T. 1985. Characterization of the size distribution of contaminants in wastewater: treatment and reuse implications. J. Wat. Pollut. Control Fed. **57**, 805-816.

Lewandowski, Z., Walser, G. and Characklis, W.G. 1991. Reaction kinetics in biofilms. Biotechnol. Bioeng. **38**, 877-882.

Lewis, D. L. (1991) Letters to the editor. ASM News. **57**, 342.

Lewis, D. L. and Gattie, D. K. 1991. The ecology of quiescent microbes. ASM News. **57**, 27-32.

Mack, W. N., Mack, J. P. and Ackerson, A. O. 1975. Microbial film development in a trickling filter. Microb. Ecol. **2**, 215-226.

MacLeod, F. A., Guiot, S. R. and Costerton, J. W. 1990. Layered structure of bacterial aggregates produced in an upflow anaerobic sludge bed and filter reactor. Appl. Environ. Microbiol. **56**, 1598-1607.

Palleroni, N. J. 1984. Genus I. Pseudomonas. In: Bergey's Manual of Systematic Bacteriology, Volume 1. Ed. N. R. Krieg. Williams & Wilkins, Baltimore, MD, 141-174.

Reichert, P., Ruchti, J. and Wanner, O. 1989. BIOSIM - Interactive Program for the Simulation of the Dynamics of Mixed Culture Biofilm Systems on a Personal Computer. Swiss Federal Institute for Water Resources and Water Pollution Control, Swiss Federal Institutes of Technology, CH-8600, Dubendorf, Switzerland.

Revsbech, N. P., Christensen, P. B. and Nielsen, L. P. 1989. Microelectrode analysis of photosynthetic and respiratory processes in microbial mats. In: Microbial Mats - Physiological Ecology of Benthic Communities. Ed. Y. Cohen and E. Roseberg. American Society for Microbiology, Washington, D. C, 153-162.

Rittman, B. R. and Wirtel, S. A. 1991. Effect of biofilm accumulation on colloid cohesion. J. Env. Eng. **117**, 692-695.

Robinson, J.A., Trulear, M.G. and Characklis, W.G. 1984a. Cellular reproduction and extracellular polymer formation by *Pseudomonas aeruginosa* in continuous culture. Biotechnol. Bioeng. **26**, 1409-1417.

Robinson, R. W., Akin, D. E., Nordstedt, R. A., Thomas, M. V. and Aldrich, H. C. 1984b. Light and electron microscopic examinations of methane-producing biofilms from anaerobic fixed-bed reactors. Appl. Environ. Microbiol. **48**, 127-136.

Santos, R., Callow, M. E. and Bott, T. R. 1991. The structure of *Pseudomonas fluorescens* biofilms in contact with flowing systems. Biofouling. **4**, 319-336.

Siebel, M.A. 1987. Binary Population Biofilms. Unpublished doctoral thesis, Montana State University, Bozeman, MT.

Siebel, M. A. and Characklis, W. G. 1991. Observations of binary population biofilms. Biotechnol. Bioeng. **37**, 778-789.

Siegrist, H. and Gujer, W. 1985. Mass transfer mechanisms in a heterotrophic biofilm. Water Res. **19**, 1369-1378.

Siegrist, H. and Gujer, W. 1987. Demonstration of mass transfer and pH effects in a nitrifying biofilm. Water Res. **21**, 1481-1487.

Sprouse, G. and Rittman, B. E. 1990. Colloidal removal in fluidized-bed biofilm reactor. J. Env. Eng. **116**, 314-329.

Starkey, R. L. 1985. Anaerobic corrosion - perspectives about causes. In: Biologically Induced Corrosion, Proceedings of the International Conference on Biologically Induced Corrosion. Ed. S. C. Dexter. National Association of Corrosion Engineers, Houston, Texas, 3-7.

Stewart, P. S., Karel, S. F. and Robertson, C. R. 1991. Characterization of immobilized cell growth rates using autoradiography. Biotechnol. Bioeng. **37**, 824-833.

Switzenbaum, M. S. and Eimstad, R. B. 1987. Analysis of anaerobic biofilms. Environ. Technol. Lett. **8**, 21-32.

Tiller, A. K. 1985. A review of the European research effort on microbial corrosion between 1950 and 1984. In: Biologically Induced Corrosion, Proceedings of the International Conference on Biologically Induced Corrosion. Ed. S. C. Dexter. National Association of Corrosion Engineers, Houston, Texas, 8-29.

Trulear, M. G. 1980. Dynamics of Biofilm Processes in an Annular Reactor. Unpublished Master of Science thesis, Rice University, Houston, Texas.

Trulear, M. G. and Characklis, W. G. 1982. Dynamics of biofilm processes. Journal Wat. Pollut. Cont. Fed. **54**, 1288-1310.

Turakhia, M.H. and Characklis, W.G. 1989. Activity of *Pseudomonas aeruginosa* in biofilms: effect of calcium. Biotechnol. Bioeng. **33**, 406-414.

van der Wende, E. 1991. Biocide Action of Chlorine on *Pseudomonas aeruginosa* Biofilm. Unpublished doctoral thesis, Montana State University, Bozeman, MT.

Visser, F.A., van Lier, J.B., Macario, A.J.L. and de Macario, E.C. 1991. Diversity and population dynamics of methanogenic bacteria in a granular consortium. Appl. Environ. Microbiol. **57**, 1728-1734.

Wang, A. K. and Gerhar, L. W. 1974. Turbulent couette flow. Trans. ASME, Journal of Fluids Engineering. **96**, 265-271.

Wanner, O. 1989. Modelling population dynamics. In: Structure and Function of Biofilms. Ed. W. G. Characklis and P. A. Wilderer. John Wiley & Sons, New York, 91-110.

Westrin, B. A. and Axelsson, A. 1991. Diffusion in gels containing immobilized cells: a critical review. Biotechnol. Bioeng. **38**, 439-446.

APPENDICES

APPENDIX A: ROTOTORQUE DIMENSIONS

Table 6. RotoTorque dimensions.

Inner cylinder:	
- wetted height	177 mm
- diameter	101 mm
- wetted surface area (vertical)	56200 mm^2
- wetted surface area (horizontal)	16000 mm^2
- total cylinder wetted surface area	72200 mm^2
Draft tubes:	
- number	4
- diameter	10 mm
- length	180 mm
- angle of inclination	80°
- surface area	23100 mm^2
Outer cylinder:	
- wetted height	188 mm
- diameter	117 mm
- wetted surface area (vertical)	69100 mm^2
- wetted surface area (horizontal)	21500 mm^2
- total outer cylinder wetted surface area	90600 mm^2
Slides:	
- number of slides	12
- thickness	0.5 mm
- width	17 mm
- wetted length	192 mm (maximum)
- wetted slide surface area (maximum)	3264 mm^2
Reactor:	
- total wetted surface area including slides and tubes	0.186 m^2
- slide surface area as fraction of whole reactor (excluding tubes)	0.25
- slide surface area as fraction of whole reactor (including tubes)	0.21
- liquid volume at 200 rpm*	0.575 x 10^{-3} m^3
- surface/volume ratio (excluding tubes)	0.28 mm^{-1}
- surface/volume ratio (including tubes)	0.32 mm^{-1}
- width of annular gap	8.0 mm
- hydraulic residence time at a flow rate of 38 ml min^{-1} and at 200 rpm	15 min

* liquid volume measured by pumping a measured volume of water into reactor with the inner cylinder turning at 200 rpm

APPENDIX B: CONCENTRATION OF DISSOLVED OXYGEN IN EQUILIBRIUM WITH AIR

APPENDIX B: CONCENTRATION OF DISSOLVED OXYGEN IN EQUILIBRIUM WITH AIR

The following is a calculation of the saturated dissolved concentration for dissolved oxygen in water in Bozeman at MSU.

The ground elevation in front of Roberts Hall is just under 4900 ft. above sea level. The fourth floor of Cobleigh Hall is somewhat over 4900 ft. We will use 5000 ft. for the calculation.

At 25°C, the saturated concentration of dissolved oxygen in water (C_{sat}) at sea level is 8.38 mg L^{-1} (from Standard Methods).

The decrease in atmospheric pressure with increasing altitude is described by:

$$dP = -\frac{M_a * g}{R * T} P dz \qquad (11)$$

Where: P = pressure (N m^{-2})

M_a = molecular weight of air = 28.97 kg $kmole^{-1}$

g = acceleration due to gravity = 9.81 m sec^{-2}

R = universal gas constant = 8.314 J $°K^{-1}$ $mole^{-1}$

T = temperature = 25°C = 298°K

z = altitude above sea level = 5000 ft = 1524 m

Separating variables and integrating from sea level (z = 0, P = P_o) to z = 1524 m produces:

$$\ln\frac{P}{P_o} = -\frac{M_a * g * z}{R * T} \qquad (12)$$

where: P_o = pressure at sea level

Or:

$$\frac{P}{P_o} = \exp\frac{-M_a * g * z}{R * T} \qquad (13)$$

Computing P/P_o gives:

$P/P_o = 0.840$

Dalton's Law of partial pressure states that the partial pressure of oxygen changes by 0.84 as well, if the volume fraction of oxygen in air does not change. Actually, it does change, because lighter gases become enriched at higher altitudes. In the range of altitude under consideration, the assumption that the volume of oxygen to total air not changing between 0 and 1524 m is not bad.

Therefore, C_{sat} for oxygen is 0.84 * 8.38 = 7.04 mg L^{-1}.

APPENDIX C: RAW DATA

Table 7. Experiment A-1 biofilm data.

Time (h)	Beads (# m^{-2})	Beads (gSS m^{-2})	Beads Std.Dev.	Cells (# m^{-2})	Cells (gC/cell)	Cells (gC m^{-2})
24	1.5E+10	0.00601	0.00259	2.9E+11	4.7E-14	0.0136
48	1.6E+10	0.00641	0.00344	4.2E+11	4.7E-14	0.0197
72	1.4E+10	0.00561	0.00269	4.6E+11	4.7E-14	0.0216
96	9.9E+09	0.00397	0.00299	4E+11	5.3E-14	0.0212
120	8.1E+09	0.00325	0.00139	4.8E+11	6.9E-14	0.0331
144	4.7E+09	0.00188	0.00057	6.5E+11	4.8E-14	0.0312

Time (h)	Cells Std.Dev.	TOC (mg/L)	TOC (mg/L)	Buffer Adjusted avg. TOC (mg/L)	TOC (gC m^{-2})	TOC std.dev.
24	0.00269	5.916	4.85	4.79	0.0909	0.00162
			5.795	4.729		
48	0.0108	7.245	6.179	6.062	0.106	0.00288
			7.011	5.945		
72	0.00966	8.771	7.705	7.603	0.140	0.00265
			8.567	7.501		
96	0.00933	2.866	1.8	1.693	0.0346	0.00104
			2.652	1.586		
120	0.0138	8.64	7.574	7.55	0.147	0.00136
			8.591	7.525		
144	0.0135	11.76	10.694	10.58	0.191	0.00294
			11.53	10.464		

Time (h)	EPS (gC m^{-2})	EPS std.dev.	L_f (μm)	L_f std.dev.
24	0.0773	0.00314	2	0.7
48	0.0859	0.0112	7.5	2
72	0.118	0.0100	14	3.4
96	0.0134	0.00939	25	1.3
120	0.114	0.0139	26	3.3
144	0.160	0.0138	29	4

Table 8. Experiment A-1 effluent data.

Time (h)	Beads (#/mL)	Beads (gSS m^{-3})	Beads std.dev.	Cells (#/mL)	Cells (gC/cell)	Cells (gC m^{-3})
24	78000	0.0313	0.0265	3900000	5E-14	0.195
48	2000	0.000802	0.00131	3500000	5E-14	0.175
72	10400	0.00417	0.00367	6900000	7.8E-14	0.538
96	61600	0.0247	0.0237	6500000	7E-14	0.455
120	51500	0.0206	0.0172	6800000	5E-14	0.34
144	27700	0.0111	0.00736	6900000	6E-14	0.414

Time (h)	Cells std.dev.	TOC (gC m^{-3})	avgTOC (gC m^{-3})	TOC std.dev.	Glucose (gC m^{-3})	avgGluc (gC m^{-3})	Glucose std.dev.
24	0.163	3.726	3.769	0.061	1.16	1.04	0.17
		3.812			0.92		
48	0.162	2.163	2.145	0.025	0.68	0.7	0.03
		2.127			0.72		
72	0.126	3.02	2.916	0.146	0.56	0.56	0
		2.813			0.56		
96	0.32	2.866	2.759	0.151	0.96	0.8	0.23
		2.652			0.64		
120	0.202	2.124	2.122	0.003	0.64	0.64	0
		2.12			0.64		
144	0.294	2.423	2.379	0.062	0.84	0.68	0.23
		2.335			0.52		

Time (h)	EPS (gC m^{-3})	EPS std.dev.
24	2.534	0.243
48	1.27	0.167
72	1.818	0.193
96	1.504	0.422
120	1.142	0.202
144	1.285	0.378

Influent glucose sample was lost.

Table 9. Experiment A-2 biofilm data.

Time (h)	Beads (# m^{-2})	Beads (gSS m^{-2})	Beads Std.Dev.	Cells (# m^{-2})	Cells (gC/cell)	Cells (gC m^{-2})
24	1E+10	0.004008	0.00216	5.6E+11	1.06E-13	0.0594
48	6.5E+09	0.002605	0.00132	1.3E+12	9.8E-14	0.1274
72	1.3E+10	0.00521	0.00611	2.1E+12	1.06E-13	0.2226
96	1.2E+10	0.004809	0.00527	6.2E+11	1.24E-13	0.0769
120	5.6E+09	0.002244	0.00198	8.3E+11	1.02E-13	0.0847
144	1.1E+10	0.004409	0.00309	1E+12	1.15E-13	0.115

Time (h)	Cells Std.Dev.	TOC (mg/L)	Buffer Adjusted TOC (mg/L)	aveTOC (mg/L)	TOC (gC m^{-2})	TOC std.dev.	EPS (gC m^{-2})
24	0.0248	8.805	7.739	7.714	0.239	0.0011	0.179
		8.756	7.69				
48	0.04516	29.43	28.364	28.184	0.873	0.0079	0.745
		29.07	28.004				
72	0.04398	20.48	19.414	19.524	0.604	0.0048	0.382
		20.7	19.634				
96	0.033	33.16	32.094	31.884	1.048	0.0098	0.971
		32.74	31.674				
120	0.03383	48.81	47.744	47.554	1.580	0.0089	1.496
		48.43	47.364				
144	0.04138	12.02	10.954	10.699	0.352	0.0119	0.237
		11.51	10.444				

Time (h)	EPS std.dev.	L_f (μm)	L_f std.dev.
24	0.025	2.2	1.5
48	0.046	12	1.3
72	0.044	12	1.4
96	0.034	22	5.5
120	0.035	16	4.1
144	0.043	19	1.9

Table 10. Experiment A-2 effluent data.

Time (h)	Beads (#/ml)	Beads (gSS m^{-3})	Beads std.dev.	Cells (#/mL)	Cells (gC/cell)	Cells (gC m^{-3})
24	2600000	1.042	0.669	6700000	9.16E-14	0.614
48	120000	0.048	0.019	9700000	9.8E-14	0.951
72	11000	0.0044	0.015	12000000	1E-13	1.2
96	17000	0.0068	0.0154	7400000	1.15E-13	0.851
120	38000	0.0152	0.0268	11000000	1E-13	1.1
144	48000	0.0192	0.0316	19000000	9.72E-14	1.85

Time (h)	Cells (gC m^{-3})	Cells std.dev.	TOC (gC m^{-3})	aveTOC (gC m^{-3})	TOC std.dev.	Glucose (gC m^{-3})
24	0.614	0.232	4.107	4.104	0.0042	2.00
			4.101			2.10
48	0.951	0.341	9.467	9.504	0.0523	0.781
			9.541			0.781
72	1.2	0.474	3.224	3.234	0.0134	0.756
			3.243			0.683
96	0.851	0.321	4.556	4.434	0.12	1.048
			4.316			1.00
			4.43			
120	1.1	0.364	6.086	6.159	0.103	0.537
			6.232			0.416
144	1.85	0.547	18.41	18.52	0.1556	0.634
			18.63			0.513

Time (h)	avgGluc (gC m^{-3})	Glucose std. dev.	EPS (gC m^{-3})	EPS std.dev.
24	2.05	0.0687	1.44	0.24
48	0.781	0	7.77	0.35
72	0.720	0.0518	1.31	0.48
96	1.02	0.067	2.56	0.35
120	0.476	0.086	4.58	0.39
144	0.574	0.086	16.1	0.58

Influent glucose sample was 5.39 gC/m^{-3}.

Table 11. Experiment B-1 biofilm data.

Time (h)	Beads (# m^{-2})	Beads (gSS m^{-2})	Beads std.dev.	Cells (# m^{-2})	Cells (gC/cell)	Cells (gC m^{-2})
144	1.2E+10	0.00481	0.00989	2.5E+12	1.16E-13	0.290
168	8.7E+09	0.00349	0.00537	2E+12	1.16E-13	0.232
192	3.9E+09	0.00156	0.00378	4.9E+12	1.07E-13	0.522
216	1.5E+09	0.000601	0.00074	4.2E+12	1.07E-13	0.447
240	1.7E+09	0.000681	0.00108	4E+12	9.8E-14	0.392
264	1.1E+09	0.000441	0.00041	2.5E+12	9.3E-14	0.232

Time (h)	Cells std.dev.	TOC (mg/L)	Buffer Adjusted TOC (mg/L)	avgTOC (mg/L)	TOC (gC m^{-2})	TOC std.dev.
144	0.137	6.267	5.201	4.554	0.141	0.0283
		4.973	3.907			
168	0.174	15.73	14.66	13.69	0.424	0.0427
		13.78	12.71			
192	0.220	21.67	20.60	19.63	0.608	0.0273
		20.48	19.41			
		19.95	18.88			
216	0.214	19.52	18.45	17.67	0.545	0.0218
		18.52	17.45			
		18.16	17.09			
240	0.166	11.84	10.77	9.879	0.306	0.0392
		10.05	8.984			
264	0.0446	5.916	4.85	4.936	0.153	0.0038
		6.088	5.02			

Time (h)	EPS (gC m^{-2})	EPS std.dev.	L_f (um)	L_f std.dev.
144	-0.149	0.140	30	11
168	0.192	0.179	27	-
192	0.0886	0.222	33	-
216	0.0997	0.215	-	-
240	-0.0862	0.171	39	7.3
264	-0.0797	0.0448	38	10

Table 12. Experiment B-1 effluent data.

Time (h)	Beads (#/ml)	Beads (gSS m^{-3})	Beads Std.Dev.	Cells (#/ml)	Cells (gC/cell)	Cells (gC m^{-3})
24				11000000	5E-14	0.55
48				32000000	6E-14	1.92
72				19000000	7E-14	1.33
96				22000000	8.5E-14	1.87
120				21000000	8.5E-14	1.78
144	960000	0.385	0.331	24000000	1.2E-13	2.88
168	94000	0.0377	0.0617	21000000	1.2E-13	2.52
192	89000	0.0357	0.0356	21000000	1.2E-13	2.52
216	7600	0.00305	0.00733	16000000	1.2E-13	1.92
240	6000	0.00240	0.00862	23000000	1.2E-13	2.76
264	4000	0.00160	0.00194	24000000	1.2E-13	2.88

Time (h)	Cells std.dev.	TOC (gC m^{-3})	avgTOC (gC m^{-3})	TOC Std.Dev.	Glucose (gC m^{-3})	avgGluc. (gC m^{-3})
24	0.199	4.51	4.51	0.001	2.74	2.69
		4.509			2.64	
48	0.770	2.543	2.59	0.069	0.614	0.550
		2.641			0.487	
72	0.353	3.095	3.07	0.032	0.386	0.386
		3.05			0.386	
96	0.454	2.752	2.64	0.16	0.31	0.297
		2.526			0.284	
120	0.453	1.848	1.895	0.066	0.31	0.335
		1.942			0.360	
144	0.658	4.379	4.08	0.428	0.436	0.373
		3.774			0.31	
168	1.30	4.251	4.30	0.062	0.386	0.297
		4.339			0.208	
192	0.745	21.22	21.0	0.332	0.436	
		20.75				
216	0.629	3.393	3.40	0.013	0.284	
		3.412				
240	0.815	4.348	4.34	0.013	0.360	
		4.329				
264	0.787	8.423	8.208	0.304	0.360	
		7.993				

Table 12 (continued). Experiment B-1 effluent data.

Time (h)	Glucose std.dev.	EPS (gC m^{-3})	EPS Std.Dev.
24	0.0716	1.27	0.211
48	0.0897	0.122	0.778
72	0	1.36	0.354
96	0.0181	0.472	0.482
120	0.0356	-0.225	0.459
144	0.0894	0.823	0.790
168	0.125	1.48	1.31
192		18.5	0.816
216		1.48	0.629
240		1.58	0.815
264		5.33	0.844

Influent glucose = 4.92 gC m^{-3} from t = 0 to t = 145.9 h.

Influent glucose = 4.88 gC m^{-3} after t = 145.9 h.

Table 13. Experiment B-2 biofilm data.

Time (h)	Beads (# m^{-2})	Beads (gSS m^{-2})	Beads std.dev.	Cells (# m^{-2})	Cells (gC/cell)	Cells (gC m^{-2})
144	8.4E+09	0.003367	0.004010	2.2E+12	1.1E-13	0.242
168	4.3E+09	0.001723	0.002830	2E+12	1.1E-13	0.220
192	2E+09	0.000802	0.002070	1.2E+12	1.1E-13	0.132
216	1.3E+09	0.000521	0.000882	1.6E+12	1.1E-13	0.176
240	4.1E+08	0.000164	0.000251	4.3E+11	1.1E-13	0.047
264	2.2E+08	0.000088	0.000076	1.2E+12	1.1E-13	0.132

Time (h)	Cells std.dev.	TOC (mg/L)	Buffer Adjusted TOC (mg/L)	avgTOC (mg/L)	TOC (gC m^{-2})	TOC std.dev.
144	0.114	15.80	14.73	14.73	0.492	-
168	0.080	12.20	11.13	12.53	0.414	0.040
		14.20	13.13			
		14.40	13.33			
192	0.064	9.34	8.27	8.02	0.264	0.012
		8.83	7.77			
216	0.074	13.74	12.67	12.41	0.409	0.012
		13.21	12.14			
240	0.014	3.70	2.64	2.69	0.088	0.003
		3.82	2.75			
264	0.042	11.60	10.53	10.06	0.333	0.022
		10.66	9.59			

Time (h)	EPS (gC m^{-2})	EPS std.dev.	L_f (um)	L_f std.dev.
144	0.250	0.114	35	8.8
168	0.194	0.0892	11	7.4
192	0.132	0.0652	9	4.8
216	0.233	0.0750	13	3.2
240	0.041	0.0140	12	6.8
264	0.201	0.0475	17	6.1

Table 14. Experiment B-2 effluent data.

Time (h)	Beads (#/mL)	Beads (gSS m^{-3})	Beads Std.Dev.	Cells (#/mL)	Cells (gC/cell)	Cells (gC m^{-3})
0				9400000	1.25E-13	1.175
24				24000000	1.25E-13	3.000
48				27000000	1.25E-13	3.375
72				18000000	1.25E-13	2.250
96				3500000	1.25E-13	0.438
120				5700000	1.25E-13	0.713
144	510000	0.20451	0.20900	18000000	1.25E-13	2.250
168	7100	0.00285	0.01330	10000000	1.25E-13	1.250
192	1700	0.00068	0.00420	12000000	1.25E-13	1.500
216	20000	0.00802	0.00898	15000000	1.25E-13	1.875
240	9400	0.00377	0.00437	23000000	1.25E-13	2.875
264	250	0.00010	0.00074	12000000	1.25E-13	1.500

Table 14 (continued). Experiment B-2 effluent data.

Time (h)	Cells Std.dev.	TOC (gC m^{-3})	aveTOC (gC m^{-3})	TOC Std.Dev.	Glucose (gC m^{-3})	aveGluc. (gC m^{-3})
0	0.247	6.017	6.044	0.038	4.081	4.056
		6.071			4.031	
24	0.543	3.148	3.122	0.038	0.498	0.510
		3.095			0.522	
48	0.797	3.203	3.181	0.031	0.373	0.361
		3.159			0.348	
72	0.516	3.476	3.537	0.086	0.323	0.311
		3.598			0.298	
96	0.096	3.557	3.543	0.021	0.323	0.336
		3.528			0.348	
120	0.474	3.353	3.329	0.034	0.323	0.298
		3.305			0.274	
144	0.885	4.872	4.983	0.156	0.373	0.373
		5.093			0.373	
168	0.530	2.819	2.843	0.034	0.348	0.348
		2.867			0.348	
192	0.408	3.432	3.578	0.129	0.323	0.323
		3.628			0.323	
		3.674				
216	0.815	6.168	6.207	0.055	0.174	0.224
		6.246			0.274	
240	0.553	10.200	10.220	0.028	4.379	4.031
		10.240			3.682	
264	0.616	3.919	3.943	0.024	0.298	0.323
		3.967			0.348	

Table 14 (continued). Experiment B-2 effluent data.

Time (h)	Glucose Std.Dev.	EPS (gC m^{-3})	EPS Std.Dev.
0	0.035	0.813	0.252
24	0.018	-0.388	0.545
48	0.018	-0.555	0.798
72	0.018	0.976	0.523
96	0.018	2.769	0.100
120	0.035	2.318	0.477
144	0.000	2.359	0.899
168	0.000	1.245	0.531
192	0.000	1.755	0.427
216	0.070	4.108	0.820
240	0.493	3.314	0.741
264	0.035	2.120	0.617

influent glucose from t=0 to t=157 h = 7.89 gC m^{-3}.
influent glucose after t=157 h = 8.45 gC m^{-3}.

Table 15. Experiment B-3 biofilm data.

Time (h)	Beads (#/ml)	Beads (# m^{-2})	Beads (gSS m^{-2})	Beads std.dev. (#/ml)	Beads std.dev.
120.1	6000000	9.49E+10	0.0380	320000	5.06E+09
120.3	8100000	1.49E+11	0.0599	950000	1.75E+10
144.1	9500000	2.49E+11	0.0997	2100000	5.5E+10
192	7800000	2.72E+11	0.1091	800000	2.79E+10
216	6100000	2.47E+11	0.0990	620000	2.51E+10

Time (h)	Beads std.dev.	Cells (#/ml)	Cells (# m^{-2})	Cells (gC/cell)	Cells (gC m^{-2})
120.1	0.0020	77000000	1.22E+12	2.4E-14	0.0292
120.3	0.0070	45000000	8.3E+11	2.4E-14	0.0199
144.1	0.0220	34000000	1.2E+12	2.4E-14	0.0288
192	0.0112	24000000	1.6E+12	2.4E-14	0.0384
216	0.0101	23000000	4.3E+11	3.2E-14	0.0138

Time (h)	Cells std.dev. (#/ml)	Cells std.dev.	Cells std.dev.	Cells std.dev.	TOC (mg/L)	Buffer TOC (mg/L)
120.1	10000000	1.58E+11	2.4E-14	0.0038	11.700	0.774
					11.370	0.774
120.3	11000000	2.03E+11	2.4E-14	0.0049	8.407	0.774
					8.135	0.774
144.1	7000000	1.83E+11	2.4E-14	0.0044	8.412	0.774
					8.205	0.774
192	4300000	1.5E+11	2.4E-14	0.0036	8.512	0.774
					8.313	0.774
216	5000000	2.02E+11	3.2E-14	0.0065	7.341	0.774
					7.051	0.774
					7.093	0.774

Table 15 (continued). Experiment B-3 biofilm data.

Time (h)	Buffer Adjusted TOC (mg/L)	avgTOC (mg/L)	TOC (gC m^{-2})	TOC std.dev.	EPS (gC m^{-2})	EPS std.dev.
120.1	10.926	10.761	0.170	0.0037	0.141	0.0053
	10.596					
120.3	7.633	7.497	0.138	0.0036	0.118	0.0060
	7.361					
144.1	7.638	7.535	0.197	0.0038	0.168	0.0058
	7.431					
192	7.738	7.539	0.267	0.0049	0.228	0.0061
	7.539					
216	6.567	6.388	0.259	0.0063	0.245	0.0091
	6.277					
	6.319					

Time (h)	SOC (mg/L)	Buffer Adjusted SOC (mg/L)	avgSOC (mg/L)	SOC (gC m^{-2})	SOC stddev	Dry Density (gSS m^{-2})
120.1	7.318	6.544	6.406	0.101	0.0031	0.914
	7.041	6.267				
120.3						1.17
144.1	5.146	4.372	4.298	0.113	0.0028	1.15
	4.997	4.223				
192	4.675	3.901	3.811	0.133	0.0044	1.02
	4.495	3.721				
216	5.477	4.703	4.460	0.181	0.0086	1.64
	5.137	4.363				
	5.087	4.313				

Table 15 (continued). Experiment B-3 biofilm data.

Time (h)	L_f (um)	L_f (um)
120.1	16	4.0
120.3	19	5.1
144.1	19	5.0
192	13	3.2
216	12	6.8

Influent glucose concentration = 5.31 gC m^{-3}
calculated from TOC

Table 16. Experiment MP-1 biofilm data.

Time (h)	Beads (# m^{-2})	Beads (gSS m^{-2})	Beads std.dev.	Cells (# m^{-2})	Cells (gC/cell)	Cells (gC m^{-2})
24	7.9E+10	0.0317	0.0038	8.3E+11	3.3E-14	0.0274
24	4.4E+10	0.0176	0.0030	5.2E+11	3.3E-14	0.0172
72	2.8E+11	0.1122	0.0521	3.2E+12	3.3E-14	0.1056
96	7.8E+10	0.0313	0.0132	1.5E+12	3.3E-14	0.0495
120	5.8E+10	0.0232	0.0100	2.1E+12	3.3E-14	0.0693
120	9.4E+10	0.0377	0.0152	2.4E+12	3.3E-14	0.0792
144	1.2E+11	0.0481	0.0184	2.9E+12	3.3E-14	0.0957
144	9.4E+10	0.0377	0.0144	2E+12	3.3E-14	0.0660
168	1.3E+11	0.0521	0.0096	2.9E+12	3.3E-14	0.0957

Time (h)	Cells std.dev.	TOC (mg/L)	Adjusted TOC (mg/L)	avgTOC (mg/L)	TOC (gC m^{-2})	TOC std.dev.
24	0.0139	7.737	7.211	7.089	0.245	0.165
		7.427	6.901			
		7.681	7.155			
24	0.0059	4.274	3.748	3.570	0.124	0.155
		3.993	3.467			
		4.021	3.495			
72	0.0287	15.550	15.024	14.307	0.658	0.621
		14.460	13.934			
		14.490	13.964			
96	0.0122	9.934	9.408	9.199	0.405	0.296
		9.516	8.990			
120	0.0218	13.900	13.374	12.524	0.508	0.822
		12.990	12.464			
		12.260	11.734			
120	0.0059	11.160	10.634	10.464	0.560	0.240
		10.820	10.294			
144	0.0317	10.490	9.964	9.250	0.488	0.668
		9.672	9.146			
		9.166	8.640			
144	0.0224	10.560	10.034	9.627	0.534	0.621
		9.438	8.912			
		10.460	9.934			
168	0.0215	11.530	11.004	10.664	0.553	0.421
		10.850	10.324			

Table 16 (continued). Experiment MP-1 biofilm data.

Time (h)	EPS (gC m^{-2})	EPS std.dev.	L_f (um)	L_f std.dev.
24	0.218	0.179	16	42
24	0.106	0.161	18	50
72	0.552	0.650	460	620
96	0.356	0.308	250	150
120	0.439	0.844	410	260
120	0.480	0.246	520	330
144	0.392	0.700	290	240
144	0.468	0.643	500	330
168	0.457	0.442	330	290

Time (h)	Dry Density (g m^{-2})
72	6.96
80.5	4.01
96.1	2.94
120	3.73
120.5	3.13
144.2	4.71
144.5	1.54
168	3.49

Table 17. Experiment MP-1 effluent data.

Time (h)	Beads (#/ml)	Beads (gSS m^{-3})	Beads std.dev.	Cells (#/ml)	Cells (gC/cell)
24	46000	0.0184	0.0028	12000000	3E-14
48	33000	0.0132	0.0033	9400000	3E-14
48	7100	0.0028	0.0010	10000000	3E-14
96	29000	0.0116	0.0018	19000000	3E-14
144	13000	0.0052	0.0009	6800000	3E-14
168	22000	0.0088	0.0024	5300000	3E-14

Time (h)	Cells (gC m^{-3})	Cells std.dev.	TOC (mg/L)	avgTOC (gC m^{-3})	TOC std.dev.	Glucose (gC m^{-3})
24	0.360	0.096	2.628	2.482	0.128	0.737
			2.431			0.737
			2.387			
48	0.282	0.168	1.588	1.487	0.097	0.000
			1.477			0.000
			1.395			
48	0.300	0.075	1.972	1.839	0.116	0.000
			1.791			0.032
			1.755			
96	0.570	0.030	2.456	2.355	0.090	0.091
			2.283			0.150
			2.327			
144	0.204	0.022	2.039	1.972	0.058	0.384
			1.934			0.443
			1.942			
168	0.159	0.036	2.398	2.344	0.077	0.326
			2.289			0.384

Table 17 (continued). Experiment MP-1 effluent data.

Time (h)	avgGluc (gC m^{-3})	Glucose std.dev.	EPS (gC m^{-3})	EPS std.dev.
24	0.737	0.000	1.385	0.224
48	0.000	0.000	1.205	0.265
48	0.016	0.023	1.523	0.214
96	0.121	0.042	1.665	0.162
144	0.414	0.042	1.354	0.122
168	0.355	0.041	1.830	0.154

Influent glucose = 5.9 gC m^{-3} from 0 to 104 h
6.48 gC m^{-3} after 104 h.

Table 18. Binary population biofilm data. Cell concentrations provided by S. Handran.

Time (h)	*P. aeruginosa* cells (gC m^{-2})	*K. pneumoniae* cells (gC m^{-2})	L_f (μm)	L_f Std.dev.
0	0.0005	0.0005	-	-
87	0.0056	0.0048	25	5.5
138	0.0225	0.0041	23	11
184	0.0255	0.0064	17	7.7

Table 19. Binary population effluent data. Cell concentrations provided by S. Handran.

Time (h)	*P. aeruginosa* cells (gC m^{-3})	*K. pneumoniae* cells (gC m^{-3})	Glucose (gC m^{-3})
0	0.0019	0.015	13.7
87	0.116	0.06	1.22
138	0.2	0.2	0.364
184	0.166	0.22	0.097

APPENDIX D: MICROBEAD PROFILE DATA

APPENDIX D: MICROBEAD PROFILE DATA

Table 20. Bead profile data from Experiment A-1 at 48 h. Symbols are as described in Figure 3. The data are presented in Figure 7. Distances are in μm.

z	L_f	z	L_f	z	L_f	z	L_f
0.8	8.4	0.5	13.9	0	8.9	11.5	22.8
0.8	8.4	0.5	13.9	1.2	8.9	11.5	22.8
2.1	8.4	1	13.9	2.2	9.5	11.5	22.8
3	8.4	1	13.9	2.2	9.5	11.5	22.8
3	8.4	3	13.9	2.2	9.5	11.5	22.8
0.8	6.3	3	13.9	3.3	9.5	13.7	22.8
0.8	6.3	3	13.9	0.1	12.6	13.7	22.8
0.5	5.4	5.4	13.9	2.1	12.6	13.7	22.8
0.5	5.4	0.9	13.3	6.4	10.7	13.7	22.8
3.6	4.9	1.8	13.3	6.4	10.7	13.7	22.8
1.6	4.9	1.8	13.3	3.8	13.5	13.7	22.8
1.6	4.9	1.8	13.3	5.1	13.5	16.8	22.8
1.1	5.1	8	11.1	5.1	13.5	16.8	22.8
0.5	6.3	0.5	14.4	5.1	13.5	16.8	22.8
0.5	6.3	0.5	14.4	7.7	13.5	16.8	22.8
0.5	6.3	0.5	14.4	7.7	13.5	16.8	22.8
0.1	6.5	0.5	14.4	8.7	13.5	20.2	22.8
0.1	6.5	0.5	14.4	8.7	13.5	20.2	22.8
0.1	6.5	0.5	14.4	0.8	14.3	20.2	22.8
0.5	6.5	1.8	14.4	0.5	10.7	20.2	22.8
0.5	6.5	1.8	14.4	2.4	6.5	20.2	22.8
1	6.5	0.5	14.2	3.8	4.3	20.3	22.8
2.2	6.5	1.6	14.2	0.6	5.8	20.3	22.8
2.2	6.5	3.8	14.2	0.6	5.8	21.9	22.8
4.3	6.5	1.7	13.9	1.5	5.8	21.9	22.8
4.3	6.5	0.7	13.9	1.5	5.8	12.3	22
4.3	6.5	0.5	14.3	2.9	5.8	12.3	22
2.5	11.3	0.5	14.3	3.5	5.8	12.3	22
1.5	11.1	0.5	10.4	0.5	2.9	12.3	22
3.5	8.9	0.6	8.4	1.1	2.9	12.3	22
5	8.9	0.7	7.2	0	3	14.2	22
5	8.9	0.5	6.9	2	5.6	14.2	22
5	8.9	1	6.9	3	5.6	14.2	22

Table 20 (continued). Bead profile data from Experiment A-1 at 48 h.

z	L_f	z	L_f	z	L_f	z	L_f
2.4	7	0.5	9.9	2.2	9.2	17.9	22
0.5	6.4	0.7	9.9	2.2	9.2	17.9	22
0.5	6.4	0.5	7.1	2.2	9.2	17.9	22
2.4	7	0.7	7.1	2.2	9.2	20	22
0.5	6.4	3.9	7.2	4.5	9.2	20	22
0.5	6.4	3.4	10.2	4.5	9.2	20	22
2.3	6.4	3.5	8.8	4.5	9.2	11.2	23.4
1	12.3	0.5	8.7	4.5	9.2	11.2	23.4
1.6	12.3	0.4	8	1.9	11.3	12.7	23.4
4.9	12.3	0.6	5.2	1.9	11.3	12.7	23.4
3.3	12.3	2.1	5.2	1.9	11.3	14.7	23.4
1.2	6.4	2.1	5.2	3.7	11.3	14.7	23.4
0.6	5.9	4.1	5.2	3.7	11.3	18.2	23.4
1	7.3	4.1	5.2	3.7	11.3	18.2	23.4
0.5	8.5	2.3	10.4	3.7	11.3	18.2	23.4
0.5	8.5	1.2	10	0.6	12	18.2	23.4
0.5	8	0.5	4.5	0.6	12	15.6	23.2
0.4	8	2.8	7.1	0.6	16	15.6	23.2
0.4	7.8	3	7.4	12.1	16	19.4	23.2
0.7	8.2	0.5	6.1	12.1	16	19.4	23.2
5.2	10.3	2	6.1	14.5	16	21.1	23.2
0	7.9	2.2	6.1	0.5	14.8	21.1	23.2
0	7.9	1.8	6	0.5	14.8	22.7	23.2
0	7.9	1.8	6	0.9	14.8	12.8	23
0	6.2	1.8	6	7.2	15.5	12.8	23
0.5	6.2	1.8	6	8.1	15.5	12.8	23
2.1	6.2	4.1	6	6.4	15.2	14.2	23
2.1	6.2	4.1	6	6.4	15.2	14.2	23
2.1	6.2	2.9	8.6	3.1	14.5	14.2	23
2.1	6.2	3.7	8.6	3.1	14.5	14.2	23
4.3	8.6	3.7	8.6	3.1	14.5	17	23
0.8	12.1	0.5	6	3.1	14.5	17	23
0.5	12.1	0.5	6	5.2	14.5	17	23
0.5	12.1	1.8	6	5.2	14.5	17	23
0.4	13.8	0.7	6.3	5.2	14.5	17.4	23
1.3	11	0.6	5.4	5.2	14.5	17.4	23
0.5	9.8	0.4	9.8	5.2	14.5	19.5	23
5.2	9.3	0.5	10.8	6.4	14.5	19.5	23
0.4	10.6	1	10.8	6.4	14.5	19.5	23

Table 20 (continued). Bead profile data from Experiment A-1 at 48 h.

z	L_f	z	L_f	z	L_f	z	L_f
0.5	12.1	1.4	10.8	6.4	14.5	0.5	14.9
1.6	12.1	3.6	7	6.4	14.5	0.5	14.9
0.5	12.6	0.5	8.1	8	14.5	1.2	14.9
2.1	13.7	0.5	6.1	8	14.5	0.8	14.9
1.1	13.1	0.5	6.1	0.5	13.3	0.8	14.9
1.1	13.1	0.5	5.7	1.3	13.3	0.6	13.4
0.5	16	1.8	8.7	6.5	24.8	0.6	13.4
0.5	13.8	0.7	10	6.5	24.8	0.3	5.6
1.2	13.8	1.2	10	4.5	24.8	0.5	12
1.2	13.8	0.5	6.3	2	21.4	0.5	12
2.4	13.8	1.2	2.4	13.7	20.9	2.3	12
2.4	13.8	1.2	2.4	13.7	20.9	1.1	13
0.5	15.6	1.4	3.4	14.5	20.9	1.1	13
0.5	15.6	2.3	3.4	14.5	20.9	3.3	13
3.9	12.2	1	6.3	14.5	20.9	3.3	13
1	14.8	1	6.3	16.5	20.9	4.5	13
3.5	12.1	1	6.3	16.5	20.9	4.5	13
7.4	13.3	1	6.3	16.5	20.9	2.6	7.2
1.3	14.1	2	6.3	16.5	20.9	3.6	10
2.7	14.1	4.9	9.2	19.8	20.9	3.6	10
1.8	5.1	2.2	9	19.8	20.9	3.6	10
2.9	5.1	0.5	6.7	19.8	20.9	6.2	10
3.9	13.1	0.9	6.7	17.1	22	6.2	10
10.3	12.7	0.9	6.7	17.1	22	6.2	10
6.2	11.6	0.6	7	17.1	22	7.8	10
5.4	12.1	0.6	7	17.1	22	0.5	5.9
8.5	12.1	0.6	7	21.5	22	0.5	5.9
10.3	12.1	0.5	7.2	10.7	21.3	2.8	5.9
12.1	12.1	0.5	7.2	12.3	21.3	4.6	5.9
12.1	12.1	3.2	8.3	12.3	21.3	4.6	5.9
9.5	18.4	3.2	8.3	12.3	21.3	5.4	5.9
13.1	17.4	2.2	8.3	12.3	21.3	5.4	5.9
11.3	24.4	0	8.4	13.8	21.3	2.5	5.7
1.3	24.4	4	7.7	13.8	21.3	3.7	8.2
11.7	24.4	4	7.7	13.8	21.3	0.5	6.9
11.7	24.4	2.1	7.7	13.8	21.3	5.4	6.8
11.7	24.4	3.6	7.7	13.8	21.3	5.4	6.8
13.6	24.4	0.5	11.2	15.3	21.3	0.4	5.1
13.6	24.4	1.2	11.2	15.3	21.3	0.4	5.1

Table 20 (continued). Bead profile data from Experiment A-1 at 48 h.

z	L_f	z	L_f	z	L_f	z	L_f
15.1	24.4	2.4	11.2	15.3	21.3	0.4	5.1
15.1	24.4	2.4	11.2	15.3	21.3	1	5.1
17.2	24.4	2.6	11.2	17.4	21.3	1	5.1
17.2	24.4	3.3	11.2	17.4	21.3	1	5.1
17.2	24.4	3.3	11.2	17.4	21.3	1.9	5.1
17.2	24.4	1.3	12.2	19.5	21.3	1.9	5.1
18.9	24.4	6.4	15.3	19.5	21.3	1.9	5.1
18.9	24.4	4.1	16.5	19.5	21.3	1.9	5.1
20.9	24.4	0.8	13.1	19.5	21.3	1.9	5.1
20.9	24.4	1.7	13.1	21	21.3	0.5	5.1
20.9	24.4	3.9	10.2	21	21.3	0.5	5.1
23.4	24.4	6.8	9.4	11.5	17	0.5	5.1
23.4	24.4	5.7	9.6	11.5	17	0.7	6.2
12.3	23.3	3.1	10.6	11.8	17	0.7	6.2
12.3	23.3	1.6	7.4	11.8	17	1.2	5.5
14.3	23.3	2.4	7.4	10	15.1	2.7	5.5
14.3	23.3	5.4	6	10.6	14.9	2.7	5.5
14.3	23.3	2.7	6	10.6	14.9	0.3	6.7
15.3	23.3	1.2	7.3	2	15.7	1.7	6.7
15.3	23.3	1.5	7.3	2	15.7	1.7	6.7
15.3	23.3	1.3	9.3	2	15.7	1	10.8
17.2	23.3	6	6.8	1.9	11.8	1	10.8
17.2	23.3	4.7	6.8	3.8	11.8	2.3	10.8
17.2	23.3	4.7	6.8	2.8	6.1	2.3	10.8
17.2	23.3	5.2	6.8	4.1	6.1	4.3	10.8
19.1	23.3	2.9	13.6	4.1	6.1	4.3	10.8
19.1	23.3	3.9	13.6	2.2	6.2	0.5	14.8
19.1	23.3	3.9	13.6	10.7	12	0.5	14.8
20.8	23.3	3	13.6	12.1	13.2	0.5	8.7
20.8	23.3	2.5	13.6	3.8	5.2	1.2	8.7
20.8	23.3	1.6	13.3	3.8	5.2	1.2	8.7
16.3	20.9	1.7	12.3	4.8	7.1	3.5	8.7
18.5	20.9	0.5	12.3	4.8	7.1	3.5	8.7
18.5	20.9	0.5	12.3	3.7	7.5	3.5	8.7
19.9	20.9	3.1	12.3	0.5	8	4.2	8.7
1.2	14.8	2.4	12.3	0.9	8	4.2	8.7
1.2	14.6	5.7	10.9	0.6	9.9	4.2	8.7
0.4	12.9	2.5	6.3	0.8	13.4	4.2	8.7
0.4	12.9	3	6.3	0.8	13.6	4.2	8.7

Table 20 (continued). Bead profile data from Experiment A-1 48 h.

z	L_f	z	L_f	z	L_f	z	L_f
1.1	12.9	3.9	6.3	2.1	13.6	6.6	8.7
1.1	12.9	3.3	6.3	0.1	14.8	6.6	8.7
1.1	12.9	3.3	6.3	3.7	13.8	6.6	8.7
1.1	12.9	4.8	6.3	3.7	13.8	7.3	8.7
1.1	12.9	0.9	6.9	4.5	13.8	5.8	13.9
1.1	12.9	3	6.9	1.4	13.8	5.8	13.9
2.6	12.9	3	6.9	2.5	13.8	7.3	13.9
2.6	12.9	3.1	6.9	4.7	11.5	7.3	13.9
2.6	12.9	0.4	7.4	0	10	0.6	12.7
2.6	12.9	1.6	4.7	1	9.9	0.6	12.7
2.6	12.9	5.7	10.6	0.5	11.9	0.6	12.7
2.6	12.9	7.3	10.6	0.5	11.9	6.8	12.5
4.7	12.9	2.9	4.6	3	9.3	8.5	12.5
4.5	12.9	2.9	4.6	1.5	6.2	8.5	12.5
4.2	14	3.8	4.2	0.5	2.9	8.5	12.5
0.3	6	1.3	4.7	8.3	13.2	8.5	12.5
1.4	6	2.6	4.7	0.1	6.2	8.9	12.5
1.6	5.7	1.3	3	6.2	7.4	8.9	12.5
2.9	5.7	1.4	5.8	3.4	6.6	0.5	7.8
0.5	8.4	5.5	7.9	5.2	6.6	0.5	7.3
0.5	8.4	2.1	5.4	4.2	12	0.5	7.3
0.5	7.7	2.1	5.4	1.8	12	0.5	7.3
2.4	5.5	7	15.8	3.1	13	0.5	7.3
2.4	5.5	7	15.8	8.1	13.3	0.9	7.3
1.6	6	6.2	13.6	1.8	14.8	1.9	7.3
1.3	6	0.8	16.8	1.4	11.1	1.9	7.3
0.6	10.4	2	16.8	2.1	11.1	1.9	7.3
1.3	8.9	7.6	22.8	2.1	11.1	1.9	7.3
1.3	8.9	10	22.8	0.8	14.4	3.5	7.3
2.1	8.9	10	22.8	8.6	13.8	3.5	7.3
3	8.9	10	22.8	8.6	13.8	0.8	3.1
0	8.9	11.5	22.8	9.4	13.8	0.8	3.1
1.8	13.8	2.2	3.5	1.6	13.1	0.8	3.1
3.1	13.8	0.8	5.5	3.9	8.6	15.6	22
0.5	8.3	0.5	13.7	3.9	8.6	15.6	22
0.5	8.3	5.4	9.9	1	9.2	17.9	22
3.1	7	1.3	14.1	3.9	8.6	15.6	22
1.1	7.4	0.6	14.1				

Table 21. Bead profile data from Experiment A-1 at 72 h. Symbols are as described in Figure 3. The data are presented in Figure 7. Distances are in μm.

z	L_f	z	L_f	z	L_f	z	L_f
1.9	11.7	6.2	12	5.6	14	5.7	13.3
11.7	16.3	7.3	12	4.5	14	7	13.3
3.3	10	0.5	14.6	4.5	14	2.6	14.8
0.5	15	0.8	16.2	2.6	10.8	2.9	12.1
1.6	8.7	2.6	10.9	1.6	6	4.2	12.1
1.2	10.7	0.5	16.1	1.1	6.9	1	12.1
2.2	12	3.4	16.1	3.2	16.5	2.7	12.1
3.8	13.7	2.9	18.5	0.5	9.5	5.2	12.1
3.8	13.7	5.7	21.3	1.3	6.5	6.3	12.1
3.8	13.7	7.3	21.3	0.7	7.8	7.3	12.1
5.4	14.4	0.5	9.8	2.3	9.8	2.1	12.5
5.4	14.4	0.6	9.6	0.5	13.5	2.1	12.5
7.9	14.4	0.6	9.6	1.8	13.5	4.7	12.5
9.7	18	0.6	9.6	5.6	31.8	8.1	12.5
8.2	17.7	2.1	9.6	13.6	31.8	8.1	12.5
13	17.7	2.1	9.6	8.7	12.6	8.1	12.5
0.5	11.6	4.4	9.6	9.3	11.5	7	11.8
2.8	18.8	4.4	9.6	8.4	11.5	5.9	11.8
1.2	18.8	6.7	12.8	6.6	12.5	5.9	11.8
1.2	18.8	5.4	14.2	1.1	4.3	2	9.9
2.2	18.8	4.2	15.5	2.7	8.9	2	9.9
2.8	19.5	2.6	15.5	5	8.9	5.6	9.9
2.8	9.3	4	15.5	1.9	8.1	2.9	10.5
5.3	11.9	4.4	15.5	0.8	8.1	1.9	8.9
4.7	11.6	7	15.5	0.5	10.2	0.8	8.6
0.5	6.5	2.2	10.8	0.5	7.4	0.5	15.1
0.6	9.9	2.4	11.3	0.5	7.4	5.8	15.1
2	9.9	0.5	12.6	1.9	7.4	3.1	13.8
3.7	9.8	2.1	17.2	1.9	7.4	2	11.5
3.7	9.8	2.6	17.2	1.9	7.4	4.6	11.5
1.4	8.6	4.3	17.2	3.7	7.4	4.6	11.5
0.5	18.1	3.6	9.4	4.3	7.4	1	8.9
1.1	18.1	2.7	12.3	7.2	12.7	0.8	11.2
1.1	18.1	2.8	13.9	0.5	23.2	0.5	15
1.1	18.1	4.1	8.9	0.5	23.2	1.6	15
2.9	18.1	2.6	10.2	7.2	23.2	2.6	15

Table 21 (continued). Bead profile data from Experiment A-1 at 72 h.

z	L_f	z	L_f	z	L_f	z	L_f
23	30.3	2.4	11.3	8.6	23.2	4	15
23	30.3	3.8	11.3	8.6	23.2	4.4	15
23	30.3	1.6	8.9	8.6	23.2	7.1	15
23.1	30.3	3.7	8.9	11.6	23.2	7.1	15
23.1	30.3	0.5	7.4	11.6	23.2	2.7	18.1
23.1	30.3	2.8	7.4	0.5	5.3	8.3	18.1
25.6	30.3	1.9	7.4	3.9	16.4	0.5	18.5
25.6	30.3	1.9	7.4	3.9	16.4	2.4	18.5
25.6	30.3	3.5	10	1.9	13.6	0.1	20.2
27.6	30.3	1	8.3	4.7	8.8	0.1	20.2
27.6	30.3	1.5	8.3	4.7	8.8	2.9	20.2
29.8	30.3	1.5	10.3	4.7	8.8	0.5	10.1
29.8	30.3	3.1	8.9	4.7	8.8	1.6	16.8
1.5	7.3	1.1	9.5	2.3	8.8	2.6	11.7
0.5	3.4	0.6	14	1.2	9.5	1.8	11.2
0.5	3.4	1.9	10.6	2.3	9.5	2.1	11.2
0.9	2.9	1.1	10.6	1.8	9.5	0.5	10.8
1.7	4.1	1.9	9.4	4.1	9.5	9.5	12.5
0.5	7.4	3.8	9.4	1.6	12.2	2.5	11.2
1.8	4.4	0.6	10.8	2	12.2	3.4	9.1
0.4	7.1	3.1	10.8	0.5	8.9	5.7	12.8
2.1	7.5	2.9	8.4	1.1	8.2	8.1	12.8
5.2	6.2	2.7	9.6	0.5	8.2	2.2	10.9
5.2	6.2	0.5	11.4	1.6	9.7	0.5	10.3
5.2	6.2	1.1	11.4	0.5	9.7	1.9	10.3
5.2	6.2	1.1	11.4	1.4	9.7	4.5	10.2
1.8	6.2	2.1	11.4	5	7.9	0.5	9.6
4	5	2.1	11.4	3.4	7.9	1	9.6
2.9	4.2	2.1	11.4	4.2	11	2.6	9.6
1.6	9.6	3	11.4	2.1	11	3.1	9.6
2.9	10.4	5.2	11.4	5.5	8.6	3.1	9.6
2.9	10.4	5.2	11.4	0.5	10.6	4.7	9.6
2.9	10.4	0.5	23.3	1.1	13.3	1.3	10.7
1.2	5.4	3.3	27.6	5.1	13.3	0.5	10.7
1.3	7.2	3.3	27.6	3.4	14.6	2.1	8.6
1.3	7.2	4.8	27.6	1.3	14.6	4	8.6
2.5	7.2	4.8	27.6	0.8	14.6	2.2	6.9
0.3	4	4.8	27.6	2.5	12.2	7	18.8

Table 21 (continued). Bead profile data from Experiment A-1 at 72 h.

z	L_f	z	L_f	z	L_f	z	L_f
1.6	6.2	4.8	27.6	1.7	12.2	7	18.8
1.6	6.2	5.5	27.6	6	9.9	7	18.8
2.5	6.2	7.2	27.6	1.3	13.8	9.8	18.8
2.5	6.2	7.2	27.6	1	17.8	9.8	18.8
1.8	11.5	7.2	27.6	3.4	11.1	9.8	18.8
3.4	7.3	7.2	27.6	4.8	11.1	9.8	18.8
1.1	8.2	8.3	27.6	5.6	11.1	10.3	18.8
3.3	11.5	8.3	27.6	0.5	15.8	10.3	18.8
4	11.5	10.3	27.6	2.9	6.9	12.5	18.8
4	11.5	10.3	27.6	2.6	14.5	12.5	18.8
4.6	12.9	10.3	27.6	4.4	20.3	14.8	18.8
0.5	14	1.2	9.5	5.4	20.3	10	19
1.7	14	0.5	13.3	6	20.3	9.1	19
1.7	14	2.9	13.3	0.5	13.3	3.5	17.7
1.7	14	2.9	13.3	2	13.3	0.5	8.3
2.5	14	4.2	13.3	4.4	12	5.7	13.3
19.7	30.3	1.3	10.7	8.6	23.2	4	15
3.5	14						

Table 22. Bead profile data from Experiment A-1 at 120 h. Symbols are as described in Figure 3. The data are presented in Figure 7. Distances are in μm.

z	L_f	z	L_f	z	L_f	z	L_f
11.7	12.2	3.25	38.4	9.4	13.6	9.5	27.1
16.7	24.2	3.25	38.4	10.6	13.6	10.2	27.1
4.6	24.2	1.45	38.4	0.6	18.2	4.8	30
6	28.2	1.65	38.4	1.1	18.2	4.8	30
10.2	30.2	0.8	38.4	2.25	18.2	4.6	22.3
12.9	30.2	0.8	38.4	2.9	17	5	22.3
9.2	30.2	1.5	38.4	0.8	9.4	6.5	22.3
6.9	30.2	1.2	46.4	1.65	5.7	7.9	22.3
11.8	30.2	1.2	46.4	1.5	6.8	7.9	22.3
7.8	31.0	1.8	46.4	1.5	6.8	8.4	22.3
13.1	31.0	2.4	46.4	3.3	26.9	2.6	30.7
11.2	32	3.6	45.1	3	26.9	1.8	30.7
11.9	33.5	1.1	31.2	2.4	26.9	1.3	30.7
16.4	33.5	1.1	31.2	1.5	26.9	7.4	29.5
5	10.2	1.8	31.2	0.7	26.9	1.4	36.3
1.2	9.8	1	31.2	1.8	26.9	1.4	36.3
2.6	22.9	0.7	20.2	1.8	26.9	2.0	36.3
3.3	15.6	2.6	18.8	3	26.9	28.6	36.9
1.7	21.8	3.6	18.8	3	26.9	29.1	36.9
3.2	21.8	1.8	8.4	4	26.9	29.1	36.9
1.3	16.1	1.4	13.7	7.6	11.6	29.6	36.9
1.3	16.1	3.3	13.2	5.4	7.4	29.6	36.9
12.6	12.9	3.3	13.2	1	8.3	29.6	36.9
12.2	12.5	1.35	17.4	1.2	7.0	31.1	36.9
8	9	2	16.6	1.7	7.0	33.0	36.9
6	9	2.7	9	2	7.0	33.0	36.9
0.6	8.2	0.6	9	2	7.0	33.8	36.9
9.4	10	0.6	9	2	7.0	33.8	36.9
3.9	24.4	1.4	9	3.3	7.0	33.8	36.9
4.2	23	7	13.6	3.3	7.0	33.8	36.9
4.2	23	9	13.6	0.7	4.5	9.5	42
3.9	17.6	5.7	14.9	1.5	6	16.8	42
5	17.6	1.5	11.6	2.5	6	17.3	42
2.5	19.6	2.6	11.6	4	6	17.9	42
2.4	24.3	2.6	11.6	4	6	18.7	42
1.7	29.7	4.6	11.6	4	6	19.0	42

Table 22 (continued). Bead profile data from Experiment A-1 at 120 h.

z	L_f	z	L_f	z	L_f	z	L_f
13.5	28	5.6	11.6	4	6	11.5	34.9
0.6	20.6	5.6	11.6	4.8	6	19.3	34.9
0.6	20.6	6.8	11.6	5.2	6	21.6	34.9
2.4	20.6	8	11.6	0.5	13	21.6	34.9
2.8	20.6	8.9	11.6	1.3	13	22.7	34.9
1.4	20.6	8.9	11.6	3.9	13	23.3	34.9
2.6	20.6	10	11.6	1.7	14.1	22.4	34.9
2.6	20.6	10.4	11.6	2.5	14.1	23.4	34.9
0.7	19.9	10.4	11.6	2.45	14.1	23.4	34.9
0.7	19.9	11.4	11.6	5.5	18.2	23.4	34.9
2.8	19.9	1.85	5.8	3.05	4.8	24.8	34.9
2.2	19.9	2.7	5.8	1	5.2	24.8	34.9
2.2	19.9	2.7	5.8	0.6	2.9	24.9	34.9
0.9	15.9	2.7	5.8	0.7	36.8	25.5	34.9
2.6	8.5	3.4	5.8	1.9	36.8	26.5	34.9
2.8	3.5	4	5.8	2.4	36.8	26.9	34.9
2.8	3.5	4	5.8	3.15	36.8	4.6	36.1
3.9	8.5	4	5.8	1.7	39.2	5.8	36.1
3.9	8.5	4.9	5.8	1	48.4	5.6	36.1
4.3	7.7	5.6	5.8	2.8	48.4	6.8	36.1
4.7	7.7	0.8	4.2	0.5	48.4	11.2	36.1
5.4	7.7	1.8	4.2	3.2	44.2	13.3	36.1
0.7	7.7	1.9	4.2	4	44.2	14.8	36.1
1.3	4.7	1.9	4.2	4	44.2	21.9	36.1
2.5	4.7	2.7	34.1	5.3	44.2	22.6	36.1
2.5	4.8	2.7	34.1	5.3	44.2	22.6	36.1
3.2	5.2	33.5	34.1	6.3	44.2	24.0	36.1
2.7	22.1	0.5	33.2	6.3	44.2	24.3	36.1
5	8.8	0.5	33.2	7.5	44.2	24.3	36.1
10.4	30.8	2.7	4.2	7.5	44.2	25.2	36.1
11.5	30.8	0.5	34.1	16.0	43.2	25.2	36.1
12	30.8	1.9	34.1	17.2	43.2	26.6	36.1
16.9	30.8	1.9	34.1	18	43.2	26.6	36.1
7.5	30.2	1.1	33.2	23.2	43.2	2.3	27.4
7.5	30.2	1.5	33.2	26.0	43.2	2.7	27.4
9.2	30.2	1.5	33.2	27.4	43.2	3.8	27.4
10.3	30.2	1.5	33.2	28.4	43.2	3.8	27.4
11.9	30.2	0.5	34.9	29	43.2	3.8	27.4
13	30.2	1	34.9	29.4	43.2	4.9	27.4

Table 22 (continued). Bead profile data from Experiment A-1 at 120 h.

z	L_f	z	L_f	z	L_f	z	L_f
13	30.2	1.5	34.9	29.4	43.2	4.9	27.4
5.6	24.2	4	34.9	2.1	37.5	6.5	27.4
4.2	20.0	4.8	34.9	2.8	37.5	7.5	27.4
17.3	25.7	4.8	34.9	3.3	37.5	7.5	27.4
11.2	13.8	4.8	34.9	3.3	37.5	2.4	29.0
4.5	17.3	4.8	34.9	5.4	37.5	14.6	29.0
6	13.2	4.8	34.9	5.4	37.5	15.6	29.0
8.8	33.4	5.4	34.9	6.9	37.5	17	29.0
10	33.4	5.4	34.9	2.2	36.7	18.8	29.0
11.8	33.4	5.4	34.9	1.4	36.7	1.6	27.8
11.8	33.4	5.4	34.9	1.4	36.7	24.8	30.1
13.4	33.7	5.4	34.9	2.5	36.7	24.8	30.1
16.0	33.7	5.4	34.9	2.5	36.7	25.6	30.1
16.0	33.7	6.3	34.9	3.6	36.7	25.6	30.1
5.6	18.2	6.3	34.9	3.6	36.7	26.4	30.1
6.6	18.2	6.3	34.9	4.3	36.7	26.4	30.1
6.6	18.2	6.3	34.9	4.8	36.7	26.6	30.1
6.6	18.2	7.4	34.9	2.4	35.9	26.6	30.1
7.2	18.2	7.8	34.9	2.4	35.9	26.8	30.1
7.9	18.2	8.3	34.9	2.6	35.9	26.8	30.1
1.6	16.8	15.4	34.9	3.6	35.9	27.9	30.1
0.5	17.1	3.4	35.2	3.6	35.9	28	30.1
5.2	29.1	4.4	35.2	3.6	35.9	0.8	36.8
3.8	27.7	5.2	35.2	4.7	35.9	5.0	36.8
1.8	34.4	6.6	35.2	4.7	35.9	17.3	36.8
2	22.9	7.5	35.2	4.7	35.9	18.4	36.8
4.4	19.1	5.3	35.2	4.7	35.9	18.4	36.8
6.3	19.1	13.9	34.3	5.6	35.9	3.8	39.4
4.7	22.2	14.2	33	1.8	36.2	1.9	46.6
5.8	19.8	6	31.2	3.1	36.2	2	14.8
5.1	19	0.7	33.2	3.6	36.2	3.2	16.7
10.1	37.6	17.0	36.6	3.6	36.2	3.2	16.7
10.1	37.6	16.2	36.6	3.6	36.2	3.6	16.7
12.1	37.6	17	36.6	4.8	36.2	3.6	16.7
12.7	37.6	18	36.6	4.8	36.2	3.2	14.6
16.3	37.6	18.7	36.6	4.8	36.2	2.8	14.6
8.4	22.4	18.7	36.6	4.2	36.2	3.8	14.6
10.9	34.2	1.8	32.5	5.0	36.5	5.8	14.6
1.2	32.2	1.8	32.5	5.0	36.5	2.2	21.9

Table 22 (continued). Bead profile data from Experiment A-1 at 120 h.

z	L_f	z	L_f	z	L_f	z	L_f
6.1	24.4	9	29.4	0.6	37.8	3.4	21.9
3	19.2	9.2	29.4	2.1	37.8	4.6	21.9
3	18	10.4	29.4	3	37.8	5.1	21.9
10.6	29.4	14.6	29.4	3	37.8	2.8	22.5
11.3	29.4	11.0	35.5	4.0	37.8	2.8	22.5
11.8	29.4	15.7	35.5	4.0	37.8	2.9	22.5
3.2	9.4	12.9	32.9	5.2	37.8	4.0	22.5
4.8	10.9	13.6	32.9	5.2	37.8	4.0	22.5
2.4	21.2	14.4	32.9	1.4	39.8	2.2	25.2
3.0	21.2	15.2	32.9	2	39.8	4	14
2.4	16.6	0.8	30.7	4.4	39.8	3.3	14
3.1	16.6	2.2	30.7	4.4	39.8	3.8	14
3.1	16.6	6.1	30.7	4.8	39.8	3.8	14
1.9	16.6	6.1	30.7	5.6	39.8	4.6	14
0.7	15.7	7	30.7	5.6	39.8	4.6	14
10.5	15.7	7	30.7	7	39.8	2.4	16.3
11.8	15.7	7	30.7	7	39.8	3.0	16.3
11.8	15.7	7	30.7	7	39.8	3.0	16.3
12.6	15.7	7	30.7	7.7	39.8	3.0	16.3
12.6	15.7	7.9	30.7	8.2	39.8	3.0	16.3
12.6	15.7	7.9	30.7	0.6	35.9	4	16.3
13.4	15.7	7.9	30.7	2.4	35.9	4.2	16.3
3.2	15.5	8.8	30.7	2.4	35.9	5	16.3
4.2	15.5	8.8	30.7	2.4	35.9	5	16.3
5.4	15.5	10	30.7	3.4	35.9	5	16.3
5.6	15.5	10	30.7	4.4	35.9	5	16.3
5.6	15.5	11.3	30.7	3.8	35.9	5	16.3
5.8	15.5	11.3	30.7	3.8	35.9	5	16.3
6.2	15.5	12.4	30.7	2	35.9	5.7	16.3
6.2	15.5	12.4	30.7	2	35.9	5.7	16.3
6.2	15.5	12.4	30.7	2.2	35.9	5.7	16.3
6.2	15.5	13.1	30.7	1.2	35.9	6.3	16.3
7.0	15.5	9.2	29.1	5.0	35.9	6.3	16.3
7.6	15.5	9.2	29.1	5.6	35.9	6.3	16.3
7.6	15.5	9.2	29.1	3.8	34.2	7.2	16.3
7.8	15.5	5.8	29.1	1.9	35.5	7.6	16.3
8.5	15.5	6	29.1	1.9	35.5	7.6	16.3
8.5	15.5	6	29.1	0.5	33.9	8.2	16.3
9.3	15.5	6.8	29.1	1.5	33.9	1.6	14

Table 22 (continued). Bead profile data from Experiment A-1 at 120 h.

z	L_f	z	L_f	z	L_f	z	L_f
9.8	15.5	7.7	29.1	2.4	33.9	1.6	14
10.6	15.5	9.2	29.1	2.4	33.9	1.6	14
11.1	15.5	9.2	29.1	2.4	33.9	2.3	14
11.1	15.5	12.3	29.1	2.4	33.9	2.3	14
11.7	15.5	6	29.7	3.2	33.9	2.3	14
11.7	15.5	6	29.7	3.2	33.9	2.8	22
11.7	15.5	6.9	29.7	3.6	33.9	2.8	22
6.7	13.6	7.8	29.7	3.6	33.9	3.8	22
7.4	13.6	1.3	26.6	0.6	38.4	4.4	21.2
7.4	13.6	1.4	25.3	1.1	38.4	2.2	18.1
8.0	13.6	1.7	25.3	1.6	38.4	4.3	11
8.0	13.6	1.7	25.3	1.6	38.4	3.1	11
9.4	13.6	1.7	25.3	2	38.4	1.8	18.9
9.4	13.6	2.7	25.3	2	38.4	3.6	18.9
9.4	13.6	3.2	25.3	2	38.4	3.6	18.9
1.5	24.1	5.6	11.6	4	6	2.6	34.9
1.4	19.5						

Table 23. Bead profile data from Experiment B-2 at 144.75 h. Symbols are as described in Figure 3. The data are presented in Figure 8. Distances are in μm.

z	L_f	z	L_f	z	L_f	z	L_f
35.5	37	8.5	16.2	34.8	44.9	24.5	37.5
6	38.5	9.7	13.3	34.8	44.9	24.5	37.5
11	38	11.6	13.4	34.8	44.9	24.5	37.5
16	39	13.9	14.3	34.8	44.9	24.5	37.5
19	38	7.1	7.5	34.8	44.9	24.5	37.5
30	33.5	4.1	7.5	34.8	44.9	27.4	37.5
25.5	31.5	4.1	7.5	34.8	44.9	27.4	37.5
13.5	31.3	4.1	7.5	34.8	44.9	30.8	37.5
30.5	32	4.1	7.5	34.8	44.9	30.8	37.5
29.5	34	4.1	7.5	34.8	44.9	36.3	37.5
31.5	34.5	7.2	12.5	34.8	44.9	36.3	37.5
29	34.5	7.2	12.5	34.8	44.9	15.4	40.8
29	34.5	9.1	12.5	34.8	44.9	15.4	40.8
29	34.5	9.1	12.5	34.8	44.9	15.4	40.8
29	34.5	10.9	12.5	34.8	44.9	15.4	40.8
29	34.5	9.3	15.5	34.8	44.9	15.4	40.8
20.5	29	10.9	15.5	45.5	48.7	15.4	40.8
20.5	33	13	15.5	45.5	48.7	15.4	40.8
12.5	30.5	13	15.5	45.5	48.7	15.4	40.8
14.5	25.5	13	15.5	41.5	45.1	15.4	40.8
13	23	13	15.5	41.5	45.1	15.4	40.8
4.5	15.5	13	15.5	44.4	45.1	15.4	40.8
14.7	19.7	13	15.5	42.5	43.5	15.4	40.8
4.2	24.8	13	15.5	42.5	43.5	25	40.8
16.7	25	7.4	14.2	42.5	43.5	25	40.8
16.7	25	13.8	14.2	39.9	43.5	25	40.8
3.1	24.2	12.7	13.2	39.9	43.5	25	40.8
13.8	27.8	12.7	13.2	39.9	43.5	25	40.8
13.8	27.8	12.2	17.4	39.9	43.5	25	40.8
13.8	27.8	12.2	17.4	39.9	43.5	25	40.8
24.7	28.5	12.2	17.4	36.7	43.5	25	40.8
24.7	28.5	12.2	17.4	36.7	43.5	25	40.8
11.4	21.2	1.8	8.4	36.7	43.5	25	40.8
16.9	24.2	4	8.4	31.1	43.5	25	40.8
3.6	16.4	6.6	8.4	31.1	43.5	25	40.8
25.8	30.3	6	7.4	32.1	38.5	39.6	40.8
45.5	47.4	14.2	16.6	21.1	26.3	8.7	32.2

Table 23 (continued). Bead profile data from Experiment B-2 at 144.75 h.

z	L_f	z	L_f	z	L_f	z	L_f
36.4	43.6	9.6	10	32.1	38.5	39.6	40.8
25.8	53.6	28.5	36.5	36.2	38.5	36.6	40.8
41.7	52.1	28.5	36.5	36.2	38.5	36.6	40.8
41.7	52.1	28.5	36.5	36.2	38.5	36.6	40.8
41.7	52.1	28.5	36.5	36.2	38.5	36.6	40.8
29.9	32.2	23.6	36.5	36.2	38.5	40.7	41.1
26.5	38.2	23.6	36.5	18.4	38.5	17.6	40
29.1	40.9	23.6	36.5	18.4	38.5	17.6	40
26.4	43.2	19.2	36.5	16.9	38.7	17.6	40
28.8	46.2	19.2	36.5	16.9	38.7	17.6	40
31	32	19.2	36.5	12.3	38.5	17.6	40
33.6	35.8	18.7	35.8	12.3	38.5	17.6	40
48.9	58.9	18.7	35.8	12.3	38.5	17.6	40
51.9	62.5	18.7	35.8	9	38.6	12.5	40
51.9	62.5	27.2	35.8	9	38.6	26.8	40
33.2	48.8	18.2	34.9	11.6	38.5	26.8	40
33.2	48.8	18.2	34.9	11.6	38.5	26.8	40
28.2	49.9	18.2	34.9	6.6	39.2	26.8	40
33.7	42.8	18.2	34.9	6.6	39.2	26.8	40
15.6	47.4	19.1	32.9	10.6	40.8	26.8	40
29.7	44.7	25.9	33.5	10.6	40.8	26.8	40
29.7	44.7	25.9	33.5	10.6	40.8	26.8	40
30.8	34.6	25.9	33.5	10.6	40.8	26.8	40
25.3	34.9	25.9	33.5	34.9	41.4	26.8	40
31	35.1	29.5	33.5	38.1	41.4	26.8	40
15.5	23.5	29.5	33.5	38.1	41.4	26.8	40
10.9	38	29.5	33.5	38.1	41.4	26.8	40
10.9	38	18.4	30.4	32.9	41.9	26.8	40
10.9	38	28.2	30.4	35.5	41.9	32.4	40
10.9	38	25.9	29.1	38.1	41.9	32.4	40
10.9	38	25.9	29.1	39	40.7	32.4	40
10.9	38	22.6	29.4	39	40.7	32.4	40
10.9	38	22.6	29.4	40.8	41.8	32.4	40
10.9	38	22.6	29.4	40.8	41.8	39.5	40
10.9	38	14.6	29.4	11.5	41.7	35.8	38.6
9.8	35	14.6	29.4	15.7	41.7	35.8	38.6
9.8	35	31.1	34.1	15.7	41.7	35.8	38.6
20.8	34	31.1	34.1	15.7	41.7	24.6	28.6
29.6	35.2	31.1	34.1	15.7	41.7	4.3	12.7

Table 23 (continued). Bead profile data from Experiment B-2 at 144.75 h.

z	L_f	z	L_f	z	L_f	z	L_f
29.6	35.2	31.1	34.1	15.7	41.7	4.3	12.7
29.6	35.2	31.1	34.1	32.7	38.4	4.3	12.7
29.6	35.2	31.1	34.1	37.8	39.9	4.3	12.7
29.6	35.2	31.1	34.1	37.8	39.9	4.3	12.7
5.8	33.8	31.1	34.1	30.3	38.5	4.3	12.7
5.8	33.8	31.1	34.1	34.8	36.8	4.3	12.7
2.4	33.3	35.9	38.7	32.1	36.8	7.6	12.7
8.4	34.4	35.9	38.7	32.1	36.8	11.3	11.8
22.4	37.9	21.1	26.8	32.1	36.8	5.4	10.4
27	36.5	13.9	23.1	32.1	36.8	5.4	10.4
33	37.4	12.9	22.9	31.7	35.9	5.4	10.4
29.3	37.3	12.9	22.9	31.7	35.9	2.1	10.4
32.2	35	22.4	22.9	32.5	34.4	8.7	10.4
30	33.1	11.2	22.2	32.5	34.4	8.7	10.4
24	27.7	13.4	22.2	22	23.8	8.7	10.4
24	27.7	13.4	22.2	18.5	20.6	8.7	10.4
21.5	27.7	13.4	22.2	3.6	4.9	9.8	10.4
21.5	27.7	17	22.2	3.6	4.9	0	9.8
0.6	17.5	17	22.2	3.4	3.9	13.7	16.8
13.2	17.3	20.5	22.2	2.4	3	13.7	16.8
13.2	17.3	10.7	19.8	2.4	3	13.7	16.8
13.2	17.3	18.2	19.8	2.4	3	13.7	16.8
12	16.3	18.2	19.8	0.4	2.6	39.1	44.7
2.8	14.8	17.7	19.1	25	38.6	31.3	40.5
5	17.2	17.7	19.1	19.5	43.9	31.3	40.5
7.8	15.9	16.5	17	23.5	44.4	35.1	40.5
7.8	15.9	25.6	26	46	51	35.1	40.5
21	29.3	28.1	28.6	46	51	38.7	40.5
21	29.3	24.4	28	46	51	38.7	40.5
11.5	31	26.2	27.4	40.3	45	24.5	35.9
24.4	29.7	28.1	30.9	36.6	45	28.6	35.9
24.4	29.7	26	31.6	36.6	45	28.6	35.9
24.4	29.7	26	31.6	36.6	45	28.6	35.9
24.4	29.7	29	31.6	49.7	52	28.6	35.9
24.4	29.7	29	31.6	30.5	35.7	32	35.9
24.4	29.7	28.8	39.6	30.5	35.7	32	35.9
20.3	36.2	28.8	39.6	33.7	35.7	32	35.9
20.3	36.2	28.8	39.6	33.7	35.7	33.9	37.9
20.3	36.2	38.8	44	33.7	35.7	35.6	43.1

Table 23 (continued). Bead profile data from Experiment B-2 at 144.75 h.

z	L_f	z	L_f	z	L_f	z	L_f
26.1	34.9	38.8	44	35.1	37.7	41.2	43.1
29.7	34.1	38.8	44	26.5	32	41.2	43.1
29.7	34.1	43.5	44	26.5	32	33.7	41.6
23.5	28.8	40.2	45.3	26.5	32	33.7	41.6
23.5	28.8	40.2	45.3	26.5	32	33.7	41.6
23.5	28.8	40.2	45.3	26.5	32	33.7	41.6
4.3	24.5	40.2	45.3	26.5	32	33.7	41.6
4.3	24.5	41.9	42.3	26.5	32	33.7	41.6
9.5	24	37.1	42.3	26.5	32	38.2	41.6
9.5	24	37.1	42.3	26.5	32	38.2	41.6
13.6	24.7	20.3	42.3	26.5	32	38.2	41.6
13.6	24.7	20.3	42.3	26.5	32	31.2	46.4
18.1	21.9	22	42.3	26.5	32	31.2	46.4
15.8	18.2	22	42.3	26.5	32	31.2	46.4
1.8	21.9	22	42.3	26.5	32	35.2	46.4
15.8	18.2	22	42.3	26.5	32	35.2	46.4
1.8	29	25	42.3	26.5	32	39.2	46.4
18	26.3	25	42.3	15	20.6	44.2	46.4
9.1	24.8	31.8	42.3	15	20.6	44.2	46.4
24	28.3	31.8	42.3	5.8	15.6	44.2	46.4
14.4	26.6	31.8	42.3	5.8	15.6	44.2	46.4
22.5	24.6	35.1	41.1	9.4	10.7	30.9	45.5
13.4	28.4	35.1	41.1	4.6	8.6	30.9	45.5
21	23.9	35.1	41.1	4.6	8.6	30.9	45.5
10.5	23.8	29.6	43.5	17.4	22.4	30.9	45.5
0.4	5.8	29.6	43.5	17.4	22.4	30.9	45.5
3.8	8	29.6	43.5	17.4	22.4	38.4	45.5
2.4	13	29.6	43.5	20	26.4	27.8	45.2
8.8	28.1	35.1	43.5	22	25.7	30.5	42.7
11	16.3	35.1	43.5	22.9	27.6	30.5	42.7
1.2	19	35.1	43.5	25.4	28	27.6	42.7
1.2	19	35.1	43.5	18.1	28.7	34.4	42.7
2.6	19.5	35.1	43.5	18.1	28.7	34.4	42.7
1.2	20.4	32.7	49.3	18.1	28.7	34.4	42.7
8.3	20.4	32.7	49.3	18.1	28.7	34.4	42.7
7.2	13.8	32.7	49.3	18.1	28.7	38.8	42.7
14.4	16	32.7	49.3	12.3	28.7	38.8	42.7
6.9	17.1	32.7	49.3	12.3	28.7	41.8	42.7
13.4	17.6	32.7	49.3	12.3	28.7	29.8	43.4

Table 23 (continued). Bead profile data from Experiment B-2 at 144.75 h.

z	L_f	z	L_f	z	L_f	z	L_f
9.8	17.3	32.7	49.3	13.5	19.5	29.8	43.4
9.8	17.3	32.7	49.3	17.9	19.1	29.8	43.4
9.8	17.3	32.7	49.3	23	29.2	29.8	43.4
9.8	17.3	32.7	49.3	20.1	31.6	33.1	43.4
9.8	17.3	32.7	49.3	18.7	31.7	33.1	43.4
9.8	17.3	32.7	49.3	42.2	46.6	33.1	43.4
9.8	17.3	33.5	49.1	42.2	46.6	33.1	43.4
9.8	17.3	33.5	49.1	36.8	43.5	34.2	43.4
9.8	17.3	36.6	45.7	36.8	43.5	34.8	43.4
1.6	23.4	36.6	45.7	39.3	43.6	34.8	43.4
6.9	18.6	18.3	45.3	39.3	43.6	41.8	43.4
6.9	18.6	18.3	45.3	42.1	43.6	41.8	43.4
6.9	18.6	18.3	45.3	42.1	43.6	29.8	43.4
6.9	18.6	24.6	25.6	25	34.4	29.8	43.4
10	17.7	24.6	25.6	25	34.4	29.8	43.4
14.8	18.5	1.4	14.9	25	34.4	29.8	43.4
14.8	18.5	9.3	14.5	25	34.4	33.1	43.4
15.9	16.5	9.3	14.5	25	34.4	33.1	43.4
15.9	16.5	9.3	14.5	18.1	34.4	33.1	43.4
17	18	18.1	20	18.1	34.4	33.1	43.4
18.9	19.9	21.6	24.1	21.5	34.4	34.2	43.4
19.3	22.3	1.3	10.4	18.8	34.1	34.8	43.4
19.3	22.3	21.4	22.2	18.8	34.1	34.8	43.4
25.1	28.9	19.9	22.7	25	32.7	41.8	43.4
38.8	40.7	19.9	22.7	25	32.7	41.8	43.4
44	49.8	19.9	22.7	30.5	32.7	29.1	47.6
17.2	43.8	30.2	30.7	30.5	32.7	29.1	47.6
24	48.5	30.4	32.4	33.8	34.2	29.1	47.6
24	48.5	30.4	32.4	26.5	34.2	29.1	47.6
24	48.5	30.4	32.4	26.5	34.2	27.2	47.6
24	48.5	30.4	32.4	26.5	34.2	27.2	47.6
24	48.5	30.6	31.4	26.5	34.2	27.2	47.6
24	48.5	11	17.2	23.1	34.2	33.9	47.6
24	48.5	39.5	40.3	23.1	34.2	33.9	47.6
24	48.5	39.5	40.3	23.1	34.2	33.9	47.6
24	48.5	35.7	36.8	20.7	35.6	30.7	47.6
24	48.5	16.3	17.7	20.7	35.6	30.7	47.6
24	48.5	11.5	29.2	20.7	35.6	30.7	47.6
24	48.5	11.5	29.2	20.7	35.6	34.9	47.6

Table 23 (continued). Bead profile data from Experiment B-2 at 144.75 h.

z	L_f	z	L_f	z	L_f	z	L_f
24	48.5	11.5	29.2	34.6	35.6	34.9	47.6
35.1	39.1	24.3	40.4	9	27.7	46.1	47.6
24	48.5	11.5	29.2	23.8	33.4	34.9	47.6
24	48.5	11.5	29.2	23.8	33.4	37.6	47.6
24	48.5	11.5	29.2	27	32.1	37.6	47.6
24	48.5	12.8	33.1	27	32.1	42	47.6
24	48.5	12.8	33.1	27	32.1	42	47.6
34.7	43.9	15.8	33.1	27	32.1	46.1	47.6
38.3	41.4	15.8	33.1	30.5	32.1	46.1	47.6
44.1	50.7	22.1	33.1	30.5	32.1	46.1	47.6
1.6	19.8	24.3	40.4	9	27.7	46.1	47.6
6.8	21.9	20.4	41.5	6.5	21.6	27.4	48.2
6.4	34.7	26	41.5	40.3	41.8	31.1	48.2
6.4	34.7	26	41.5	35.6	36	31.1	48.2
6.4	34.7	26	41.5	28.5	34.2	31.1	48.2
6.4	34.7	26	41.5	28.5	34.2	35.5	48.2
6.4	34.7	26	41.5	28.5	34.2	39.4	48.2
6.4	34.7	26	41.5	28.5	34.2	39.4	48.2
7.5	32.1	26	41.5	34.4	34.6	39.4	48.2
7.5	32.1	26	41.5	31.7	34.2	39.4	48.2
7.5	32.1	26	41.5	26.5	34.2	39.4	48.2
7.4	34.4	26	41.5	34	34.7	39.4	48.2
7.4	34.4	26	41.5	23.2	40.9	39.4	48.2
11.7	33.5	26	41.5	26.8	39.9	39.4	48.2
11.7	33.5	30.9	41.5	40.3	43.8	39.4	48.2
14.1	32.7	30.9	41.5	37.5	41	39.4	48.2
14.5	31	34.6	41.5	42.7	52.6	50.7	51.4
14.5	31	34.6	41.5	42.7	52.6	39.8	48.7
17.4	34	34.6	41.5	42.7	52.6	39.8	48.7
17.4	34	34.4	42.7	39.7	41.8	39.8	48.7
17.4	34	34.4	42.7	27.4	36	39.8	48.7
29	31.9	34.4	42.7	31.5	33.1	38.2	47.3
29	31.9	43.1	44.4	31.5	33.1	38.2	47.3
3.4	36.8	43.1	44.4	26.6	32.4	38.2	47.3
32.4	36.8	17.5	41.6	26.6	32.4	41.8	47.3
18.3	24.6	17.5	41.6	26.6	32.4	41.8	47.3
6.8	23.7	17.5	41.6	25.3	32.4	41.8	47.3
9.4	23.7	21.7	41.6	25.3	32.4	41.8	47.3
45.5	47.4	5.1	9.9	21.1	26.3	29.5	40.1

Table 23 (continued). Bead profile data from Experiment B-2 at 144.75 h.

z	L_f	z	L_f	z	L_f	z	L_f
9.4	23.7	21.7	41.6	21.3	32.4	41.8	47.3
11.5	23.7	32.7	37.8	18.3	29.8	41.8	47.3
5.4	10.3	32.7	37.8	26.6	29.8	45.1	47.3
5.4	10.3	27.9	40.7	26.6	29.8	45.1	47.3
3	10.2	42.1	43.4	26.6	29.8	36	45.7
24.3	31.8	42.1	43.4	26.6	29.8	36	45.7
24.3	31.8	42.1	43.4	23.9	25.1	36	45.7
24.3	31.8	19.6	37.8	15.2	25.1	36	45.7
28	32.8	2.8	36.3	15.2	25.1	40.5	45.7
28	32.8	27.2	29.9	15	21.5	40.5	45.7
1.4	12	27.2	29.9	15	21.5	40.5	45.7
23.7	27	27.2	29.9	18.3	21.5	40.5	45.7
18.3	22.3	24.8	26.2	10.1	20	37.2	49
11.9	20.9	26.4	32.1	16.9	24	37.2	49
4.6	18.8	26.4	32.1	25.3	31.9	37.2	49
7.2	17.6	26.4	32.1	36.4	41.5	37.2	49
12.3	17.3	30.5	32.5	36.4	41.5	37.6	50.4
12.3	17.3	30.5	32.5	36.4	41.5	37.6	50.4
10.7	19.5	30.5	32.5	36.4	41.5	37.6	50.4
10.7	19.5	33.9	34.4	36.4	41.5	37.6	50.4
13.8	25.7	19.3	34.2	36.4	41.5	40.4	50.4
20.6	25.7	32	32.5	36.4	41.5	40.4	50.4
20.6	25.7	35.5	35.9	36.4	41.5	35.7	44.7
24	25.7	29	39.8	36.4	41.5	35.7	44.7
10.6	23.6	29	39.8	36.4	41.5	35.7	44.7
10.6	23.6	29	39.8	36.4	41.5	35.7	44.7
10.6	23.6	29	39.8	36.4	41.5	40.8	44.7
16.2	24.4	29	39.8	36.4	41.5	40.8	44.7
37.4	51.5	33.3	39.8	36.4	41.5	40.8	44.7
37.4	51.5	33.3	39.8	36.4	41.5	36.6	45.7
37.4	51.5	25.4	39.8	36.4	41.5	36.6	45.7
42.6	52.5	25.4	39.8	36.4	41.5	36.6	45.7
42.6	52.5	25.4	39.8	36.4	41.5	43.3	45.7
43.6	54.6	25.4	39.8	24.4	41.3	43.3	45.7
43.6	54.6	27.7	39.8	24.4	41.3	43.3	45.7
46.4	53.4	27.7	39.8	24.4	41.3	43.3	45.7
49.2	52.4	24.7	38.5	24.4	41.3	44.4	46.8
49.2	52.4	31.4	38.5	24.4	41.3	50.2	51.4
40.7	53.4	31.4	38.5	24.4	41.3	37.3	42.6

Table 23 (continued). Bead profile data from Experiment B-2 at 144.75 h.

z	L_f	z	L_f	z	L_f	z	L_f
49.2	52.4	28.8	37.7	24.4	41.3	37.3	42.6
49.2	52.4	28.8	37.7	24.4	41.3	37.3	42.6
40.7	53.4	22	37.2	24.4	41.3	42.2	54
51.1	54.2	22	37.2	24.4	41.3	29.2	49.4
51.1	54.2	22	37.2	24.4	41.3	36.5	46.8
46.4	54	22	37.2	24.4	41.3	36.5	46.8
46.4	54	22	37.2	24.4	41.3	36.5	46.8
49.5	54	22	37.2	24.4	41.3	39.8	46.8
49.5	54	22	37.2	24.4	41.3	39.8	46.8
55.8	56.6	22	37.2	8.7	41.3	41.6	46.8
47.9	56.6	22	37.2	15.8	36.6	41.6	46.8
54.1	56.2	29.4	37.2	15.8	36.6	41.6	46.8
54.1	56.2	29.4	37.2	15.8	36.6	32.6	44.4
54.1	56.2	29.4	37.2	15.8	36.6	23.4	42.4
54.1	56.2	29.4	37.2	15.8	36.6	23.4	42.4
54.1	56.2	21.5	43.6	22	36.6	38.5	42.4
50.4	53.5	21.5	43.6	22	36.6	33.1	37.2
49.5	52	21.5	43.6	22	36.6	36.4	36.9
46.4	50.9	21.5	43.6	22	36.6	36.4	36.9
43	49.2	19.1	43	22	36.6	12	37.6
34.2	37.3	19.1	43	22	36.6	12	37.6
28	38.4	19.1	43	26.8	36.6	45.9	54.9
34.8	36.5	19.1	43	26.8	36.6	45.9	54.9
34.8	36.5	25.3	43	26.8	36.6	58.7	59.2
3.3	12.4	25.3	43	31	36.6	31.5	42.2
3.3	12.4	25.3	43	31	36.6	31.5	42.2
9.2	12.4	27.6	44.3	31	36.6	26.1	38.8
9.2	12.4	25.7	45.5	26.5	29.7	26.1	38.8
9.2	12.4	25.7	45.5	26.5	29.7	1	38.8
9.2	12.4	30.3	45.4	26.5	29.7	1	38.8
13	15	17.6	34.8	26.5	29.7	6.8	22.8
2	19.4	17.6	34.8	17.5	27.4	6.8	22.8
2	19.4	17.6	34.8	17.5	27.4	13	22.8
2	19.4	17.6	34.8	17.5	27.4	13	22.8
2	19.4	8.8	21.7	14	27.4	13	22.8
10.8	19.4	9.9	18.5	14	27.4	13	22.8
10.8	19.4	9.9	18.5	14	27.4	13	22.8
10.8	19.4	9.9	18.5	14	27.4	13	22.8
10.8	19.4	13.4	18.5	11.4	27.4	10.9	22.8

Table 23 (continued). Bead profile data from Experiment B-2 at 144.75 h.

z	L_f	z	L_f	z	L_f	z	L_f
10.8	19.4	13.4	18.5	10.4	27.4	10.9	22.8
10.8	19.4	15	18.5	21.6	23	10.9	22.8
10.8	19.4	15	18.5	21.6	23	10.9	22.8
10.8	19.4	17.6	18.5	18.7	23	0.9	22.8
17.6	19.4	15.8	18.3	2.1	19.9	16.5	22.8
17.6	19.4	15.8	18.3	7	7.7	16.5	22.8
7.7	21.2	15.8	18.3	7	7.7	16.5	22.8
7.7	21.2	15.8	18.3	7	7.7	16.5	22.8
25	26.8	15.8	18.3	1.8	7.5	16.5	22.8
23.4	27.3	15.8	18.3	1.8	7.5	16.5	22.8
22.5	31.4	3	19.3	1.8	7.5	16.5	22.8
29.3	31	3	19.3	1.8	7.5	16.5	22.8
28	40.1	3	19.3	1.8	7.5	16.5	22.8
28	40.1	3	19.3	5.3	6.5	16.5	22.8
13	29.9	3	19.3	5.3	6.5	16.5	22.8
9.6	30.8	3	19.3	5.3	6.5	16.5	22.8
9.6	30.8	3	19.3	5.3	6.5	16.5	22.8
27.5	29.9	3	19.3	5.3	6.5	16.5	22.8
27.5	29.9	3	19.3	6.1	6.4	15.1	22.2
26.5	27.9	3	19.3	6.1	6.4	15.1	22.2
26.5	27.9	9.2	19.3	6.1	6.4	8.7	20.7
16.5	27.7	9.2	19.3	3.8	6.4	8.7	20.7
25.3	27.7	9.2	19.3	3.8	6.4	8.7	20.7
25.3	27.7	9.2	19.3	4.8	6.4	8.7	20.7
21.6	27.7	9.2	19.3	26.4	33.6	8.7	20.7
21.6	27.7	9.2	19.3	34.6	38.2	16.8	20.7
19.7	21.8	9.2	19.3	34.6	38.2	16.8	20.7
19.7	21.8	9.2	19.3	34.6	38.2	16.8	20.7
19.7	21.8	9.2	19.3	34.6	38.2	16.8	20.7
19.7	21.8	9.2	19.3	34.6	38.2	16.8	20.7
13.6	20.8	9.2	19.3	34.6	38.2	13.8	21.6
13.6	20.8	9.2	19.3	34.6	38.2	13.8	21.6
12.4	21	9.2	19.3	34.6	38.2	13.8	21.6
12.4	21	9.2	19.3	34.6	38.2	13.8	21.6
12.4	21	9.2	19.3	34.6	38.2	13.8	21.6
12.4	21	9.2	19.3	34.6	38.2	13.8	21.6
9	21	9.2	19.3	30	38.2	13.8	21.6
17.5	20.6	9.2	19.3	30	38.2	25.6	29.1
12.6	27.4	15.6	18.6	30.4	38.7	29.2	32.4

Table 23 (continued). Bead profile data from Experiment B-2 at 144.75 h.

z	L_f	z	L_f	z	L_f	z	L_f
6.3	29.7	15.6	18.6	30.4	38.7	26.8	28.4
43.1	55.7	17.4	18.6	37.4	38.7	26	26.4
38.4	51.6	17.4	18.6	37.4	38.7	26	26.4
30.8	40.7	10.7	18.6	37.4	38.7	26	26.4
17.4	36.4	10.7	18.6	37.4	38.7	26	26.4
16.3	37.9	10.7	18.6	34.4	37.8	26	26.4
16.3	37.9	10.7	18.6	34.4	37.8	23.5	30
16.3	37.9	9.1	18.6	16.9	37.7	23.5	30
16.3	37.9	9.1	18.6	30.4	37.7	23.5	30
16.3	37.9	15.4	25	33.2	37.7	23.5	30
16.3	37.9	15.4	25	33.2	37.7	23.5	30
16.3	37.9	15.4	25	36.9	37.7	23.5	30
16.3	37.9	15.4	25	36.9	37.7	23.5	30
16.3	37.9	15.4	25	31.3	37.7	29.5	30
16.3	37.9	15.4	25	31.3	37.7	29.5	30
16.3	37.9	15.4	25	33.8	37.7	22.9	28.7
16.3	37.9	15.4	25	33.8	37.7	22.9	28.7
16.3	37.9	15.4	25	37.3	37.7	28.2	28.7
16.3	37.9	15.4	25	36.6	39.1	28.2	28.7
16.3	37.9	15.4	25	36.6	39.1	3.2	21.6
16.3	37.9	22.3	25	37.5	41.4	2.7	25.6
16.3	37.9	22.3	25	37.5	41.4	2.7	25.6
16.3	37.9	26.4	26.8	25.1	38.9	2.7	25.6
16.3	37.9	26.7	29.6	16.7	38.9	0	13.8
21.1	37.2	19.4	29.6	28.4	40	14.4	18.4
21.1	37.2	29.6	30.1	28.4	40	15.3	17.8
24.4	37.2	29.6	30.1	28.4	40	15.3	17.8
24.4	37.2	22.1	29.6	28.4	40	15.3	17.8
24.4	37.2	22.1	29.6	28.4	40	15.3	17.8
24.4	37.2	22.1	29.6	32.7	40.4	27	34
29.6	37.2	22.1	29.6	32.7	40.4	31.5	34
29.6	37.2	13.7	29.6	28.8	36	31.5	34
29.6	37.2	13.7	29.6	28.8	36	31.5	34
31	37.2	13.7	29.6	7.8	34.1	31.5	34
13.2	33.7	16.9	29.6	22.4	38.4	31.5	34
17.2	36.6	16.9	29.6	22.4	38.4	31.5	34
34	41.8	16.9	29.6	35.8	36.2	25.9	32
34	41.8	16.9	29.6	21.1	25.9	31.6	32
34	41.8	16.9	29.6	21.1	25.9	2.6	11.5

Table 23 (continued). Bead profile data from Experiment B-2 at 144.75 h.

z	L_f	z	L_f	z	L_f	z	L_f
34	41.8	16.9	29.6	21.1	25.9	6.7	7.1
34	41.8	16.9	29.6	4.3	25.4	4.1	26.1
39.5	42.2	21.6	29.6	20.7	23.7	9.5	22.8
39.5	42.2	21.6	29.6	21.8	23.7	18.8	22.9
39.5	42.2	21.6	29.6	21.1	23.7	18.8	22.9
39.5	42.2	21.6	29.6	25.7	27	18.8	22.9
42.2	43.3	21.6	29.6	25.7	27	15.7	25.1
42.2	43.3	21.6	29.6	24.3	27	24	25.1
42.2	43.3	21.6	29.6	24.3	27	24	25.1
42.7	47.7	27.7	29.6	21.9	26.1	20.5	33
42.7	47.7	27.7	29.6	27.8	28.6	25.2	33
37.7	52	20.8	29.4	27.8	28.6	25.2	33
34.9	53.2	20.8	29.4	27.8	28.6	25.2	33
34.9	53.2	20.8	29.4	18.1	28.6	25.2	33
34.9	53.2	20.8	29.4	28.6	30.3	25.2	33
33.3	53.2	20.8	29.4	30.8	31	25.2	33
33.3	53.2	16.9	28.9	16.1	30.3	28.4	33
33.3	53.2	16.9	28.9	31.6	32.1	28.4	33
31.1	53.2	16.9	28.9	32.1	33.6	28.4	33
29.4	54.5	16.9	28.9	32.1	33.6	32.3	33
29.4	54.5	16.9	28.9	31	32.2	24.7	29.5
29.4	54.5	16.9	28.9	31	32.2	28.2	29.5
29.4	54.5	16.9	28.9	27	32.2	28.2	29.5
29.4	54.5	16.9	28.9	16	31.5	8	8.6
40	59.6	22.6	28.9	23.7	26.6	13.9	16.1
40	59.6	22.6	28.9	23.7	26.6	13.9	16.1
50.5	60.3	22.6	28.9	23.7	26.6	13.9	16.1
25	54.6	22.6	28.9	23.7	26.6	13.9	16.1
25	54.6	22.6	28.9	23.7	26.6	13.9	16.1
25	54.6	22.6	28.9	23.7	26.6	13.9	16.1
25	54.6	22.6	28.9	23.7	26.6	19.8	24.2
29.3	54.6	22.6	28.9	23.7	26.6	19.8	24.2
29.3	54.6	22.6	28.9	23.7	26.6	19.8	24.2
29.3	54.6	22.6	28.9	23.7	26.6	19.8	24.2
29.3	54.6	22.6	28.9	12	15.2	19.8	24.2
34.6	54.6	22.6	28.9	6.1	16.3	19.8	24.2
34.6	54.6	22.6	28.9	31.6	33.1	19.8	24.2
34.6	54.6	17.8	33.1	5.2	32.2	19.8	24.2
34.6	54.6	17.8	33.1	5.2	32.2	19.8	24.2

Table 23 (continued). Bead profile data from Experiment B-2 at 144.75 h.

z	L_f	z	L_f	z	L_f	z	L_f
36.2	47.4	32	33.1	3.2	34.1	19.8	24.2
36.2	47.4	32	33.1	3.2	34.1	19.8	24.2
36.2	58	31.4	36.6	3.2	34.1	28	28.4
48.8	58	10.4	22	33.5	34.1	6	34.3
48.8	58	10.4	22	33.5	34.1	6	34.3
48.8	58	20.6	31.9	0.3	34.5	6	34.3
48.8	58	20.6	31.9	21.9	33.5	6	34.3
50.8	55.8	31.5	33.2	21.9	33.5	6	34.3
34.8	44.9	31.5	33.2	1.2	33.3	6	34.3
34.8	44.9	14.2	17	10	33.3	6	34.3
34.8	44.9	14.2	17	36	40.3	6	34.3
34.8	44.9	12.6	18.9	36	40.3	6	34.3
34.8	44.9	18	18.9	36	40.3	0.8	33.1
34.8	44.9	22.8	29.4	36	40.3	0.8	33.1
34.8	44.9	27.1	29.4	28.2	35.7	7.5	33.1
34.8	44.9	28.5	33.3	28.2	35.7	7.5	33.1
34.8	44.9	34.8	36.7	20.8	27.8	31.6	33.1
34.8	44.9	24.5	37.5	20.8	27.8	21.1	26.3
26.1	27.8	21.1	26.3	34.4	48	13.7	14.2
20.1	23.1	8	25.4	46.7	48	3.8	27
20.1	23.1	8	25.4	27.6	50.8	3.8	27
20.1	23.1	8	25.4	27.6	50.8	25.9	31.8
18.2	24.5	8	25.4	26.3	50.3	18.5	28.3
18.2	24.5	14.7	25.4	26.3	50.3	15.6	25.9
18.9	23	22.6	27.6	26.3	50.3	15.6	25.9
18.9	23	20.3	26	37.5	42.4	30	30.6
16.9	22.5	20.3	26	37.5	42.4	43.6	46.3
4.4	22.5	20.3	26	37.5	42.4	52	53.5
21.8	22.6	20.3	26	37.5	42.4	34.5	52.5
18.1	20.5	20.3	26	40.3	42.4	29.3	50.4
18.1	20.5	20.3	26	40.3	42.4	12.3	21.9
24.1	26	21.1	23.4	40.3	42.4	12.3	21.9
24.1	26	16	25.6	38	38.5	14	17.1
23.8	26.7	15.3	15.7	33.1	33.6	25.6	27.8
23.8	26.7	9	13.9	29.1	35.2	10.2	29.1
25.3	26.4	10.5	11.3	8	11	5	26.8
21.1	22.2	8.4	9.7	6.1	9.6	10.6	24.4
17.5	19.4	8.4	9.7	7.5	8	12.3	15.7
17.5	19.4	13.5	24.3	4.5	8.9	3.1	23.2

Table 23 (continued). Bead profile data from Experiment B-2 at 144.75 h.

z	L_f	z	L_f	z	L_f	z	L_f
13.8	16.1	16.7	24.5	5.6	10.6	3.1	23.2
6.7	10.5	22	26.1	4.5	8.9	10	23.2
6.7	10.5	24.4	26.3	5.6	10.6	14.2	21.9
6.7	10.5	24.4	26.3	8.4	10.2	14.2	21.9
9.4	10.7	25.6	27	12.2	16.5	22.8	24.8
9.4	10.7	25.6	27	12.2	16.5	22.8	24.8
0	6.8	25.6	27	12.2	16.5	22.9	26.2
2.3	6.8	24.7	28.8	8.9	16.6	29	29.8
4.5	6.8	22.4	22.9	8.9	16.6	6.5	30.6
4.5	6.8	4.6	22	8.9	16.6	6.5	30.6
5.4	23	4.6	22	13.2	16.6	14.4	30.6
28	33.3	1.3	16.6	6.1	19.8	26.4	27.4
28	33.3	4.3	16	6.1	19.8	11.2	26.9
30	33.3	4.3	16	6.1	19.8	9.9	25.6
30.8	32.9	4.3	16	7.3	21.8	25.1	25.6
30.8	32.9	2	16	10.9	18.3	31.8	33.2
30.8	32.9	7.7	15.6	6.6	17.7	12	32.2
30.8	32.9	7.7	15.6	0.9	5.8	29.3	30.6
33.4	46.2	14	15.6	0.9	5.8	16.2	37.4
33.4	46.2	14	15.6	14.5	23.2	16.2	37.4
33.4	46.2	14	15.6	14.5	23.2	26.2	28.3
36.6	46.2	4.3	11.8	21.1	26.3	26.2	28.3
36.6	46.2	4.3	11.8	21.1	26.3	11.3	24.3
37.7	46.2	14.2	16.6	21.1	26.3	2.7	17.5

Table 24. Bead profile data from Experiment B-2 at 168.6 h. Symbols are as described in Figure 3. The data are presented in Figure 8. Distances are in μm.

z	L_f	z	L_f	z	L_f	z	L_f
11.3	28.3	14.6	20	39.5	99.8	27.7	78.8
11.2	31.8	14.9	20	41.5	99.8	27.7	78.8
30.7	40.6	13.2	27.6	44.6	99.8	27.7	78.8
8.4	37.5	13.2	27.6	59.9	99.8	30.7	78.8
6.5	26.8	14.8	27.6	58	99.7	30.7	78.8
7.4	34	14.8	27.6	38.6	99.6	32.2	78.8
3.6	36	17	27.6	19.8	97	34.5	78.8
5	36	17	27.6	0.6	77.2	34.4	78.8
2.6	17.4	18.5	27.6	31.5	100.2	38	78.8
9.7	17.3	20.1	24.9	100.3	101.2	39.9	78.8
11	22.4	0.4	24.1	28.6	101.2	39.9	78.8
4.8	27.5	19.4	21.1	28.6	101.2	43	78.8
11.2	34.1	19.4	21.1	32.6	101.2	49.3	78.1
13.9	34.1	15.2	19.5	36.8	101.2	52	78.1
13.9	34.1	12.6	22.2	62	101.2	42.4	79.3
16.4	30.7	0.6	21.3	65.3	101.2	44.5	79.3
16.4	30.7	6.9	21.3	101.2	101.2	44.5	79.3
16.4	30.7	8.8	21.3	18	98.1	46.9	79.3
22.6	47.2	17.7	21.1	18.7	98.1	47.9	79.3
2.3	37.8	23.5	32.4	18.7	98.1	48.6	79.3
2.1	18.2	23.5	32.4	21.3	98.1	48.6	79.3
2.6	37.9	10.9	34.8	69.4	98.1	48.6	79.3
2.4	18.6	0.9	9.9	72.1	103.9	50.5	79.3
17.2	49.3	3.4	8.6	72.1	103.9	51.6	79.3
1.6	27.1	7.1	12	74.2	103.9	51.1	79.3
13.1	50.6	0.5	32.1	78.7	103.9	4.1	87
36.4	44	0.6	24.7	80.2	103.9	8.3	45.1
36.4	44	0.6	24.7	19.3	110	7.1	52.3
35	61.8	2.4	19.2	19.3	110	16.1	60.6
0.5	44.9	4.4	19.2	35.5	110	35.1	55.8
16.7	111.8	15.8	29	42.2	110	38.6	61
2	35.5	8.1	31	1.8	110	34.3	63
14.8	35.9	11.9	31	10.4	110	22.5	54.5
11.8	33.7	11.9	31	9.6	48.3	28	65.2
17.3	33.7	14.2	31	43.5	48.3	22.6	43.9
12.8	33.9	14.2	31	6.4	65.6	21	43.7

Table 24 (continued). Bead profile data from Experiment B-2 at 168.6 h.

z	L_f	z	L_f	z	L_f	z	L_f
0.2	54.8	16.4	31	5.4	65.6	21	43.7
11.4	58	8.8	33.9	7.8	65.6	19.6	43.7
11	45.6	12.7	26	9.9	65.6	22.8	43.7
12.8	52.4	25.4	30.2	10.1	65.6	22.8	43.7
14.6	52.4	4.6	27.6	57	63.2	14.9	41.3
14.6	52.4	4.4	31.4	47.2	74.3	14.9	41.3
11.8	44.7	3.4	48	50.8	74.3	19.5	41.3
39.9	63.9	17.8	35.8	50.8	74.3	21.3	41.3
39.9	63.9	23.4	35.8	52.7	74.3	22.4	41.3
48.5	68.2	23.4	35.8	54.8	74.3	23.8	45.8
48.5	68.2	25.6	35.8	46	72.2	14.1	57.6
46.9	67.4	25.6	35.8	44.1	72.2	14.1	57.6
46.9	67.4	27.6	35.8	47.8	72.2	21.1	57.6
48.1	67.4	27.6	35.8	47.8	72.2	21.1	57.6
8	100.9	27.6	35.8	49.9	72.2	21.1	57.6
9.9	104.6	18	43.6	7.9	91.3	23.2	57.6
75	113.4	18	43.6	3.5	96.7	23.2	57.6
69.7	114.5	20.6	43.6	8	96.6	24.6	57.6
76.3	114.5	20.6	43.6	7.6	127.1	58.4	101.6
79.4	114.5	14.9	43.9	10.5	127.1	60.5	101.6
84	114.5	6.5	27.3	10.5	127.1	58.2	100.6
67.1	114.5	15.3	58.2	13.6	127.1	58.2	100.6
66.1	112.7	1.6	57	13.6	127.1	49.9	103.8
83.9	112.7	0.3	57	15.5	127.1	14.2	115.9
13.3	112.7	25.8	52.4	13.2	127.1	89.9	141.4
13.3	112.7	17.7	66.5	13.2	127.1	92.2	141.4
14.9	112.7	0	16.8	30.6	127.1	119.4	141.4
95.2	111	0	16.8	47.3	121.5	120.1	141.4
90.7	114.4	1	16.8	12.6	128.3	125.9	141.4
97.3	114.4	1	16.8	27.6	127.5	135.6	141.4
94	114.4	3.7	19.9	27.6	127.5	91.8	142.6
96.1	111.8	0.7	25.8	20.9	128.9	91.8	142.6
99	110.9	15	48.8	24.1	139.3	93.7	142.6
102	110.9	16	48.8	26.2	139.3	132.7	142.6
29.2	103.8	23.4	37.7	26.2	139.3	132.7	142.6
23.5	103.8	12.5	61.6	28	139.3	87.2	132.9
25.7	103.8	1.1	60.2	30.3	139.3	87.2	132.9
8.6	99.1	29.2	60	32	139.3	87.2	132.9
30.9	107.2	24.7	53.9	32	139.3	90.6	132.9

Table 24 (continued). Bead profile data from Experiment B-2 at 168.6 h.

z	L_f	z	L_f	z	L_f	z	L_f
31.7	107.2	27.4	53.9	21.8	140.5	96.6	132.9
29.2	107.2	17.9	46.8	26.7	140.5	96.6	132.9
21.4	95.3	19.4	46.8	3	78.5	97.6	132.9
3.7	95.8	22	46.8	31.6	54.2	97.6	132.9
39.5	95.8	21.4	46.8	30.9	52.2	83.3	116
42.1	95.8	28.8	46.8	35.8	52.6	86	116
39.7	71.9	31.8	46.8	32.4	72.6	86	116
20.8	98.3	33.1	46.8	5.6	45.3	82.2	116
22.3	108.4	35.1	46.8	1.8	53.7	86	116
24.9	108.4	2.3	44.6	6.2	42.1	17.6	49.4
26.8	108.4	6.3	50.5	12.8	34.7	22.1	57.3
20.7	108.4	51.8	83	18.9	32.9	26.5	57.3
13.9	108.9	51.8	83	2.6	33.1	28.2	57.3
47.6	108.9	53.6	83.7	3.6	20.6	28.2	57.3
19.2	108.6	46.5	83.7	30.6	69.2	23	57.2
16.5	101.8	46.5	83.7	3.2	62.1	25.1	56.9
30.5	100.7	54.7	83.7	34	59.6	27.3	56.9
3.4	35	62.1	83.7	2.2	58.2	27.3	56.9
6.3	36.6	69.2	89.2	29.7	56.3	27.3	56.9
51.5	79.7	37.5	88.7	10.5	45.7	32.2	56.9
53.6	81.6	0.3	36.6	35.7	54.6	22.7	57.4
21.7	59.8	16.5	31.2	10.7	45.8	26.2	55.6
7.6	66.4	13	28.5	29.3	45.8	27.3	55.6
29.7	76.8	7.9	36.5	31	45.8	9.5	73.1
16.2	59.6	1.1	30.7	31	45.8	6.2	83.9
43	79	82.7	90	1.8	44.3	4.4	60.1
8.1	60.1	57	82.5	22.8	32.8	24.2	94
48.2	92.9	39.3	86.6	0.5	29.2	24.2	94
50.9	92.9	36.4	86.6	26.7	39.6	35.4	94.8
50.9	92.9	39.4	86.6	12	33	10	98.4
53.6	92.9	43.3	86.6	14.3	33	8.1	40.6
58.8	59.8	20	91.6	2.3	22.5	16.6	39.3
25.4	52.5	20	91.6	2.5	18.2	19.3	39.3
12	62.8	20.7	91.6	0	21.1	19.3	39.3
13.9	62.8	24.6	91.6	12	20.6	16.9	50.2
1	61.4	18.5	86.9	14.8	40.9	19	50.2
3.4	61.4	20.3	86.9	22.9	40.9	21.1	61.6
6.8	63.2	20.3	86.9	21.6	35.5	22.6	61.6
3.9	29.8	21.9	86.9	0.5	31.4	22.6	61.6

Table 24 (continued). Bead profile data from Experiment B-2 at 168.6 h.

z	L_f	z	L_f	z	L_f	z	L_f
74.4	96.9	24.6	86.9	4.2	28.1	21.2	61.6
29.2	97.1	19.8	85.7	11.2	45.9	21	42.7
36.8	98.4	21.5	85.7	2.1	26.7	21	42.7
38.1	98.4	22.8	85.7	7.5	28.4	7.3	31.4
38.1	98.4	24.2	85.7	12.1	18.1	8.6	31.4
40.5	98.4	26.2	85.7	13.9	18.1	6.1	20.7
42.9	98.4	26.5	85.7	16.7	18.1	8.4	20.7
42.9	98.4	27.4	85.7	11	14.8	10	28.4
24.6	98.4	30.1	85.7	10.7	19.3	36.8	41
59.4	98.4	24	78.8	12.8	19.3	3.8	41
32.8	99.8	25.9	78.8	12.9	18.3	26.4	46.1
10.8	29.7	14.2	31	6.4	65.6	21	43.7
48.1	91.6	22.3	86.9	4.8	24	21.2	61.6
36.4	99.8	27.7	78.8	14.5	18.3		

Table 25. Bead profile data from Experiment B-3 at 120.05 h. Symbols are as described in Figure 3. The data are presented in Figure 10. Distances are in μm.

z	L_f	z	L_f	z	L_f	z	L_f
24.6	26	32.7	46.4	30.8	34.4	53.7	55.6
25.8	26.2	32.8	46.4	31.7	34.4	55.1	55.6
25.8	26.2	35.3	46.4	33.0	34.4	38.7	39.1
30.0	31.6	36.5	46.4	32.8	33.2	38.2	38.7
33.0	34.3	37.4	46.4	33.4	34.8	38.2	38.7
34.1	34.3	37.8	46.4	34.4	34.8	36.8	37.1
35.4	35.8	38.6	46.4	35.8	36.2	36.8	37.1
35.4	35.8	34.4	42.1	37.8	39.0	36.4	36.9
33.8	34.2	32.7	33.1	38.4	39.0	8	36.6
28.8	33.6	32.1	33.5	38.4	39.0	9.3	36.6
29.5	33.6	33.1	33.5	38.6	39.0	11.3	36.6
30.4	31.8	30.8	31.2	29.0	32.4	12.6	36.6
29.6	31.8	51.8	53.5	30.4	32.4	14.6	36.6
29.6	31.8	52.1	53.5	31.7	32.1	36.2	36.6
28.2	30.6	52	53.6	32.2	32.6	36.2	36.6
26.5	30.2	53.2	53.6	38.8	39.2	33.8	35.3
27.6	30.2	28.2	28.7	40.0	40.4	32.2	35.1
28.5	30.2	25.8	30.4	40.0	40.4	33.8	35.1
28.7	30.2	29.2	30.4	37.2	37.6	33.6	35.4
29.8	30.2	28.7	30.4	35	35.4	34.9	35.4
38.2	38.6	30	30.4	36.2	36.6	34.9	35.4
36.4	36.8	29	29.4	29.8	31.5	33.9	34.3
36.4	36.8	29	29.4	30.1	31.5	18.1	22
36.4	36.8	26	26.4	30.1	31.5	18.8	22
35.8	36.8	26	26.4	31.1	31.5	19.2	22
31.9	35.4	21.2	22.2	31.1	31.5	19.4	22
31.9	35.4	21.2	22.2	31.8	32.2	18	18.4
34.0	35.4	33	33.4	32.8	33.2	30.4	30.9
35.0	35.4	37.7	48.2	32.8	33.2	32.1	32.5
25	26.6	33.1	45.7	32.7	33	34.9	35.3
27.6	28.0	46	46.5	32.7	33	34.9	35.3
31.3	34.4	45.8	48.2	32.7	33	32.2	32.6
42.2	42.6	54	54.4	28.9	46.1	32.9	39.2
43	43.4	54.9	56	38.6	46.1	28.7	40.4
36.7	37.1	55.6	56	38.6	46.1	29.7	40.4
37.4	38.4	30	55.6	37.7	46.1	29.7	40.4

Table 25 (continued). Bead profile data from Experiment B-3 at 120.05 h.

z	L_f	z	L_f	z	L_f	z	L_f
32	34.4	47	48.2	26.4	27.9	26.2	26.6
33.0	34.4	47.8	48.2	26.8	27.9	31.4	31.8
34.0	34.4	32.2	50.5	27.5	27.9	35.9	37.6
34.0	34.4	50	50.5	38.8	39.2	37.1	37.6
34.7	35.1	33.5	54.5	38	38.4	36.6	37.4
35.8	36.2	32.1	54.5	39	39.7	22.1	35
26.8	27.2	33	54.5	26.3	32.3	22.1	35
54.8	55.4	52.5	54.5	31.9	32.3	24	35
54.8	55.4	56.9	57.3	11.2	24.6	28	35
39.6	41.6	57.9	58.3	16.2	24.6	28	35
39.6	41.6	59.4	59.8	17.5	24.6	31	35
40.6	41.6	60	60.4	21.9	24.6	23.5	24
41.2	41.6	63.3	63.8	23.4	23.8	23.2	25.4
28.6	29.0	70.2	71.5	24.4	24.8	24.9	25.4
30.4	30.8	44.3	44.7	23.8	24.2	24	24.6
30.4	30.9	44.3	44.7	19.1	19.5	24.5	25
30.4	30.9	32.9	45.6	19.3	19.7	33.1	34.5
27.4	27.8	45.1	45.6	13.3	22.4	33.2	36.3
22.6	24	44.6	45.1	19.7	22.4	33.2	36.3
23.3	24	30	44.1	19.7	22.4	35.5	36.3
23.6	24	30	44.1	20.9	22.4	35.8	36.3
24.4	24.8	30.9	44.1	20.9	22.4	32.6	36.7
25.4	25.9	31.6	44.1	20.9	22.4	33.8	36.7
25.4	25.9	32.4	44.1	22.0	22.4	34.6	36.7
29.2	29.6	34.2	44.1	26.0	31.7	35.6	36.7
29.0	29.4	28.7	41	27.6	31.7	35.6	36.7
28.1	28.9	27.2	27.6	30.8	31.7	36.3	36.7
28.7	29.1	27.2	27.6	30.8	31.7	36.3	36.7
28	28.5	28	28.4	31.3	31.7	26	31.2
28	28.5	39.7	40.1	27.3	33.0	30.7	31.2
27.2	28.5	25	25.4	28.0	33.0	30.7	31.2
27.5	29.5	23.2	25.3	31.2	33.0	23.1	23.6
28.2	29.5	24	25.3	32.0	33.0	18	40.6
28.3	29.5	36.3	41.2	32.0	33.0	23	44.5
29.1	29.5	37.1	41.2	32.6	33.0	23.9	44.5
32.6	33.1	42.2	45.9	30.8	31.2	21.6	43.4
32.6	33.0	45.5	45.9	30.8	31.2	20.9	42.8
34.4	35.5	36.3	41.3	28.3	28.7	24.8	25.3
35.3	35.7	26.8	27.2	28.3	28.7	24.8	25.3

Table 25 (continued). Bead profile data from Experiment B-3 at 120.05 h.

z	L_f	z	L_f	z	L_f	z	L_f
33.4	35.8	28	28.4	29.8	30.2	23.9	24.4
34.2	35.8	28.6	30	29.8	30.2	18.8	19.2
35.4	35.8	29.6	30	22.6	23	15.9	16.4
33.4	34.4	29.7	30.1	23.6	24	17.2	17.7
34.0	34.4	30.4	30.8	23.8	24.6	20.2	20.7
34.2	34.8	29.1	29.5	24.2	24.6	22.9	23.3
32.8	33.2	28.6	29.7	24.2	28.8	24.6	26
19.6	20.0	31.7	32.1	28.2	28.6	25.6	26
43	43.4	34.6	36.8	29.4	30.4	23.1	24.5
43	43.4	33.9	36.2	30.9	31.5	24	24.5
46.4	46.75	30.5	31	30.2	30.6	25.5	26
60.0	60.6	39	39.4	20.8	24.3	24.7	26
57.7	58.1	39	39.4	25.2	26.5	25.6	26
56.8	58.1	39.9	40.3	28.1	28.5	23.3	23.7
57.8	59.6	39.8	40.2	21.4	21.8	22.6	23
59.0	59.6	39.8	40.2	25.8	26.3	22.2	22.7
59.2	59.8	34.2	36.6	29.4	29.8	20.8	21.2
15.4	59.2	34.8	36.6	25.4	27.8	25.7	26.6
21.1	59.2	35.7	36.6	27.4	27.8	28	28.4
59.4	59.8	36.2	36.6	27.4	27.8	26.7	28.8
58.3	59.2	37.1	37.5	27.4	27.8	26.7	28.8
59	59.5	32	34.4	28	28.4	26.7	28.8
22.4	59.7	32.9	34.4	28.2	28.6	26.9	28.8
24.4	59.7	33.9	34.4	27.9	29.6	26.9	28.8
24.4	59.7	33.9	34.4	27.9	29.6	27.8	28.8
29	59.7	34.8	35.2	28.3	29.6	28.4	28.8
48.8	59.7	34.8	35.2	28.3	29.6	26.9	27.4
55.8	59.7	35.8	36.2	29.2	29.6	27.4	27.8
56.8	57.8	37.4	37.8	31.6	32.0	26.8	27.2
56.8	57.8	37.4	37.8	33.3	34.4	21.8	22.3
55.8	57.8	34.7	35.1	34.0	34.4	22.5	23
54.2	57.8	34.2	34.7	33	33.8	23.4	23.9
54.2	57.8	36.9	37.3	33.4	33.8	31.6	32
54.4	59.2	37.5	38.9	33.6	34.0	31.5	31.9
54.3	59.2	38.3	38.7	31.1	31.5	32.8	33.2
58.8	59.2	36.6	39.6	13.6	15.5	27.7	30.1
57.4	62.0	22.4	25.4	13.6	15.5	28.5	30.9
57.4	62.0	26.1	28.2	15.1	15.5	30.4	30.9
60.9	62.0	27.8	28.2	15.1	15.5	33.2	33.7

Table 25 (continued). Bead profile data from Experiment B-3 at 120.05 h.

z	L_f	z	L_f	z	L_f	z	L_f
61.6	62.0	27.2	27.6	23.9	24.3	34.8	35.3
60.8	61.2	28.4	29.7	26.7	27.1	33.6	35.1
60.8	61.2	29.3	29.7	26.7	27.1	34.6	35.1
60.7	63.0	29	29.4	26.8	27.2	35.7	36.2
62.5	63.0	24.5	25	25.5	25.9	35.1	36.3
59.9	61.6	26.1	26.5	21.9	23.8	35.1	36.3
61.2	61.6	26.1	26.5	23.4	23.8	35.8	36.3
61.2	61.6	35.8	37.1	24.5	26	31.7	34.3
61.2	62.9	36	37.1	25.6	26	33.1	34.3
62.5	62.9	36.4	36.8	32.4	43.8	34.3	34.8
62.5	62.9	36.7	37.1	38.9	39.3	31.4	32.7
61.9	63.2	36.2	36.6	42.8	43.4	32.2	32.7
62.8	63.2	34.8	35.2	42.8	43.2	30.5	32.5
62.8	63.2	34.8	35.2	44.4	44.8	31.3	32.5
62.0	62.4	28.1	32.2	44.3	44.7	31.3	32.5
31.1	54.6	28.7	29.9	43.4	43.8	25.9	26.4
31.1	54.6	29.5	29.9	42.4	42.8	26	26.5
31.1	54.6	28.8	29.2	37.3	37.7	20.9	21.4
30.4	52.8	19.7	20.1	34.8	36.6	21	27.8
31.4	52.8	25.7	27.5	36.1	36.6	20.2	27.8
46.4	49.8	27.1	27.5	35.2	35.7	25.7	26.2
49.4	49.8	26.5	26.9	35.8	36.2	26.8	27.3
40.1	40.6	31.3	31.7	21.2	21.7	27.3	27.7
40.1	40.6	31.5	31.9	25.6	27.2	27.3	27.7
42.4	43.8	32.5	32.9	29.8	31.2	26.3	26.7
42.4	43.8	23	23.4	30.8	31.2	21.4	27.3
43.4	43.8	23	23.4	32.4	32.8	22.5	27.3
44.8	45.2	32.1	32.5	32.6	33	22.5	27.3
44.8	45.2	33.1	33.5	34.1	34.5	23	27.3
31.4	32.8	25.5	25.9	34.7	35.1	24.2	27.3
32.4	32.8	27.9	28.4	36.5	37	24.2	27.3
32.8	33.2	20.7	21.1	26.7	27.1	24.7	27.3
28.9	33.1	20.7	21.1	36.1	36.5	28.8	33.2
29.5	33.1	21.3	23.3	35	35.9	27.3	32.4
29.5	33.1	22.9	23.3	36.8	38.2	28	32.4
30.7	33.1	29.9	30.3	37.8	38.2	28	32.4
28.7	30	32.2	32.6	36.6	37	28.9	32.4
29.6	30	33.1	33.5	36.9	37.3	29.7	32.4
32.4	32.8	32.6	33	22.6	23	31	32.4

Table 25 (continued). Bead profile data from Experiment B-3 at 120.05 h.

z	L_f	z	L_f	z	L_f	z	L_f
33.9	34.3	32.6	33	29.2	29.7	31.9	32.4
28.8	29.2	31.9	32.3	29.3	31.6	27.3	27.8
23.7	24.1	23	32.2	30.2	31.6	21.8	22.8
25	25.5	31.4	32.2	31.1	31.6	22.4	22.8
25	25.5	34.4	34.8	30.4	32	17.8	18.7
27.8	28.2	35.6	36	31.6	32	25.5	26
34.6	35.0	30.3	35.1	33	33.4	25.5	26
31.5	35.9	32.2	35.1	33.5	33.9	21.5	23.1
35.5	35.9	33.7	35.1	34.4	34.8	27.4	27.8
35.0	35.4	35.8	36.2	34.2	34.6	32.6	34.4
32.5	35.4	35.3	35.7	26.3	28.4	29.8	34
33.6	37.0	26.4	28	28.5	31.3	31.3	34
36.6	37.0	27.5	28	29.8	31.3	33.6	34
31.2	36	31	31.4	29.7	31	33.6	34
32.3	36	31.9	32.3	30.6	31	24.5	37.3
33.4	36	28.5	32.5	29.5	30.8	26.6	37.3
33.4	36	40.3	40.7	28.6	31.6	33	37.3
34.8	36	40.8	42.4	29.6	31.6	31.9	37.3
34.8	36	42	42.4	31.2	31.6	33.6	37.3
26.4	42.0	42	42.4	26.3	28.2	34.8	36.1
27.6	42.0	42.4	42.9	27.8	28.2	33.1	37.4
40.8	41.2	44.8	45.3	28.3	28.7	33.5	37.4
40.8	41.2	37.6	44.8	53.7	55.3	34	37.4
40.2	41.2	43.6	44.8	54.8	55.3	35.8	37.4
38.5	42.3	44.7	45.2	54.1	54.6	36.9	37.4
40.1	42.3	31	42.4	58.6	64	27.2	37.6
41.3	42.3	40.2	42.4	56.2	63.4	28.8	37.6
41.3	42.3	41.9	42.4	56.4	56.8	36.4	37.6
37.1	42.5	17.2	42.5	52.8	53.2	37.2	37.6
42	42.5	19.4	42.5	52	52.4	29.9	35.9
41	41.5	24	42.5	38.3	54.4	30	35.9
42.3	42.7	42	42.5	39.3	54.4	31.6	35.9
42.3	42.7	23.8	24.2	43.3	54.4	31.6	35.9
41.6	43	27.7	28.8	44.7	54.4	32.7	35.9
34.7	35.2	25.3	28.5	45.2	54.4	34.1	35.9
36.7	46.6	26.6	28.4	47.1	54.4	34.1	35.9
52	52.4	26.2	29.5	52.6	54.4	36.1	39
52.6	53.0	29.1	29.5	52.6	54.4	37	39
52.8	53.2	27.7	29.3	53.9	54.4	38	39

Table 25 (continued). Bead profile data from Experiment B-3 at 120.05 h.

z	L_f	z	L_f	z	L_f	z	L_f
52.0	52.4	28.1	28.6	53.9	54.4	38.6	39
49.3	49.7	26.3	27.8	24.3	54.8	38.6	39
46.8	47.2	27.2	27.8	24.7	54.8	27.5	27.9
46.8	47.2	18.3	26.1	25.5	54.8	23.1	43.7
46.8	47.2	42.4	42.9	24.4	54.8	30.8	43.7
37.3	37.7	41.9	42.3	26.7	54.8	31	43.7
40.4	40.8	38.8	40.5	53.1	54.8	28.9	43.8
43.0	43.4	40	40.5	54.3	54.8	28.3	40.8
43.0	43.4	38.4	39.7	24.8	55.7	29.9	44.1
44.6	45	39.2	39.7	26.6	60.6	26.1	40.3
46.0	46.4	34.7	38.6	63.1	63.5	27.8	40.3
46.0	46.4	36.8	38.6	62.4	62.8	39.9	40.3
47.4	47.8	37.8	38.6	61.7	62.1	26.8	32
47.4	47.8	36.1	37.8	60.7	61.1	26.9	31.1
38.4	43.0	37.4	37.8	62.1	62.5	28.2	31.1
39.	43.0	36.4	36.9	26.4	58.1	28.9	31.1
39.4	43.0	37.5	39.2	29.3	58.1	29	31.3
40.4	43.0	37	38.3	31.9	58.1	29.6	31.3
40.4	43.0	36.4	36.9	32.8	58.1	30.8	31.3
41.4	43.0	37.5	39.2	33.4	58.1	25.3	30.3
42.6	43.0	37	38.3	57.7	58.1	27.5	30.3
42.6	43.0	36.4	40.1	55.3	55.7	27.5	30.3
36.1	39.6	39.6	40.1	23.8	53	28.5	30.3
37.4	39.6	39.8	40.3	26.5	53	29.1	30.3
38.6	39.6	37.7	41.7	27.4	51.4	29.1	30.3
38.6	39.6	39.3	41.7	51.4	53	29.8	30.3
39.2	39.6	40	41.7	37.1	47.5	25.5	26
22.6	32.3	40.6	41.7	47	47.5	26.6	31.2
23.6	32.3	41.3	41.7	48.3	48.7	27.4	29.8
24.7	32.3	24.5	24.9	41.8	43.8	28.6	31.2
24.7	32.3	20.2	20.7	42.6	43.1	29.3	29.8
26.5	32.2	16.7	17.2	43.3	43.7	29.3	29.8
27.5	32.2	27.4	27.8	41.4	41.8	30.8	31.2
28.6	29.0	27.4	27.8	32.4	32.8	31.8	34
28.6	29.0	20.8	21.2	31.3	32.9	23	32.1
35.2	35.7	33.4	33.9	32.5	32.9	23	32.1
43.3	43.7	37.1	37.5	28.8	29.3	24.1	32.1
31.9	32.4	35.1	35.6	30.1	30.5	28.5	32.1
34.2	35.7	35.2	35.6	30.5	30.9	29.8	32.1

Table 25 (continued). Bead profile data from Experiment B-3 at 120.05 h.

z	L_f	z	L_f	z	L_f	z	L_f
35.3	35.7	34.1	34.6	28	29.5	16.7	33.1
34.7	35.1	32.9	34.5	29.1	29.5	17.4	34.2
34.6	37	34	34.5	28.9	29.4	17.8	35.5
34.6	37	32.5	33	37.4	37.8	17.8	35.5
35.8	37	29.4	30.5	40	42.1	18.9	35.5
35.8	37	24.3	24.8	39.6	42.1	18.9	35.5
27.2	36.2	24.3	24.8	41	44.6	30.3	31.8
28.7	36.2	24	27.6	41.9	44.6	31.1	31.8
28.3	28.7	16.7	36.2	42.9	44.6	31.3	31.8
28.3	28.7	17.4	36.2	44.2	44.6	31.9	34.7
29.0	29.4	32.2	36.2	44	46.9	33.2	34.7
28.7	30.2	14.5	33.2	46.5	46.9	34.3	34.7
29.8	30.2	14.8	33.2	43.2	43.9	30.5	32.6
25.6	29.6	15.4	33.2	33.9	34.3	31.1	32.6
27.3	29.6	16.7	33.2	33.9	34.3	32.2	32.6
28.2	29.6	40	40.6	33.7	34.4	17.1	17.6
29.2	29.6	40.3	40.8	43.1	43.6	20.5	23.3
38.0	39.8	38.3	40.5	44.6	45	22.1	23.3
39.2	39.8	38.6	40.5	44.3	45.9	22.9	23.3
41.8	42.2	40	40.5	45.4	45.9	18.5	23
41.3	41.7	40	40.5	44.7	45.1	19.6	23
40.8	41.2	40.6	41.1	45.1	45.5	22.5	23
36.2	36.6	42.1	42.6	44.3	44.8	23.7	24.1
35.0	35.4	48	48.4	44.7	45.1	21.8	25.2
36.8	38.4	20	52.6	44.7	45.1	24	25.2
28.5	31.7	20	52.6	42.1	45.3	24.8	25.2
29.4	31.7	20.8	52.6	44.1	45.3	31.9	33
30.5	31.7	21.7	52.6	44.8	45.3	23.5	26.1
31.3	31.7	50.9	52.6	45.9	46.3	24.3	26.1
37.2	37.6	51.5	52.6	41.9	42.6	25.6	26.1
38.7	42	52.1	52.6	44.8	46.3	26	26.5
39.4	42	26	53.5	45.9	46.3	25.7	26.8
40.8	42	53	53.5	47.1	47.5	26.4	26.8
41.6	42	50.6	52.9	44.7	46.6	31.7	33.2
40.6	44.4	50.6	52.9	44.8	47	32.8	33.2
42.5	44.4	51.6	52.9	46.6	47	35.5	39.2
42.5	44.4	51.6	52.1	30.8	31.3	35.5	39.2
42.5	44.4	48.6	52.8	32.6	46.8	36	39.2
37.8	43.1	48.6	52.8	37.1	46.8	36.9	39.2

Table 25 (continued). Bead profile data from Experiment B-3 at 120.05 h.

z	L_f	z	L_f	z	L_f	z	L_f
38.4	43.1	49.8	52.8	38	46.8	37.7	39.2
38.4	43.1	50.1	52.8	38.9	46.8	38.7	39.2
38.4	43.1	51	52.8	38.9	46.8	36.1	36.5
39.9	43.1	52.4	52.8	36.8	47.3	20.1	36
40.6	43.1	48.4	54.4	24.8	46.1	15.4	39.2
40.6	43.1	49.9	54.4	28.9	46.1	27.3	39.2
31.9	46.4	35.4	35.8	53.7	55.6	31.1	46.4
38.0	38.4	47	55.6	39.2	46.1	30.6	40.4
31.7	40.4						

Table 26. Bead profile data from Experiment B-3 at 122.9 h. Symbols are as described in Figure 3. The data are presented in Figure 10. Distances are in μm.

z	L_f	z	L_f	z	L_f	z	L_f
23.1	30.4	37.0	40.9	29.0	39.1	25.4	25.9
27.4	30.4	38.4	40.9	29.0	39.1	26.3	26.8
27.4	30.4	38.4	40.9	29.3	39.1	29.0	31.0
30.0	30.4	39.4	40.9	29.3	39.1	30.6	31.0
30.0	30.4	39.4	40.9	38.3	39.1	38.4	40.5
29.9	31.8	34.8	41.3	42.5	46.8	40.0	40.5
31.4	31.8	34.9	41.3	43.8	46.8	33.9	46.0
31.4	31.8	35.6	41.3	44.4	46.8	34.9	46.0
21.4	30.8	37.1	41.3	44.5	46.8	36.3	46.0
22.1	30.8	37.3	41.3	44.5	46.8	38.7	46.0
17.8	31.6	38.3	41.3	45.1	46.8	40.6	46.0
17.8	31.6	39.4	41.3	29.7	41.4	40.6	46.0
17.8	31.6	39.8	41.3	29.7	41.4	42.1	46.0
18.4	31.6	40.9	41.3	30.0	41.4	42.1	46.0
18.4	31.6	18.1	24.4	31.8	41.4	42.6	46.0
31.2	31.6	25.5	31.4	33.7	41.4	42.6	46.0
18.3	33.9	27.7	31.1	37.9	41.4	43.6	46.0
19.2	33.9	27.7	31.1	37.9	41.4	34.8	44.2
20.0	33.9	28.3	31.1	38.8	41.4	39.8	44.2
20.0	33.9	28.3	31.1	40.1	41.4	42.1	44.2
20.2	33.9	28.3	31.1	41.0	41.4	42.1	44.2
20.2	33.9	29.3	31.1	30.6	40.6	43.7	44.2
21.4	33.9	29.3	31.1	32.3	40.6	19.6	43.0
21.4	33.9	28.7	29.5	32.3	40.6	19.6	43.0
21.7	33.9	30.2	32.7	32.3	40.6	41.2	43.0
22.5	33.9	31.2	32.7	35.4	40.6	41.2	43.0
22.5	33.9	32.3	32.7	35.4	40.6	41.8	43.0
22.3	33.9	14.8	31.1	36.6	40.6	42.6	43.0
22.0	33.9	28.9	30.8	36.6	40.6	23.2	41.7
22.9	33.9	29.1	30.8	36.6	40.6	23.2	41.7
22.9	33.9	29.8	30.8	36.6	40.6	24.6	41.7
23.5	33.9	29.8	30.8	37.6	40.6	24.6	41.7
23.8	33.9	29.8	30.8	37.6	40.6	25.7	41.7
24.9	33.9	30.4	30.8	38.8	40.6	25.7	41.7
24.9	33.9	31.1	31.5	38.8	40.6	25.7	41.7
26.6	33.9	31.1	31.5	38.8	40.6	25.9	41.7

Table 26 (continued). Bead profile data from Experiment B-3 at 122.9 h.

z	L_f	z	L_f	z	L_f	z	L_f
29.4	33.9	21.6	30.5	27.8	32.4	26.9	32.8
30.4	33.9	22.4	30.5	29.0	32.4	28.6	32.8
30.8	33.9	23.7	30.5	29.8	32.4	29.4	32.8
31.2	33.9	23.7	30.5	31.2	32.4	31.8	35.5
30.8	33.9	23.7	30.5	31.7	32.4	33.4	35.5
30.8	33.9	25.1	33.8	31.2	32.4	20.5	39.9
31.9	33.9	25.0	33.8	31.2	32.4	34.3	39.9
31.9	33.9	25.0	33.8	31.2	32.4	39.4	39.9
31.8	33.9	26.6	33.8	30.3	32.4	36.4	39.9
32.7	33.9	26.6	33.8	30.3	32.4	34.9	35.6
32.7	33.9	27.7	33.8	32.0	32.4	36.8	39.1
33.5	33.9	29.0	33.8	32.0	32.4	36.8	39.1
33.5	33.9	29.0	33.8	41.6	43.2	36.8	39.1
26.5	26.9	30.0	33.8	41.5	43.2	38.1	41.0
29.7	31.5	30.0	33.8	42.7	43.2	28.4	42.3
30.0	31.5	30.0	33.8	23.7	43.7	29.7	42.3
30.0	31.5	30.0	33.8	24.2	43.7	29.7	42.3
31.1	31.5	31.0	31.5	24.2	43.7	30.3	42.3
31.1	31.5	31.0	31.5	25.9	43.7	32.3	42.3
30.9	34.1	32.2	32.6	26.3	43.7	32.4	42.3
32.1	34.1	19.4	25.8	26.6	43.7	33.7	42.3
32.1	34.1	39.2	39.6	27.6	43.7	41.3	42.3
32.1	34.1	41.6	43.5	37.3	37.7	29.5	43.1
32.0	34.1	43.1	43.5	38.5	42.2	31.1	43.1
32.0	34.1	36.9	41.2	38.5	38.9	32.0	43.1
33.7	34.1	38.8	41.2	39.7	40.1	35.5	43.1
25.6	31.7	40.8	41.2	41.4	41.8	35.5	43.1
26.6	31.7	39.3	40.3	41.4	41.8	36.8	43.1
29.6	31.7	39.8	40.3	25.4	41.6	36.8	43.1
29.6	31.7	38.8	40.3	39.1	41.6	37.7	43.1
30.7	31.7	39.8	40.3	39.1	41.6	37.7	43.1
30.7	31.7	38.2	40.0	40.1	41.6	42.1	43.1
31.3	31.7	39.6	40.0	40.1	41.6	42.1	43.1
24.7	25.2	27.8	47.8	40.7	41.6	33.0	41.9
25.2	29.6	27.8	47.8	40.7	41.6	33.0	41.9
29.2	29.6	28.3	47.8	41.1	41.6	33.8	41.9
30.7	31.4	28.8	47.8	21.4	30.4	34.7	41.9
32.3	32.7	28.8	47.8	22.7	30.4	39.7	41.9
31.6	32.0	28.8	47.8	22.7	30.4	39.7	41.9

Table 26 (continued). Bead profile data from Experiment B-3 at 122.9 h.

z	L_f	z	L_f	z	L_f	z	L_f
26.4	31.6	41.2	44.3	45.6	46.5	38.8	39.3
26.4	31.6	41.2	44.3	46.1	46.5	33.6	34.8
27.4	31.6	15.8	44.4	46.0	46.9	19.8	39.2
27.4	31.6	40.3	44.4	44.3	46.9	20.5	39.2
27.9	31.6	40.3	44.4	39.7	45.4	21.2	39.2
28.5	31.6	15.8	43.1	39.7	45.4	36.4	39.2
29.7	32.2	39.9	43.1	40.4	45.4	24.1	40.0
14.7	33.2	16.6	41.7	40.4	45.4	25.3	40.0
14.7	33.2	36.6	41.7	41.8	45.4	27.0	40.0
15.4	33.2	35.8	41.7	41.8	45.4	28.1	40.0
16.4	33.2	35.8	41.7	43.6	45.4	28.1	40.0
29.1	32.5	20.8	41.0	43.6	45.4	28.8	40.0
29.1	32.5	20.8	41.0	38.6	43.9	29.3	40.0
30.6	32.5	21.2	41.0	37.9	43.9	29.3	40.0
30.6	32.5	22.3	41.0	39.3	43.9	30.6	40.0
31.6	32.5	32.3	41.0	42.2	43.9	30.6	40.0
24.8	30.6	35.3	41.0	42.2	43.9	30.6	40.0
24.5	30.6	20.0	39.7	43.5	43.9	30.6	40.0
24.5	30.6	21.7	39.7	43.5	43.9	31.9	40.0
24.4	30.1	21.7	39.7	34.5	41.7	32.6	40.0
24.4	30.1	21.7	39.7	35.9	41.2	33.4	40.0
23.2	30.5	21.3	39.7	36.3	41.2	33.8	40.0
23.2	30.5	23.4	39.7	37.0	41.2	35.0	40.0
22.5	30.5	24.9	39.7	38.8	41.2	35.6	40.0
23.6	30.5	24.9	39.7	39.1	40.5	35.6	40.0
24.2	30.5	27.6	39.7	40.0	40.5	35.6	40.0
20.6	30.4	19.8	23.3	40.0	40.5	36.2	40.0
23.1	30.4	20.5	23.3	40.0	40.5	38.5	40.0
23.1	30.4	21.2	23.3	38.6	39.0	38.5	40.0
23.5	30.4	21.2	23.3	32.6	37.8	39.2	40.0
24.4	30.4	21.9	23.3	30.9	31.3	34.0	38.8
24.4	30.4	21.3	25.0	31.6	32.0	34.0	38.8
24.4	30.4	19.1	25.0	28.0	30.6	34.0	38.8
23.2	28.9	22.9	26.4	28.9	30.6	38.3	38.8
26.2	28.9	24.1	26.4	37.3	42.9	22.5	40.1
25.0	28.9	25.2	26.4	39.4	42.9	38.2	40.1
26.2	28.9	26.0	26.4	41.0	42.9	38.2	40.1
21.6	29.2	31.4	34.6	45.6	46.3	40.5	47.6
21.6	29.2	34.0	40.5	46.5	46.9	23.6	48.0

Table 26 (continued). Bead profile data from Experiment B-3 at 122.9 h.

z	L_f	z	L_f	z	L_f	z	L_f
22.0	27.6	43.2	44.1	42.7	48.2	34.4	48.0
22.9	27.6	43.2	44.1	42.7	48.2	34.4	48.0
22.9	27.6	31.0	47.0	43.9	48.2	34.4	48.0
23.6	27.6	34.8	47.0	43.9	48.2	35.1	48.0
23.9	27.6	31.7	47.4	43.9	48.2	42.9	48.0
22.3	31.5	32.3	47.4	43.9	48.2	44.7	48.0
25.9	27.1	32.7	47.4	43.9	48.2	44.7	48.0
26.7	27.1	33.3	47.4	44.6	48.2	45.3	48.0
17.9	24.4	32.3	47.4	44.6	48.2	46.2	48.0
19.5	24.4	33.1	47.4	44.6	48.2	46.5	48.0
21.1	24.4	32.4	48.2	44.6	48.2	34.9	45.8
21.7	24.4	32.4	48.2	44.6	48.2	38.9	45.8
20.8	24.4	34.6	48.2	45.7	48.2	34.8	43.2
22.4	24.4	34.6	48.2	45.7	48.2	42.1	43.2
22.4	24.4	32.7	48.2	45.7	48.2	37.4	40.1
22.4	24.4	33.5	48.2	46.4	48.2	37.4	40.1
22.4	24.4	33.5	48.2	47.1	48.2	42.3	43.0
23.7	24.4	33.9	48.2	47.1	48.2	40.5	44.8
23.7	24.4	35.7	48.2	47.8	48.2	40.5	44.8
23.7	24.4	35.2	47.8	45.7	47.7	44.3	44.8
23.7	24.4	35.8	47.8	45.7	47.7	39.9	43.8
24.0	24.4	35.8	47.8	45.7	47.7	42.0	44.3
21.4	21.8	36.5	47.8	45.7	47.7	43.3	44.3
21.4	21.8	37.0	47.8	44.6	47.7	26.0	35.9
20.4	21.8	37.8	47.8	45.2	47.7	31.9	35.9
17.6	19.8	29.4	49.1	46.6	47.7	35.0	35.9
32.1	35.3	33.5	49.1	46.6	47.7	35.4	35.9
33.0	35.3	33.9	49.1	46.6	47.7	38.9	39.4
33.7	35.3	33.9	49.1	46.7	47.8	38.9	39.4
34.9	35.3	34.8	49.1	47.4	47.8	37.0	41.1
31.4	31.8	36.2	49.1	43.4	47.3	38.4	41.1
28.7	31.1	36.2	49.1	44.5	47.3	39.1	41.1
23.6	29.1	37.5	49.1	46.9	47.3	39.1	41.1
23.4	26.5	38.4	49.1	45.5	47.5	39.1	41.1
24.7	26.5	39.0	49.1	46.5	47.5	40.2	41.1
24.7	26.5	29.2	53.3	45.1	46.8	38.8	42.3
25.4	26.5	46.8	53.3	41.9	46.0	41.8	42.4
26.1	26.5	49.8	53.3	42.9	46.0	23.6	30.6
26.1	26.5	51.3	53.3	44.1	46.0	26.4	26.9

Table 26 (continued). Bead profile data from Experiment B-3 at 122.9 h.

z	L_f	z	L_f	z	L_f	z	L_f
29.4	45.5	37.7	42.0	21.7	42.1	26.7	43.6
29.4	45.5	38.4	42.0	24.0	42.2	27.6	43.6
30.4	45.5	32.6	34.3	29.2	42.2	26.4	42.7
30.4	45.5	32.6	34.3	22.8	42.4	26.4	42.7
29.1	45.5	33.8	34.3	24.2	42.4	27.6	42.7
31.4	45.5	34.1	34.5	30.3	42.4	28.6	42.7
31.4	45.5	41.3	42.3	27.6	43.1	28.6	42.7
31.8	45.5	41.1	42.4	31.3	43.1	29.7	42.7
32.6	45.5	40.6	41.1	32.9	43.1	29.7	42.7
33.0	45.5	39.6	40.1	33.6	43.1	30.6	42.7
34.8	45.5	32.7	40.1	32.6	43.1	26.7	44.6
34.8	45.5	34.1	38.0	25.9	43.2	28.2	44.6
36.0	45.5	37.5	38.0	30.6	43.2	28.2	44.6
36.0	45.5	37.0	39.1	27.5	43.6	29.5	44.6
26.9	45.8	38.8	39.2	29.2	43.6	29.7	44.6
29.1	45.8	32.9	34.2	29.6	43.6	30.5	44.6
29.1	45.8	26.9	34.7	33.0	43.6	30.5	44.6
24.3	45.8	28.7	34.7	29.2	43.4	30.5	44.6
31.9	45.8	30.2	34.7	31.4	43.4	31.3	44.6
30.3	45.8	32.4	34.7	32.4	43.4	31.7	46.8
30.7	45.8	20.0	30.1	33.4	43.4	31.7	46.8
31.6	45.8	26.9	30.1	30.4	42.9	33.6	46.8
44.0	45.8	27.0	30.1	31.8	42.9	35.1	46.8
17.5	45.4	23.2	43.2	32.3	42.9	35.1	46.8
20.1	45.4	33.3	43.2	24.5	42.0	36.2	46.8
20.1	45.4	34.2	43.2	25.8	41.3	32.8	45.4
24.4	45.4	34.8	43.2	36.1	41.3	32.8	45.4
24.4	45.4	35.6	43.2	28.6	38.9	32.8	45.4
20.4	45.4	36.2	43.2	25.4	37.8	32.8	45.4
24.9	45.4	36.7	43.2	22.1	42.4	32.8	45.4
24.9	45.4	37.6	43.2	24.0	42.4	33.7	45.4
28.2	45.4	38.4	43.2	24.9	42.4	34.4	45.4
28.3	45.4	38.8	43.2	24.9	42.4	34.4	45.4
28.6	45.4	38.8	43.2	26.7	42.4	35.2	45.4
30.2	45.4	38.8	43.2	26.7	42.4	28.7	45.1
18.1	27.5	39.6	43.2	26.7	42.4	28.7	45.1
13.4	27.5	40.8	43.2	27.3	42.4	35.3	45.1
15.5	27.5	40.6	43.2	28.2	42.4	34.4	40.6
27.1	27.5	41.3	43.2	30.6	42.4	34.8	45.1

Table 26 (continued). Bead profile data from Experiment B-3 at 122.9 h.

z	L_f	z	L_f	z	L_f	z	L_f
31.7	42.2	36.5	40.3	31.8	43.1	34.3	43.3
31.2	43.0	36.5	40.3	33.3	43.1	36.5	43.3
21.4	42.4	36.5	40.3	33.3	43.1	35.5	44.1
25.4	42.4	37.2	40.3	24.0	43.1	35.5	44.1
25.4	42.4	35.5	39.0	26.8	43.1	36.6	44.1
25.9	42.4	37.8	39.0	27.4	43.1	36.3	44.1
26.3	42.4	38.6	39.0	29.5	43.1	23.4	41.7
26.3	42.4	38.6	39.0	25.6	43.0	34.2	41.7
27.8	42.4	35.9	37.8	25.9	43.0	34.2	41.7
27.8	42.4	31.8	36.3	27.0	43.0	35.1	43.2
37.3	42.4	32.2	36.3	27.0	43.0	33.4	43.2
37.3	42.4	32.5	36.3	29.0	43.0	34.3	43.2
38.4	42.4	32.5	36.3	29.6	43.0	33.6	42.6
39.3	42.4	33.8	36.3	34.6	43.8	35.2	42.6
41.9	42.4	33.8	36.3	37.9	44.0	35.2	42.6
41.9	42.4	34.5	36.3	33.9	43.7	36.0	42.6
22.5	42.3	35.4	36.3	23.8	44.4	29.9	43.3
22.5	42.3	29.4	36.5	32.4	44.4	29.9	43.3
22.5	42.3	20.0	36.5	33.4	44.4	31.1	43.8
22.9	42.3	29.9	36.5	28.7	44.7	28.5	43.0
23.1	42.3	31.0	36.5	29.5	44.7	28.5	43.0
23.1	42.3	31.6	36.5	29.5	44.7	29.2	43.0
24.2	42.3	30.7	36.5	30.2	44.7	31.6	43.0
24.2	42.3	31.6	36.5	31.6	44.7	33.2	43.0
24.2	42.3	31.6	36.5	37.0	44.7	17.8	42.3
24.1	42.3	32.5	36.5	27.3	44.8	27.0	42.3
25.5	42.3	32.5	36.5	28.0	44.8	27.0	42.3
25.9	42.3	33.1	36.5	28.0	44.8	28.2	42.3
26.6	42.3	34.2	36.5	28.6	44.8	27.5	42.7
30.1	42.3	35.4	36.5	28.6	44.8	28.4	42.7
33.5	42.3	35.4	36.5	28.6	44.8	21.6	42.9
33.5	42.3	31.6	32.1	30.5	44.8	28.2	42.9
32.4	40.4	23.4	30.6	31.0	44.8	29.6	42.5
33.1	40.4	12.2	27.2	34.5	44.8	31.3	42.5
33.1	40.4	15.5	27.2	35.7	44.8	28.4	39.0
33.9	40.4	15.5	27.2	28.1	45.3	31.4	39.0
35.6	40.4	17.3	27.2	28.1	45.3	35.6	39.0
35.5	40.4	20.8	27.2	28.4	45.3	36.9	39.0
36.7	40.4	26.7	27.2	24.6	45.3	36.9	39.0

Table 26 (continued). Bead profile data from Experiment B-3 at 122.9 h.

z	L_f	z	L_f	z	L_f	z	L_f
41.6	42.5	37.8	40.5	32.0	44.6	42.2	44.7
41.6	42.5	37.8	40.5	29.1	41.0	43.3	44.7
42.4	42.8	39.2	40.5	28.8	41.1	29.7	42.6
39.0	42.8	40.0	40.5	28.8	41.1	34.3	42.6
42.1	42.8	21.6	35.4	35.5	41.1	27.2	40.7
42.1	42.8	22.3	35.4	36.8	41.1	26.7	40.7
34.7	39.6	29.5	35.4	36.8	41.1	27.8	40.7
35.4	39.6	30.9	35.4	38.2	41.1	32.1	40.7
35.4	39.6	32.7	35.4	26.8	34.6	32.1	40.7
35.9	39.6	32.7	35.4	28.0	34.6	34.8	37.9
37.5	39.6	33.8	35.4	29.8	34.6	30.4	42.8
26.8	39.1	33.8	35.4	31.5	40.9	33.0	42.8
27.7	39.1	34.5	35.4	33.2	40.9	40.7	42.8
27.7	39.1	34.6	35.4	34.5	40.9	33.0	44.7
37.0	40.9	34.2	44.7	27.1	32.4	24.6	32.8
26.8	33.9	31.6	32.6	36.2	37.8	39.5	44.0
26.3	33.9	18.1	31.5	35.0	37.8	38.4	41.7
26.9	33.9	18.8	31.5	33.5	35.9	40.2	44.0
26.9	33.9	18.8	31.5	34.0	35.9	40.2	44.0
27.6	33.9	20.3	31.5	34.3	35.9	42.4	44.0
27.6	33.9	20.3	31.5	34.0	36.4	42.4	44.0
27.6	33.9	20.3	31.5	30.6	34.1	43.6	44.0
28.4	33.9	21.6	30.5	25.2	32.4	24.6	32.8
28.9	33.9	21.6	30.5	45.3	45.7	38.0	39.3
25.6	31.2	28.8	47.8	23.7	30.4	40.7	41.9
30.2	30.6	29.0	47.6	23.7	30.4	32.6	41.4
30.2	30.6	29.5	47.6	24.6	30.4	34.4	39.3
30.4	30.8	28.9	47.6	27.9	30.4	35.3	39.3
30.8	31.2	28.9	47.6	29.7	30.4	35.3	39.3
24.4	31.6	38.8	46.9	36.7	39.6	35.3	39.3
24.9	31.6	32.4	45.3	40.7	44.6	36.3	39.3
26.4	31.6	34.6	45.3	42.0	44.6	38.0	39.3
26.4	31.6	40.4	44.3	42.7	48.2	33.8	48.0
22.4	29.2	33.8	40.5	43.7	45.0	27.5	48.0
22.6	29.2	35.1	40.5	44.4	45.0	27.5	48.0
23.2	29.2	40.0	40.5	42.7	44.6	28.5	48.0
23.9	29.2	35.5	42.2	42.7	44.6	28.5	48.0
24.3	29.2	36.6	42.2	43.2	44.6	28.9	48.0
23.5	30.7	36.5	44.2	43.2	44.6	30.2	48.0

Table 26 (continued). Bead profile data from Experiment B-3 at 122.9 h.

z	L_f	z	L_f	z	L_f	z	L_f
24.2	30.7	37.0	44.2	41.6	48.2	30.2	48.0
21.3	27.6	41.6	44.2	41.6	48.2	31.4	48.0
22.0	27.6	42.7	44.2	27.5	42.6	26.2	43.6
27.6	28.0	52.0	53.3	45.2	46.0	25.6	43.0
26.7	34.9	52.9	53.3	45.2	46.0	29.0	43.0
24.4	45.5	38.7	52.0	42.7	45.8	29.0	43.0
25.0	45.5	24.2	45.8	43.6	45.8	22.0	43.6
25.0	45.5	24.2	45.8	45.4	45.8	23.5	43.6
25.4	45.5	25.1	45.8	24.3	41.6	23.5	43.6
26.4	45.5	28.1	45.8	24.6	42.6	25.2	43.6
28.5	45.5	42.1	45.8	25.7	42.6	25.2	43.6
28.5	45.5	29.2	42.1	31.8	43.1	34.3	43.3
29.4	31.8	42.2	43.2	32.0	42.4	26.4	41.2
30.2	31.8	32.2	40.3	33.2	42.4	32.0	41.8
31.4	31.8	32.2	40.3	22.3	43.1	33.3	41.8
29.5	43.3	31.4	40.3	26.1	43.1	33.3	41.8
31.0	42.2	32.4	40.3	27.3	43.1	33.3	41.8
31.0	42.2	33.4	40.3	29.2	43.1	34.3	41.8
31.0	42.2	34.1	40.3	28.4	43.1	25.3	43.3
31.5	42.2	36.0	40.3	28.4	43.1	26.0	43.3
31.5	42.2	36.0	40.3	26.6	44.6	42.0	44.7
38.5	40.4	45.7	46.2	24.0	45.8	42.4	42.9
38.5	40.4	46.5	47.0	21.9	46.0	43.5	43.9
35.7	38.4	39.4	41.8	23.1	46.0	44.0	44.9
37.0	38.4	46.5	47.0	24.4	46.0	40.6	45.0
36.3	38.4	40.8	41.8	30.5	46.0	43.4	45.0
36.3	38.4	40.8	41.8	23.1	45.1	29.8	44.7
38.0	38.4	41.3	41.8	23.9	45.1	41.0	44.7
40.3	42.5	39.7	42.0	24.9	45.1	41.0	44.7
26.3	33.9	33.2	33.6	38.1	39.4	38.0	44.0
41.6	42.5	40.3	42.0				

Table 27. Bead profile data from Experiment B-3 at 128.9 h. Symbols are as described in Figure 3. The data are presented in Figure 10. Distances are in μm.

z	L_f	z	L_f	z	L_f	z	L_f
17.9	30.9	22.4	26.9	21.6	38.1	5.1	68.7
35.5	38.0	22.6	26.9	23.8	38.1	6.1	68.7
35.5	38.0	23.5	26.9	26.9	38.1	6.9	68.7
37.0	37.8	24.5	26.9	26.9	38.1	8.1	68.7
23.6	39.7	24.5	26.9	27.8	38.1	9.4	68.7
38.6	39.3	25.7	35.6	31.6	38.1	9.4	68.7
37.4	38.5	27.8	35.6	32.2	38.1	12.0	68.7
36.4	38.5	30.9	35.6	32.2	38.1	12.0	68.7
36.8	38.5	30.9	35.6	33.5	38.1	13.6	68.7
34.0	34.5	31.7	35.6	33.5	38.1	13.6	68.7
27.8	31.6	33.1	35.5	35.9	38.1	15.6	68.7
28.0	33.0	34.4	35.5	35.9	38.1	15.8	68.7
28.0	33.0	21.9	36.8	37.1	38.1	16.7	68.7
30.0	33.0	32.4	36.8	34.5	35.6	16.7	68.7
30.0	33.0	19.8	37.4	34.5	35.6	18.7	68.7
30.0	33.0	28.7	36.8	32.9	35.0	18.7	68.7
30.9	33.5	33.0	37.4	34.2	35.0	18.7	68.7
32.6	33.0	32.8	38.2	33.7	35.0	20.9	68.7
33.1	33.5	33.5	38.2	33.7	35.0	20.9	68.7
32.6	33.0	33.4	38.2	31.4	33.8	20.9	68.7
33.1	33.5	37.7	38.2	31.4	33.8	20.9	68.7
33.1	33.5	33.6	38.5	32.4	33.8	22.4	68.7
29.4	33.0	33.6	38.5	21.0	30.0	22.4	68.7
32.2	33.0	35.6	38.5	22.5	30.0	22.4	68.7
30.2	44.2	35.6	38.5	23.6	30.0	23.7	68.7
33.7	44.2	37.8	38.5	26.0	30.0	24.3	68.7
38.2	44.2	37.8	38.5	28.4	30.0	26.5	68.7
29.4	32.4	20.1	32.9	28.6	32.5	36.6	68.7
30.5	32.4	26.8	33.3	29.5	36.4	48.5	68.7
31.4	32.4	27.1	33.3	30.6	36.4	50.8	68.7
30.3	31.8	30.5	33.3	32.3	36.4	53.1	68.7
28.9	29.3	22.8	34.1	33.2	36.4	33.9	40.9
27.9	43.9	24.3	34.1	32.1	36.4	34.9	40.9
38.6	43.9	25.3	34.1	25.8	46.2	34.9	40.9
32.8	45.1	26.4	34.1	30.2	46.2	36.0	40.9
38.4	45.1	24.6	36.0	36.4	46.2	35.9	40.9

Table 27 (continued). Bead profile data from Experiment B-3 at 128.9 h.

z	L_f	z	L_f	z	L_f	z	L_f
38.7	45.1	34.8	37.8	37.5	46.2	37.6	40.9
40.3	45.1	34.8	37.8	37.5	46.2	42.4	45.6
27.0	46.0	31.2	40.8	38.7	46.2	28.5	37.0
33.2	46.0	32.0	42.0	40.1	46.2	30.6	37.0
31.7	47.2	34.6	42.0	23.8	28.2	32.3	37.0
32.6	47.2	36.9	42.0	37.8	39.2	32.3	37.0
33.8	47.2	38.6	42.0	25.6	45.9	34.3	37.0
34.5	47.2	36.4	42.7	27.6	45.9	26.3	39.3
36.0	47.2	38.2	42.7	28.0	45.9	26.3	39.3
36.0	47.2	39.6	42.7	29.1	45.9	26.3	39.3
36.0	47.2	39.6	42.7	30.3	45.9	30.2	39.3
36.0	47.2	40.1	42.7	32.0	45.9	32.0	39.3
37.6	47.2	20.8	41.5	32.0	45.9	32.0	39.3
39.2	47.2	22.2	41.5	32.8	45.9	33.5	39.3
24.2	45.9	25.9	41.5	32.8	45.9	33.5	39.3
28.9	45.9	27.9	41.5	32.5	45.9	33.5	39.3
32.2	43.6	29.0	41.5	33.9	45.9	34.3	39.3
35.1	43.6	29.4	41.5	33.9	45.9	35.2	39.3
36.0	43.6	30.4	41.5	34.1	45.9	37.0	39.3
38.1	43.6	32.2	41.5	35.1	45.9	37.0	39.3
38.1	43.6	33.6	41.5	35.1	45.9	38.2	39.3
38.1	43.6	35.4	40.0	35.1	45.9	22.5	40.4
39.3	43.6	36.2	40.0	35.1	45.9	22.5	40.4
30.4	42.5	37.5	40.0	41.4	45.9	23.6	40.4
37.4	42.5	21.3	39.3	40.7	45.8	24.4	40.4
33.6	38.3	21.0	40.0	41.5	45.8	25.5	40.4
31.7	34.0	26.6	40.0	35.7	46.4	28.5	40.4
36.2	40.9	28.0	40.0	38.1	46.4	29.6	40.4
37.8	40.9	28.0	40.0	40.6	46.4	24.5	42.2
38.9	40.9	29.3	40.0	38.2	43.3	24.5	42.2
35.4	41.3	31.6	40.0	39.6	43.3	24.5	42.2
36.9	41.3	31.6	40.0	39.6	43.3	25.9	42.2
38.0	41.3	37.5	40.0	41.0	43.3	25.9	42.2
39.9	41.3	20.4	36.9	33.7	43.2	25.9	42.2
28.3	39.3	23.3	40.0	41.5	45.8	26.5	40.4
31.4	34.0	24.8	40.0	32.7	45.8	27.1	40.4
29.1	34.0	25.7	40.0	37.7	46.4	27.1	40.4
41.0	41.4	36.4	37.1	38.2	43.2	28.8	42.2
22.6	35.4	37.2	37.7	38.6	43.2	32.2	42.2

Table 27 (continued). Bead profile data from Experiment B-3 at 128.9 h.

z	L_f	z	L_f	z	L_f	z	L_f
25.4	35.4	31.4	37.0	39.2	43.2	32.2	42.2
32.8	35.4	35.4	38.2	39.7	43.2	33.0	42.2
33.9	35.4	23.3	38.3	40.3	43.2	34.4	42.2
35.0	35.4	30.0	39.0	40.2	43.2	36.4	42.2
32.7	40.9	32.7	38.3	27.7	45.4	36.4	42.2
35.2	40.9	34.8	38.3	28.5	45.4	33.0	42.2
37.0	40.9	24.6	36.5	28.5	45.4	33.0	42.2
38.8	40.9	25.7	36.2	28.5	45.4	37.0	42.2
36.2	41.6	29.9	36.2	30.2	45.4	35.3	40.4
37.9	41.6	26.1	37.9	31.2	45.4	20.3	38.4
38.8	41.6	26.1	37.9	32.2	45.4	23.4	38.4
39.0	41.6	26.1	37.9	40.2	45.4	24.2	38.4
40.3	41.6	25.5	37.5	43.0	45.4	25.9	38.4
41.4	41.9	25.5	37.5	43.7	45.4	26.7	38.4
42.2	43.6	26.7	37.5	23.2	39.9	27.8	38.4
43.2	43.6	26.7	37.5	29.9	39.9	36.6	38.4
36.1	44.4	30.5	37.5	31.0	39.9	21.7	40.1
41.9	44.4	31.3	37.5	31.7	39.9	24.6	40.1
41.9	44.4	31.3	37.5	32.4	39.9	24.6	40.1
42.8	44.4	22.5	36.8	33.4	39.9	24.6	40.1
44.0	44.4	22.5	36.8	23.4	38.9	25.5	40.1
38.0	40.1	25.2	36.8	23.4	38.9	25.5	40.1
33.4	43.0	29.9	36.8	23.4	38.9	25.5	40.1
40.8	43.0	27.2	36.4	20.8	35.1	26.2	40.1
38.7	40.8	28.1	36.4	23.6	35.1	26.2	40.1
18.7	22.0	29.1	36.4	25.4	35.1	27.1	40.1
23.0	25.5	30.0	36.4	26.7	35.1	27.1	40.1
24.0	25.5	31.7	36.4	27.7	35.1	27.6	40.1
24.0	25.5	31.7	36.4	30.2	35.1	27.6	40.1
21.2	25.5	31.7	36.4	30.8	35.1	39.5	40.1
23.9	25.5	31.7	36.4	18.0	34.9	39.5	40.1
20.7	27.2	31.7	36.4	25.5	34.9	32.5	40.0
25.4	25.9	31.8	36.9	31.8	35.7	32.5	40.0
26.2	26.6	34.1	36.9	30.7	35.7	33.7	40.0
25.3	25.7	36.4	36.9	30.7	35.7	33.7	40.0
22.5	26.3	31.2	39.0	33.2	35.7	33.7	40.0
22.5	26.3	34.0	39.0	34.4	35.7	36.0	40.0
24.2	26.3	38.6	39.0	26.6	43.2	37.5	40.0
25.8	26.3	35.4	39.4	34.5	43.2	38.7	40.0

Table 27 (continued). Bead profile data from Experiment B-3 at 128.9 h.

z	L_f	z	L_f	z	L_f	z	L_f
27.7	38.0	36.7	39.4	31.4	34.4	38.7	40.0
30.7	38.0	39.0	39.4	32.2	34.4	39.5	40.0
30.7	38.0	33.5	40.0	33.5	34.4	39.5	40.0
30.7	38.0	33.5	40.0	33.9	34.4	39.5	40.0
34.0	41.4	33.5	40.0	29.1	38.8	32.3	46.4
34.4	41.4	33.5	40.0	33.6	41.6	33.6	46.4
34.5	41.4	33.5	40.0	41.0	41.6	34.4	46.4
35.8	41.4	35.7	40.0	39.6	40.6	34.4	46.4
35.8	41.4	37.0	40.0	40.0	40.6	34.4	46.4
39.1	41.4	38.4	40.0	31.5	33.8	35.7	46.4
41.0	41.4	38.4	40.0	31.5	33.8	35.7	46.4
30.1	40.1	39.5	40.0	26.6	31.0	38.0	46.4
31.1	40.1	39.5	40.0	26.2	28.7	38.0	46.4
32.6	40.1	35.1	41.1	20.2	29.8	26.3	29.4
34.1	40.1	35.9	36.4	21.7	29.8	26.0	27.2
35.5	40.1	34.5	36.0	19.0	29.8	15.3	15.8
29.3	31.4	33.9	35.3	23.0	29.8	15.3	16.3
23.5	30.8	24.6	40.6	24.4	29.8	12.5	17.2
18.3	24.3	25.9	40.6	25.3	29.8	11.7	16.3
21.9	24.3	26.9	40.6	27.6	29.8	16.0	18.2
21.2	23.4	26.9	40.6	28.0	29.8	17.7	18.2
19.2	26.1	27.6	40.6	29.1	29.8	18.3	18.8
21.3	26.1	27.6	40.6	29.3	29.8	17.3	17.8
24.3	26.1	28.8	40.6	26.1	28.3	16.1	18.2
11.1	22.7	28.8	40.6	8.2	16.2	21.4	22.9
12.2	22.7	28.8	40.6	5.0	16.0	17.8	24.0
17.3	22.7	28.8	40.6	19.6	20.4	19.6	24.0
19.7	22.7	30.3	40.6	18.8	20.7	20.0	24.0
20.9	22.7	30.3	40.6	25.4	25.9	21.2	24.0
13.5	23.1	31.4	40.6	27.6	30.9	18.8	22.2
18.1	24.6	32.0	40.6	28.1	30.9	19.2	22.2
18.1	24.6	33.3	40.6	28.6	30.9	20.7	22.2
19.5	24.6	33.3	40.6	30.4	30.9	17.6	23.4
21.8	23.1	34.8	40.6	30.4	30.9	22.5	23.4
24.1	24.6	38.3	40.6	23.6	30.2	22.7	24.0
24.1	24.6	33.7	36.3	29.7	30.2	22.7	24.0
21.7	24.5	34.6	36.3	29.7	30.2	22.7	24.0
23.1	24.5	31.0	56.3	30.5	32.7	19.4	23.2
23.1	24.5	31.0	56.3	31.2	32.7	22.3	23.2

Table 27 (continued). Bead profile data from Experiment B-3 at 128.9 h.

z	L_f	z	L_f	z	L_f	z	L_f
21.2	34.6	20.9	58.9	32.2	32.7	22.3	23.2
21.6	34.6	20.9	58.9	23.5	29.4	16.8	21.0
21.6	34.6	21.8	58.9	26.3	31.6	16.8	21.0
21.6	34.6	21.8	58.9	28.2	30.5	18.0	21.0
22.3	34.6	23.3	58.9	11.7	30.5	18.8	21.0
22.3	34.6	24.7	58.9	14.9	30.5	18.8	21.0
23.0	34.6	24.7	58.9	16.8	29.3	20.8	21.0
28.3	34.6	24.8	58.9	16.8	29.3	22.8	23.3
28.3	34.6	24.8	58.9	18.0	29.3	15.0	19.5
29.6	34.6	26.3	58.9	18.0	29.3	24.6	25.1
29.6	34.6	29.5	58.9	18.7	29.3	24.6	25.1
29.6	34.6	56.4	58.9	18.7	29.3	22.0	29.0
31.9	34.6	18.1	60.5	18.8	29.3	9.0	32.4
16.6	34.7	22.4	60.5	18.8	29.3	26.7	32.4
19.8	34.7	23.2	60.5	19.8	29.3	29.0	32.4
25.4	34.7	27.9	60.5	21.3	29.3	29.0	32.4
27.2	34.7	27.9	60.5	22.6	29.3	37.3	40.1
32.1	34.7	25.8	61.0	22.6	29.3	37.7	40.1
32.1	34.7	27.4	61.0	22.6	29.3	38.7	40.1
33.2	34.7	30.8	61.0	23.7	29.3	39.7	40.2
31.5	35.3	32.8	61.0	24.9	29.3	17.0	36.7
33.3	35.3	16.3	61.9	26.0	29.3	24.9	36.7
34.3	36.0	19.8	61.9	26.0	29.3	24.9	36.7
34.8	35.3	21.8	61.9	27.6	29.3	29.9	36.7
35.0	35.5	21.8	61.9	31.4	32.6	20.8	26.9
27.8	30.0	24.0	61.9	28.5	32.3	22.2	26.9
27.4	32.9	25.7	61.9	28.5	32.3	22.7	31.0
27.4	32.9	26.8	61.9	18.5	29.9	27.5	31.0
30.3	32.9	16.1	61.9	18.9	29.9	29.1	31.0
31.0	32.9	21.7	61.9	12.6	26.1	29.1	31.0
32.4	32.9	22.5	61.9	13.2	26.1	29.1	31.0
30.4	31.7	22.5	61.9	14.4	26.1	29.1	31.0
31.2	31.7	22.5	61.9	14.4	26.1	28.2	31.8
29.5	30.9	24.8	61.9	18.4	26.1	34.9	35.4
28.9	31.3	24.8	61.9	19.9	26.1	34.9	35.4
34.1	35.4	24.8	61.9	19.9	26.1	28.5	32.7
32.1	33.6	25.7	61.9	20.7	26.1	22.2	31.4
32.1	33.6	25.7	61.9	22.5	26.1	26.9	31.4
33.0	33.6	25.7	61.9	13.7	29.8	28.8	31.4

Table 27 (continued). Bead profile data from Experiment B-3 at 128.9 h.

z	L_f	z	L_f	z	L_f	z	L_f
27.8	30.9	27.0	61.9	13.7	29.8	30.1	31.3
29.3	30.9	27.0	61.9	16.8	29.8	30.1	31.3
28.1	32.1	27.5	61.9	18.2	29.8	30.1	31.3
28.9	30.1	27.5	61.9	18.2	29.8	24.8	30.0
25.6	29.5	28.8	61.9	19.9	29.8	26.1	29.9
35.6	36.4	28.8	61.9	21.5	29.8	28.6	29.9
31.9	32.3	28.8	61.9	25.3	29.8	28.5	30.8
30.2	30.6	28.8	61.9	21.5	31.7	29.9	30.8
33.9	34.4	30.0	61.9	22.7	31.7	30.0	31.6
33.9	34.4	30.0	61.9	24.3	31.7	30.7	31.6
31.0	32.1	30.5	61.9	27.9	31.7	20.9	31.4
30.2	33.2	26.6	61.9	23.9	32.0	29.3	31.4
30.2	33.2	29.2	61.9	26.2	32.0	30.2	31.4
31.2	33.2	31.5	61.9	26.2	32.0	30.2	31.4
21.3	24.9	31.5	61.9	26.2	32.0	32.0	32.5
22.1	24.9	32.8	61.9	27.1	32.0	19.2	28.9
31.9	32.4	34.7	61.9	27.1	32.0	25.5	28.9
24.3	26.8	37.0	61.9	28.4	32.0	24.8	28.4
24.9	26.8	40.0	61.9	16.9	29.1	23.6	27.7
24.9	26.8	49.4	61.9	17.6	29.1	18.7	24.5
26.3	26.8	51.3	61.9	18.7	29.1	22.3	27.8
17.4	27.8	51.3	61.9	18.7	29.1	24.5	27.3
17.6	27.8	52.4	61.9	18.7	29.1	24.5	27.3
19.2	27.8	55.4	61.9	20.9	29.1	25.5	34.4
20.5	27.8	55.4	61.9	21.6	29.1	28.7	36.6
21.4	27.8	56.4	61.9	22.1	29.1	31.1	36.6
20.8	27.8	60.7	61.9	23.7	29.1	26.6	27.0
21.6	27.8	60.7	61.9	25.4	29.1	24.0	24.9
22.5	27.8	22.6	55.5	25.9	29.1	25.6	27.0
22.5	27.8	22.6	55.5	25.9	29.1	17.5	29.8
23.3	27.8	24.8	55.5	26.8	29.1	28.5	29.6
23.8	27.8	24.8	55.5	29.0	30.3	25.6	26.1
23.8	27.8	25.8	55.5	19.7	30.9	23.6	24.0
24.1	27.8	27.7	55.5	21.7	30.9	27.4	34.9
24.9	27.8	27.7	55.5	24.3	30.9	25.0	41.3
24.9	27.8	27.7	55.5	25.6	30.9	29.5	41.3
24.2	27.8	27.7	55.5	24.0	33.0	30.8	41.3
24.2	27.8	27.7	55.5	25.0	33.0	30.8	41.3
25.2	27.8	30.0	55.5	25.0	33.0	32.2	41.3

Table 27 (continued). Bead profile data from Experiment B-3 at 128.9 h.

z	L_f	z	L_f	z	L_f	z	L_f
26.1	27.8	30.0	55.5	25.0	33.0	32.2	41.3
26.6	27.8	30.0	55.5	30.0	33.0	33.0	41.3
28.4	32.3	30.0	55.5	31.3	33.0	33.8	41.0
18.2	33.6	31.9	55.5	22.0	28.0	29.8	43.4
19.8	33.6	31.9	55.5	25.2	30.5	31.2	43.4
20.7	33.6	31.9	55.5	27.9	30.5	32.5	43.4
22.0	33.6	33.2	55.5	20.4	30.5	32.5	43.4
24.6	33.6	33.2	55.5	22.9	30.5	32.5	43.4
24.6	33.6	33.2	55.5	29.9	30.5	32.5	43.4
25.5	33.6	35.8	55.5	26.6	34.1	34.3	43.4
27.1	33.6	35.8	55.5	26.1	39.4	21.2	42.2
27.1	33.6	37.1	55.5	26.1	39.4	23.4	42.2
27.6	33.6	37.1	55.5	26.1	39.4	23.4	42.2
29.7	33.6	39.0	55.5	26.1	39.4	24.7	42.2
31.2	35.3	39.0	55.5	37.6	39.4	24.7	42.2
34.9	35.3	39.0	55.5	38.8	39.4	24.7	42.2
19.0	34.2	39.0	55.5	31.7	37.3	25.1	42.2
21.0	34.2	39.0	55.5	33.5	37.3	26.2	42.2
24.9	33.4	40.9	55.5	34.9	37.3	27.3	42.2
29.9	33.4	42.2	55.5	36.4	37.3	27.3	42.2
30.8	33.4	42.2	55.5	34.4	42.6	28.1	42.2
19.5	37.8	43.2	55.5	35.3	42.6	28.8	42.2
25.2	37.8	44.4	55.5	37.9	42.6	30.4	42.2
28.2	34.9	45.0	55.5	40.1	43.0	31.7	41.6
28.0	40.2	47.1	55.5	42.0	43.0	32.7	41.6
30.9	40.2	50.6	55.5	30.6	36.5	17.3	34.3
31.6	40.2	50.6	55.5	31.2	36.5	19.0	34.3
32.7	40.2	52.7	55.5	31.2	36.5	20.5	34.3
33.6	40.2	55.0	55.5	32.2	36.5	17.5	33.7
35.2	40.2	42.6	53.6	32.6	36.5	21.3	33.7
36.3	40.2	46.0	53.6	33.6	36.5	26.3	33.7
38.4	41.5	51.6	53.6	34.1	37.1	30.4	33.7
23.5	33.2	51.6	53.6	34.5	38.2	13.8	34.6
26.0	33.2	51.6	53.6	34.8	38.2	13.8	34.6
24.4	29.0	0.6	63.6	35.7	38.2	17.3	34.6
24.4	29.0	2.3	63.6	35.7	38.2	19.8	34.6
27.5	29.0	45.2	63.6	37.1	38.2	23.1	34.6
15.6	22.8	58.3	63.6	32.0	38.2	25.1	34.6
16.8	22.8	60.2	63.6	28.5	37.0	26.3	34.6

Table 27 (continued). Bead profile data from Experiment B-3 at 128.9 h.

z	L_f	z	L_f	z	L_f	z	L_f
18.2	22.8	1.1	65.6	28.5	37.0	28.4	34.6
19.1	22.8	40.9	65.6	30.7	37.0	30.0	34.6
19.6	22.8	49.0	65.6	31.3	37.0	30.0	34.6
19.7	22.8	52.0	68.0	31.3	37.0	12.4	33.4
20.5	22.8	53.0	68.0	32.4	37.0	13.2	33.4
20.0	22.8	53.0	68.0	34.4	37.0	13.5	33.4
21.1	22.8	53.0	68.0	35.8	37.0	13.5	33.4
21.1	22.8	54.0	68.0	25.5	33.5	14.3	33.4
22.1	22.8	1.8	68.7	33.0	33.5	14.3	33.4
22.1	22.8	3.1	68.7	17.7	26.9	15.6	33.4
22.7	23.1	4.2	68.7	20.2	26.9	16.6	33.4
17.8	19.4	4.2	68.7	21.4	26.9	18.8	33.4
38.4	45.1	27.2	36.0	36.4	46.2	37.6	40.9
17.5	38.1	5.1	68.7				

Table 28. Bead profile data from Experiment B-3 at 143.9 h. Symbols are as described in Figure 3. The data are presented in Figure 11. Distances are in μm.

z	L_f	z	L_f	z	L_f	z	L_f
21.5	22.0	8.8	23.9	16.0	33.7	14.1	40.4
20.4	21.7	20.5	31.4	17.1	33.7	16.1	40.4
17.5	21.4	10.7	20.4	17.8	35.2	17.1	40.4
14.9	21.2	12.5	20.8	19.0	35.2	17.8	40.4
14.1	22.1	21.4	24.7	18.7	37.4	17.8	40.4
16.1	22.1	24.4	34.3	18.7	37.4	18.8	40.4
17.7	22.1	22.4	35.7	20.5	37.4	18.8	40.4
19.4	22.1	23.4	35.7	20.5	37.4	20.6	40.4
20.0	22.1	15.4	30.7	21.7	37.4	20.6	40.4
21.6	22.1	10.1	35.6	33.4	37.4	20.6	40.4
21.6	22.1	19.8	35.8	19.0	20.5	21.3	40.4
8.8	23.3	22.2	35.8	13.0	18.0	21.3	40.4
8.8	23.3	26.4	35.8	20.6	23.8	22.4	40.4
11.3	23.3	20.3	35.6	7.3	25.9	23.1	40.4
6.2	24.0	21.4	35.6	8.3	25.9	18.2	39.1
7.2	24.0	23.2	35.6	25.4	25.9	29.1	38.3
7.8	24.0	23.6	34.7	4.8	23.4	23.2	38.3
10.5	24.0	15.3	32.5	7.4	23.4	10.9	40.8
14.5	18.0	17.0	32.5	8.1	23.4	22.5	40.8
15.3	18.0	21.0	32.5	14.0	23.4	24.2	40.8
5.7	23.6	24.9	32.5	14.9	23.4	36.0	40.8
7.2	23.6	26.2	30.6	18.1	23.4	16.8	41.3
7.2	23.6	20.0	31.5	19.6	23.4	21.1	40.2
8.5	23.6	9.2	45.6	5.1	24.3	22.7	40.2
8.5	23.6	9.2	45.6	6.0	24.3	30.6	40.2
14.1	23.6	10.1	45.6	6.0	24.3	33.3	40.2
21.6	23.6	11.6	45.6	6.7	24.3	33.3	40.2
23.1	23.6	11.6	45.6	8.8	24.3	38.2	40.8
23.1	23.6	13.1	45.6	12.2	24.3	39.0	40.8
20.3	23.8	13.1	45.6	13.1	24.3	13.8	36.2
7.9	9.6	14.1	45.6	23.3	24.3	13.8	36.2
19.2	25.9	14.1	45.6	11.0	31.4	14.8	24.4
19.2	25.9	21.5	45.6	17.1	31.4	16.2	24.3
16.6	25.8	22.6	45.6	17.1	31.4	18.0	23.8
23.2	25.8	13.0	46.0	17.1	31.4	21.6	23.9
21.0	24.9	13.0	46.0	17.8	31.4	17.8	24.5

Table 28 (continued). Bead profile data from Experiment B-3 at 143.9 h.

z	L_f	z	L_f	z	L_f	z	L_f
19.1	20.8	13.3	47.4	18.8	31.4	25.4	26.1
4.8	19.4	14.3	47.4	18.8	31.4	27.0	27.4
4.8	19.4	15.4	47.4	19.7	31.4	20.8	28.5
8.6	19.4	15.4	47.4	20.3	31.4	23.8	28.4
10.0	19.4	16.2	47.4	21.7	31.4	23.8	28.4
13.2	16.3	17.5	47.4	21.7	31.4	25.2	28.4
11.8	17.2	18.1	47.4	22.6	31.4	26.3	28.4
15.1	17.2	18.1	47.4	22.6	31.4	11.2	26.6
28.3	29.4	18.1	47.4	23.9	31.4	19.5	31.0
25.9	26.4	19.1	47.4	24.4	31.4	12.1	31.3
22.6	26.2	20.4	47.4	26.9	31.4	12.7	31.3
24.4	26.2	20.4	47.4	27.0	31.4	13.9	31.3
21.8	25.7	17.7	48.3	27.0	31.4	18.8	31.3
26.3	26.7	19.3	48.3	27.0	31.4	21.8	31.3
19.3	21.2	19.3	48.3	27.0	31.4	13.2	31.4
20.7	21.2	20.5	48.3	28.3	31.4	15.6	31.4
11.4	20.1	20.5	48.3	28.3	31.4	17.1	31.4
17.4	20.1	24.7	48.3	30.4	31.4	17.6	32.4
18.5	20.1	26.1	48.3	29.4	30.6	16.5	32.4
18.5	20.1	29.1	48.3	16.6	26.5	25.4	32.4
17.5	18.0	15.8	48.7	18.4	26.5	29.3	32.4
21.2	21.7	17.1	48.7	21.6	26.5	19.0	33.1
18.4	22.4	17.1	48.7	24.3	26.5	19.0	33.1
23.7	25.0	17.1	48.7	24.3	26.5	20.0	33.1
23.8	24.3	19.2	48.7	24.3	26.5	23.1	33.1
17.6	25.0	19.2	48.7	25.1	26.5	15.4	33.4
15.8	28.7	19.2	48.7	26.0	26.5	17.8	33.4
8.4	11.2	19.2	48.7	6.6	21.3	19.4	33.4
1.4	23.4	19.2	48.7	7.9	21.3	21.6	33.4
2.4	23.4	20.1	48.7	8.6	21.3	25.8	33.4
3.1	23.4	20.1	48.7	11.1	21.3	27.0	33.4
4.6	23.4	20.1	48.7	12.8	21.3	31.0	33.4
4.6	23.4	20.9	48.7	13.9	21.3	19.2	34.2
5.3	23.4	20.9	48.7	14.7	21.3	20.4	34.2
6.5	23.4	21.5	48.7	14.7	21.3	22.8	34.2
9.8	23.4	22.6	48.7	17.9	21.3	25.8	34.2
14.9	23.4	23.4	48.7	17.9	21.3	29.4	34.2
18.2	23.4	23.4	48.7	9.9	21.3	19.3	26.2
20.0	23.4	29.9	48.7	9.9	21.3	21.2	26.2

Table 28 (continued). Bead profile data from Experiment B-3 at 143.9 h.

z	L_f	z	L_f	z	L_f	z	L_f
21.8	23.4	31.8	48.7	9.9	21.3	21.2	26.2
22.6	23.4	32.7	48.7	12.4	21.3	23.2	26.2
10.6	24.5	37.3	48.7	13.8	21.3	24.7	26.2
11.8	24.5	37.3	48.7	13.8	21.3	15.6	23.0
15.7	17.2	17.0	45.7	16.9	21.3	21.3	26.4
3.6	19.4	22.5	45.7	16.9	21.3	24.5	25.7
6.5	19.4	23.6	45.7	6.8	21.9	28.3	37.5
8.1	19.4	24.4	45.7	6.8	21.9	27.1	38.8
9.9	19.4	30.1	45.7	6.8	21.9	9.2	38.3
15.2	19.4	30.3	38.2	11.1	21.9	10.2	38.3
15.2	19.4	31.9	37.5	19.4	21.9	11.4	38.3
16.4	19.4	14.7	56.7	12.3	21.0	11.4	38.3
16.4	19.4	28.8	56.7	17.8	21.0	12.7	38.3
17.6	19.4	30.7	56.7	18.7	21.0	14.1	38.3
18.4	19.4	30.7	56.7	8.5	20.8	15.8	38.3
28.5	29.0	32.8	56.7	9.8	20.8	17.8	38.3
18.6	22.0	34.4	56.7	10.6	20.8	17.8	38.3
18.4	20.6	34.4	56.7	11.9	20.8	17.8	38.3
3.4	11.0	34.4	56.7	12.3	20.8	19.2	38.3
13.6	14.1	35.2	56.7	13.7	20.8	21.8	38.3
30.2	30.7	36.8	56.7	4.3	21.1	21.8	38.3
27.9	30.7	36.8	56.7	4.3	21.1	23.6	38.3
23.2	28.2	36.8	56.7	5.4	21.1	25.5	38.3
26.1	28.2	36.8	56.7	5.4	21.1	6.9	38.2
26.1	28.2	36.8	56.7	7.8	21.1	6.9	38.2
26.1	28.2	36.8	56.7	7.8	21.1	10.5	38.2
27.1	28.2	38.7	56.7	7.8	21.1	10.5	38.2
27.7	28.2	38.7	56.7	9.0	21.1	13.2	38.2
22.4	24.0	50.7	56.7	9.0	21.1	13.2	38.2
23.4	24.0	53.2	56.7	9.0	21.1	17.8	38.2
4.7	16.9	55.9	56.7	9.7	21.1	17.8	38.2
1.5	13.8	54.9	56.7	9.7	21.1	19.5	38.2
4.1	13.8	42.5	57.8	10.9	21.1	19.5	38.2
5.1	13.8	43.6	57.8	10.9	21.1	25.1	38.2
6.3	13.8	38.2	58.6	15.2	21.1	5.1	37.5
7.5	13.8	46.5	58.6	12.4	33.1	6.9	37.5
9.2	13.8	47.8	58.6	12.4	33.1	6.9	37.5
10.0	13.8	47.8	58.6	14.6	33.1	8.6	37.5
12.2	13.8	47.8	58.6	9.3	31.8	13.6	37.5

Table 28 (continued). Bead profile data from Experiment B-3 at 143.9 h.

z	L_f	z	L_f	z	L_f	z	L_f
13.0	13.8	51.0	58.6	17.8	31.8	14.8	37.5
15.1	42.4	51.3	58.4	7.7	31.7	14.9	37.5
15.1	42.4	52.8	59.8	7.7	31.7	14.9	37.5
15.1	42.4	53.9	59.8	9.7	31.7	16.1	37.5
16.1	42.4	52.5	60.9	10.8	31.7	20.8	37.5
16.9	42.4	54.6	60.9	12.3	40.0	22.4	37.5
19.7	42.4	60.4	60.9	13.7	40.0	22.4	37.5
19.7	42.4	52.6	58.6	17.4	40.0	23.2	37.5
20.5	42.4	54.9	58.6	17.4	40.0	26.0	37.5
21.4	42.4	54.9	58.6	20.0	40.0	27.3	37.5
21.4	42.4	54.9	58.6	20.9	40.0	27.3	37.5
24.6	42.4	56.4	58.6	30.3	40.0	8.7	34.9
41.2	42.4	53.4	58.4	34.7	40.0	7.8	34.9
16.4	40.8	54.3	58.4	36.2	40.0	21.0	34.9
17.3	40.8	60.1	61.1	36.2	40.0	24.3	34.9
18.4	40.8	52.5	59.8	36.2	40.0	30.4	34.9
18.9	40.8	54.2	59.8	36.2	40.0	10.7	32.0
18.9	40.8	52.6	57.7	36.2	40.0	15.1	32.0
17.3	39.0	53.8	57.7	37.7	40.0	18.2	32.0
19.3	39.0	55.5	57.7	37.7	40.0	21.0	32.0
21.0	39.0	52.8	59.9	37.7	40.0	24.9	32.0
21.0	39.0	54.9	59.9	37.7	40.0	24.0	32.0
38.5	39.0	59.4	59.9	38.4	40.0	22.4	32.0
19.9	38.5	55.2	66.6	38.4	40.0	25.1	32.0
21.2	38.5	56.9	66.6	27.7	33.8	1.3	28.6
23.5	38.5	58.6	66.6	29.2	33.8	4.0	28.6
34.1	38.5	63.2	66.6	27.8	56.7	7.3	28.6
36.0	38.5	54.8	56.5	37.6	56.7	7.3	28.6
36.7	38.5	54.8	56.5	39.0	56.7	7.3	28.6
38.0	38.5	54.0	55.5	44.8	48.7	8.6	28.6
37.4	39.0	31.2	55.2	33.3	39.8	11.0	28.6
38.1	39.0	31.2	55.2	22.5	28.5	13.4	28.6
38.5	39.0	50.8	55.2	22.2	38.0	13.8	28.6
30.6	39.9	50.8	55.2	19.4	34.4	15.7	28.6
25.0	39.6	53.0	55.2	21.4	33.6	26.0	28.6
33.9	39.6	53.4	55.2	28.3	33.6	4.9	27.7
35.0	39.6	54.7	55.2	29.2	33.6	6.2	27.7
25.9	28.0	32.9	54.1	14.8	20.3	7.4	27.7
31.4	33.7	32.9	54.1	14.9	18.1	9.6	27.7

Table 28 (continued). Bead profile data from Experiment B-3 at 143.9 h.

z	L_f	z	L_f	z	L_f	z	L_f
31.4	33.7	33.9	54.1	17.0	18.1	13.6	27.7
31.4	33.7	33.9	54.1	17.0	18.1	18.4	27.7
32.4	33.7	35.1	54.1	17.0	18.1	23.5	27.7
33.2	33.7	35.1	54.1	17.6	18.1	8.0	19.2
22.0	26.0	50.9	54.1	18.0	28.2	3.3	21.2
24.5	26.0	50.9	54.1	19.3	25.5	8.1	21.2
18.0	26.3	53.6	54.1	12.4	18.9	11.2	21.2
24.8	26.3	36.7	50.2	11.6	21.0	13.3	21.2
20.9	26.7	37.6	50.2	17.2	21.0	9.8	24.1
24.1	26.7	38.8	50.2	16.4	25.2	22.9	23.8
15.7	16.2	41.8	50.2	19.9	25.2	23.7	24.1
10.0	13.9	45.8	50.2	23.1	25.2	23.7	24.1
11.8	13.9	45.8	50.2	23.1	25.2	22.8	25.4
13.4	13.9	48.1	50.2	23.1	25.2	15.5	23.6
21.8	27.0	7.9	36.8	23.1	25.2	19.0	21.1
23.6	27.0	11.1	36.8	26.2	29.4	16.0	27.3
26.0	27.0	12.6	36.8	19.9	29.4	24.3	27.3
26.0	27.0	14.4	36.8	19.9	29.4	21.3	24.8
27.2	36.5	9.4	34.0	21.2	29.4	24.8	29.3
32.9	36.5	10.6	34.0	21.2	29.4	24.7	26.7
34.5	36.5	10.6	34.0	20.1	26.7	24.7	26.7
36.6	38.1	11.8	34.0	21.0	26.7	19.1	27.4
38.2	38.7	11.8	34.0	21.0	26.7	27.3	27.9
37.7	39.7	11.8	34.0	25.1	26.7	17.9	29.2
37.7	39.7	13.8	34.0	26.2	26.7	21.8	29.2
38.7	39.7	14.4	34.0	27.4	29.2	24.7	29.2
32.3	34.1	14.4	34.0	16.1	20.0	24.7	29.2
33.6	34.1	15.0	34.0	9.4	17.0	27.9	29.2
25.1	27.5	13.5	32.8	6.7	23.5	24.2	28.7
19.0	23.4	16.2	32.8	18.6	23.5	26.4	28.7
20.8	23.4	13.2	32.8	21.6	23.5	24.6	28.1
12.1	39.8	14.3	32.8	19.5	25.2	27.5	28.1
11.4	39.3	12.9	26.5	23.9	25.2	24.6	28.5
41.1	42.6	13.9	26.5	19.1	26.0	27.8	28.5
13.4	41.6	9.3	23.9	21.4	26.0	27.8	28.5
14.9	41.2	9.2	25.0	22.5	26.0	29.2	29.7
39.3	41.2	10.4	25.0	26.3	34.9	19.9	30.7
39.7	41.6	11.5	25.0	24.5	37.2	23.8	30.7
41.8	42.2	12.5	25.0	31.5	37.2	27.6	30.9

Table 28 (continued). Bead profile data from Experiment B-3 at 143.9 h.

z	L_f	z	L_f	z	L_f	z	L_f
41.8	42.2	12.5	25.0	32.7	37.2	27.6	30.9
16.3	42.2	13.7	25.0	29.2	46.1	2.1	27.9
41.7	42.2	13.7	25.0	32.0	46.1	3.0	26.2
40.6	42.0	13.0	30.7	32.0	46.1	3.0	26.2
41.5	42.0	14.4	30.7	34.8	46.1	4.2	26.2
40.7	41.7	15.2	30.7	34.8	46.1	16.5	22.8
13.8	41.8	14.3	30.7	36.3	46.1	14.1	22.8
38.2	41.8	14.3	30.7	38.4	46.1	15.8	22.8
16.9	41.8	16.4	30.7	15.1	25.8	19.1	22.8
39.2	41.8	16.4	30.7	10.2	24.1	21.0	22.8
39.8	41.8	16.4	30.7	15.9	17.0	7.8	19.8
40.9	41.8	19.0	31.8	7.6	17.8	0.6	19.8
16.0	25.2	19.0	31.8	18.7	30.4	19.8	20.6
25.2	26.0	21.2	31.8	15.0	30.4	18.2	22.5
24.3	24.8	16.3	36.7	20.7	30.4	20.4	22.5
23.9	24.4	22.2	36.7	20.7	30.4	18.1	21.4
3.8	12.5	26.9	36.7	21.5	30.4	14.0	24.1
6.2	12.5	28.4	36.7	21.5	30.4	25.5	26.3
10.9	11.5	27.0	38.9	23.9	30.4	24.0	27.1
10.6	14.3	29.2	38.9	23.9	30.4	24.4	27.2
7.3	18.7	18.6	29.2	13.1	30.4	12.2	30.7
9.4	18.7	19.0	22.7	26.2	30.4	16.4	30.7
9.4	18.7	12.0	29.8	26.2	30.4	17.5	30.7
9.7	18.7	22.7	29.8	22.6	28.6	17.9	30.7
10.8	18.7	13.7	29.8	23.8	28.6	20.6	30.7
11.6	18.7	10.1	39.7	24.5	28.6	21.7	30.7
11.7	18.7	10.1	39.7	25.8	28.6	21.7	30.7
12.7	18.7	11.6	39.7	25.8	28.6	22.7	30.7
13.0	18.7	12.7	39.7	25.8	28.6	22.7	30.7
16.5	18.7	13.4	39.7	27.3	28.6	19.4	31.3
11.5	18.9	17.5	39.7	13.3	27.7	20.9	31.3
12.6	18.9	18.3	39.7	23.5	27.7	22.9	31.3
15.0	18.9	20.8	39.7	26.5	27.9	27.0	31.3
12.3	21.0	20.8	39.7	27.5	28.5	27.8	31.3
13.2	21.0	22.9	39.7	13.0	27.5	28.8	31.3
13.2	21.0	25.7	39.7	26.7	27.5	22.2	32.7
13.2	21.0	10.8	45.4	12.9	20.5	23.9	32.7
14.2	21.0	38.2	45.4	14.8	20.5	26.8	32.7
14.2	21.0	42.0	45.4	17.2	20.5	28.2	32.7

Table 28 (continued). Bead profile data from Experiment B-3 at 143.9 h.

z	L_f	z	L_f	z	L_f	z	L_f
17.1	21.0	10.7	41.3	9.7	21.3	18.8	32.6
16.2	30.6	30.2	34.2	17.9	21.3	23.7	32.6
14.6	33.7	28.8	35.5	15.8	22.8	23.7	32.6
16.0	33.7	12.2	35.8	16.4	22.8	27.9	32.6
19.7	24.9	15.5	46.0	17.8	31.4	12.6	26.1
16.0	33.7	14.8	36.1				

Table 29. Bead profile data from Experiment B-3 at 191.9 h. Symbols are as described in Figure 3. The data are presented in Figure 11. Distances are in μm.

z	L_f	z	L_f	z	L_f	z	L_f
15.4	33.1	2.4	31.8	10.4	26.2	26.0	53.6
18.4	34.2	5.7	31.8	22.7	26.2	25.1	53.6
19.5	35.3	7.0	31.8	25.7	26.2	29.4	53.6
18.5	36.4	12.9	31.5	0.5	25.1	30.3	53.6
20.0	36.4	14.3	31.5	1.7	25.9	30.3	53.6
20.0	36.4	15.0	31.5	19.5	25.9	30.9	53.6
11.2	37.4	14.2	30.3	20.5	25.2	33.4	53.6
22.8	37.4	16.5	30.3	20.5	25.2	35.5	53.6
7.1	39.8	16.9	31.4	21.7	25.2	35.5	53.6
7.1	39.8	11.2	31.8	24.7	25.2	37.3	53.6
8.1	39.8	11.2	31.8	1.7	24.9	37.3	53.6
9.0	39.8	21.0	30.8	0.5	24.9	15.7	49.8
25.2	39.8	21.0	30.8	1.2	22.6	21.3	49.8
16.3	54.1	9.9	33.3	2.8	22.6	25.4	49.8
16.3	54.1	10.0	31.2	2.8	22.6	25.4	49.8
22.0	54.1	12.0	31.2	2.8	22.6	29.5	49.8
29.2	54.1	17.2	31.7	4.0	22.6	35.9	49.8
7.4	54.3	24.0	31.7	9.4	25.3	39.6	49.8
6.2	54.7	19.4	32.5	2.8	17.7	11.0	49.6
7.4	54.7	20.5	32.5	2.8	17.7	12.3	49.6
31.2	54.7	17.9	33.2	4.6	17.7	13.6	49.6
32.9	54.7	8.4	34.1	6.8	17.7	15.7	49.6
17.8	54.1	10.8	34.1	6.5	17.7	17.7	49.6
30.3	54.1	0.5	28.6	9.5	17.7	21.2	49.6
33.4	54.1	5.5	28.6	9.5	17.7	21.2	49.6
4.3	52.2	5.5	28.6	10.6	17.7	19.7	49.6
4.3	52.2	7.6	28.6	10.6	17.7	23.1	49.6
5.5	52.2	8.2	28.6	15.6	17.7	23.1	49.6
26.3	52.2	9.3	28.6	6.6	16.0	25.1	49.6
30.6	52.2	11.3	28.6	6.6	16.0	27.9	49.6
32.8	52.2	11.3	28.6	13.1	16.0	29.0	49.6
3.6	51.7	12.2	28.6	14.3	16.0	29.0	49.6
3.0	51.7	13.4	28.6	5.0	17.2	29.7	49.6
24.3	47.1	26.7	28.6	7.9	17.2	31.4	49.6
24.3	47.1	9.1	25.7	14.8	17.2	33.6	49.6
26.7	47.1	10.8	25.7	16.0	17.2	3.9	52.4

Table 29 (continued). Bead profile data from Experiment B-3 at 191.9 h.

z	L_f	z	L_f	z	L_f	z	L_f
26.7	44.1	12.5	25.7	1.0	17.2	23.7	52.4
3.5	44.1	13.2	25.7	5.0	17.2	23.7	52.4
6.3	44.1	13.2	25.7	16.7	17.2	25.0	52.4
7.4	44.1	13.7	25.7	17.4	41.1	28.6	52.4
11.7	44.1	15.0	25.7	18.8	41.1	31.6	52.4
0.7	21.5	15.0	25.7	19.6	41.1	35.5	52.4
4.1	21.5	9.0	20.5	21.9	41.1	40.3	52.4
4.1	21.5	10.6	20.5	23.9	41.1	30.3	52.2
4.1	21.5	15.4	20.5	24.5	41.1	28.5	50.1
5.0	21.5	16.0	20.5	25.5	41.1	22.0	49.3
5.0	21.5	5.4	26.9	26.1	41.1	22.0	49.3
6.5	21.5	12.8	26.9	27.8	41.1	24.3	41.7
1.4	21.1	12.8	26.9	29.6	41.1	25.1	41.7
5.1	21.1	14.0	26.9	30.3	41.1	22.1	41.9
5.1	21.1	17.2	26.9	31.7	41.1	25.0	41.9
5.1	21.1	5.7	36.1	34.0	41.1	5.4	28.5
8.0	21.1	8.3	36.1	35.2	41.1	6.7	28.5
0.5	20.7	12.3	36.1	40.6	41.1	6.7	28.5
3.5	22.0	12.3	36.1	16.8	47.0	10.7	28.5
9.9	22.0	30.3	36.1	16.8	47.0	10.7	28.5
4.3	21.9	30.3	36.1	15.4	47.0	13.0	28.5
13.4	21.9	32.0	43.5	41.1	47.0	15.8	28.5
14.6	21.9	32.0	43.5	42.8	47.0	15.8	28.5
15.4	21.9	32.0	43.5	45.1	47.0	18.3	28.5
8.7	21.7	33.4	43.5	17.2	46.4	19.3	28.5
13.5	21.7	33.8	43.5	18.7	46.4	19.3	28.5
10.2	22.2	33.8	43.5	24.4	46.4	19.3	28.5
13.8	21.8	33.8	43.5	40.8	46.4	24.1	28.5
14.7	21.8	30.7	43.6	43.0	46.4	15.2	26.6
14.1	23.2	37.1	43.6	43.0	46.4	15.2	26.6
4.5	24.6	29.7	43.0	44.7	46.4	16.9	26.6
14.0	24.6	34.8	43.0	21.5	46.0	17.5	26.6
14.8	24.6	34.8	43.0	23.0	46.0	18.0	26.6
24.3	24.5	37.2	42.9	24.4	46.0	19.1	26.6
4.4	31.9	37.2	42.9	25.9	46.0	22.6	26.6
24.3	28.1	38.1	42.9	39.8	46.0	23.9	26.6
25.8	28.4	40.4	42.9	45.5	46.0	15.7	27.3
17.9	29.5	40.4	42.9	10.9	45.6	15.7	27.3
21.6	29.5	41.3	42.9	13.2	45.6	15.7	27.3

Table 29 (continued). Bead profile data from Experiment B-3 at 191.9 h.

z	L_f	z	L_f	z	L_f	z	L_f
24.1	29.5	42.4	42.9	13.2	45.6	20.0	27.3
24.7	30.4	33.7	43.2	14.5	45.6	20.5	27.3
11.7	31.2	36.1	43.2	19.0	45.6	20.8	27.3
24.6	31.2	42.8	43.2	38.4	45.6	22.0	27.3
17.3	31.3	38.6	42.3	42.5	45.6	22.9	27.3
25.9	31.3	38.9	42.3	13.6	48.5	23.5	27.3
26.7	31.3	40.2	42.3	16.0	48.5	2.4	27.6
20.7	32.7	41.8	42.3	16.8	48.5	4.1	27.6
20.7	32.7	36.1	37.4	21.7	48.5	7.0	27.6
21.9	32.7	36.1	37.4	24.0	48.5	18.7	27.6
22.5	32.7	7.1	33.0	40.9	48.5	21.6	27.6
23.2	32.7	8.6	32.7	16.3	47.6	24.8	27.6
10.7	33.9	10.8	32.7	20.2	47.6	12.0	27.3
22.6	33.9	9.6	32.1	22.1	47.6	18.4	27.3
22.6	33.9	11.1	32.1	22.6	47.6	21.5	27.3
21.3	35.6	13.8	32.1	31.5	47.6	5.8	27.4
22.6	35.6	12.3	32.1	33.6	47.6	5.8	27.4
22.6	35.6	15.8	32.1	33.6	47.6	7.3	27.4
23.6	35.6	6.9	32.0	35.5	47.6	15.9	27.4
24.5	35.6	16.0	32.0	38.6	47.6	20.1	27.4
25.3	35.6	27.0	31.3	38.6	47.6	20.1	27.4
23.7	36.6	27.0	31.3	15.9	46.7	15.3	27.4
25.9	36.6	17.8	30.6	22.2	46.7	21.2	27.4
18.6	39.5	20.2	30.6	23.3	46.7	10.1	27.7
7.8	27.4	20.2	30.6	23.3	46.7	12.2	27.7
10.0	27.4	14.8	25.4	24.5	46.7	15.6	27.7
12.9	27.4	20.7	30.2	24.5	46.7	4.6	22.8
8.3	27.5	21.7	30.2	31.0	46.7	7.2	22.8
10.7	27.5	12.4	32.4	32.4	46.7	9.9	22.8
10.5	30.0	15.8	32.4	34.6	46.7	10.6	22.8
17.0	30.0	16.9	32.4	38.2	46.7	12.4	20.9
12.8	31.8	22.0	32.4	38.2	46.7	8.7	37.9
4.6	31.0	24.3	32.4	41.9	46.7	14.6	37.9
5.5	31.0	11.9	31.7	45.6	46.7	16.2	37.9
8.4	31.0	13.4	31.7	14.0	45.9	17.5	37.9
8.4	31.0	19.4	31.7	16.1	45.9	17.4	39.1
9.9	31.0	20.7	31.7	17.9	45.9	18.6	39.1
12.4	34.6	13.0	33.0	21.7	45.9	12.4	39.3
12.4	34.6	9.9	34.4	23.5	45.9	14.9	33.9

Table 29 (continued). Bead profile data from Experiment B-3 at 191.9 h.

z	L_f	z	L_f	z	L_f	z	L_f
11.9	34.6	22.0	34.4	9.9	43.3	19.6	33.9
2.5	36.7	23.1	34.4	11.5	43.3	15.9	33.9
4.1	36.7	7.7	35.2	17.1	43.3	15.9	33.9
4.1	36.7	10.7	35.2	18.4	43.3	17.6	33.9
4.1	36.7	11.4	35.2	24.8	43.3	18.6	33.9
5.6	36.7	15.2	35.2	21.5	43.5	18.4	34.2
5.6	36.7	18.3	35.2	23.1	43.5	20.2	34.2
6.5	36.7	14.2	35.1	17.0	43.0	26.4	34.2
6.5	36.7	18.6	35.1	19.7	43.0	16.5	25.7
8.6	36.7	21.7	31.9	23.2	43.0	16.5	25.7
8.6	36.7	22.8	31.9	5.6	42.7	19.9	25.7
5.5	37.3	24.6	31.9	16.0	42.7	16.8	24.5
5.5	37.3	18.9	32.4	16.0	42.7	17.2	24.5
6.5	37.3	26.0	32.4	16.9	42.7	18.5	24.5
0.8	37.8	26.0	32.4	17.8	42.7	19.3	24.5
0.5	37.8	15.6	33.4	19.0	42.7	16.1	22.4
8.7	39.9	16.5	33.4	24.4	42.7	19.7	22.4
10.2	34.2	16.5	33.4	27.6	42.7	20.5	22.4
12.9	34.2	16.5	33.4	15.0	39.2	10.6	25.3
40.0	41.2	17.4	33.4	15.0	39.2	14.5	25.3
10.9	33.0	18.0	33.4	18.9	39.2	16.7	25.3
14.4	34.0	18.6	33.4	21.1	39.2	16.7	25.3
14.1	34.5	20.7	33.4	23.0	39.2	17.7	25.3
14.1	34.5	21.5	33.4	6.0	51.3	19.7	25.3
16.0	34.1	22.6	33.4	7.9	51.3	19.7	25.3
19.9	34.1	22.6	33.4	10.1	51.3	20.7	25.3
13.9	55.3	23.6	33.4	14.0	52.3	21.3	25.3
13.9	55.3	22.4	34.7	0.6	52.7	21.3	25.3
15.1	54.6	31.4	34.7	1.2	52.7	22.2	25.3
2.8	51.5	24.3	35.1	6.9	52.7	22.2	25.3
2.8	51.5	27.9	35.1	6.9	52.7	22.2	25.3
4.8	51.5	10.6	30.6	9.5	52.7	18.0	25.1
4.8	51.5	14.9	30.6	10.0	52.7	17.4	25.8
4.8	51.5	19.5	30.6	0.7	52.0	19.8	25.8
12.9	51.5	23.0	30.6	2.4	52.0	21.8	25.8
17.1	51.5	24.3	30.6	9.8	52.0	21.8	25.8
18.5	51.5	27.6	30.6	11.7	52.0	23.4	25.8
19.2	51.5	3.0	28.1	9.0	51.1	25.3	25.8
29.4	51.5	4.5	28.1	7.4	47.6	0.5	26.8

Table 29 (continued). Bead profile data from Experiment B-3 at 191.9 h.

z	L_f	z	L_f	z	L_f	z	L_f
23.5	51.5	5.7	28.1	9.8	47.6	2.4	26.8
24.5	51.5	5.7	28.1	9.1	45.7	15.1	26.8
50.2	51.5	5.7	28.1	9.1	45.7	18.0	26.8
3.4	51.5	8.2	33.7	11.1	43.3	18.0	26.8
19.0	51.5	8.2	33.7	9.9	47.1	20.3	26.8
31.2	51.5	8.7	33.9	17.1	33.7	20.3	26.8
33.3	50.9	8.7	33.9	14.8	41.6	16.6	28.1
3.0	52.5	7.4	33.8	16.7	41.6	17.8	28.1
3.0	52.5	7.4	33.8	17.5	41.6	19.4	28.1
4.5	52.5	9.0	33.8	17.5	41.6	20.2	28.1
4.9	53.1	9.0	33.8	18.1	41.6	20.2	28.1
4.9	52.2	11.3	33.8	18.1	41.6	22.9	28.1
6.2	52.2	14.1	33.8	20.6	41.6	16.1	43.3
9.1	52.2	11.2	35.0	15.0	40.7	16.1	43.3
0.5	40.2	12.4	35.0	16.6	40.7	17.4	43.3
3.6	36.8	14.0	35.0	17.6	40.7	18.7	43.3
4.8	36.8	14.0	35.0	17.6	40.7	26.9	43.3
6.7	36.8	14.0	35.0	20.0	40.7	0.8	43.3
7.4	36.8	11.8	35.5	21.6	40.7	20.2	45.4
8.6	36.8	11.8	35.5	23.9	40.7	22.1	45.4
9.6	36.8	15.2	35.5	29.3	40.7	22.8	45.4
1.6	39.6	16.1	35.5	39.7	40.7	0.6	43.4
2.8	39.6	7.2	35.9	28.2	39.9	29.8	43.4
2.8	39.6	8.4	35.9	8.4	28.2	1.4	46.6
3.8	39.6	9.2	35.9	14.0	28.2	7.1	47.3
4.4	42.0	10.6	35.9	17.5	28.2	10.0	47.3
4.4	42.0	10.6	35.9	14.1	30.3	11.6	47.3
6.0	42.0	10.6	35.9	14.3	27.2	13.3	47.3
11.5	42.0	11.5	35.9	10.4	28.6	13.3	47.3
3.5	42.8	11.5	35.9	11.2	28.6	14.1	47.3
6.0	42.8	11.0	35.9	12.8	29.7	14.1	47.3
5.0	46.2	13.1	35.9	14.1	29.7	17.0	47.3
5.0	46.2	19.3	35.9	14.1	29.7	22.0	47.3
8.3	46.2	22.1	35.9	14.5	29.7	27.4	47.3
4.7	45.7	6.9	37.9	17.0	31.5	28.8	47.3
7.4	45.7	8.6	37.9	18.9	31.5	30.4	47.3
9.7	45.7	7.6	38.3	10.2	28.7	9.4	47.9
10.7	45.7	8.3	38.3	12.0	28.7	13.5	47.9
14.7	45.7	10.3	38.3	13.1	28.7	15.7	47.9

Table 29 (continued). Bead profile data from Experiment B-3 at 191.9 h.

z	L_f	z	L_f	z	L_f	z	L_f
17.0	45.7	7.7	47.2	13.1	28.7	22.3	47.9
2.5	46.2	9.2	47.2	13.1	28.7	30.6	47.9
7.4	46.2	10.0	44.9	14.5	28.7	8.1	46.1
7.4	46.2	14.4	44.9	13.0	33.9	1.4	43.7
0.5	43.5	9.2	43.9	9.5	36.8	2.9	43.7
0.8	43.5	1.4	43.4	8.5	36.5	9.8	36.0
3.7	43.5	1.4	43.4	10.0	36.5	13.5	36.0
8.0	43.5	3.4	43.4	10.0	36.5	13.5	36.0
11.5	43.5	3.4	43.4	14.8	38.7	29.0	36.0
13.3	43.5	3.4	43.4	11.5	37.9	33.2	36.0
0.5	40.9	3.4	43.4	11.5	37.9	34.2	36.0
3.7	40.9	4.6	43.4	6.9	37.4	34.2	36.0
3.7	40.9	5.9	43.4	8.1	37.4	8.9	40.7
5.9	40.9	7.0	43.3	8.1	37.4	8.9	40.7
8.4	40.9	7.1	43.3	11.6	37.4	14.4	40.7
9.6	40.9	22.0	43.3	11.1	37.4	15.8	40.7
11.0	40.9	23.6	43.3	10.1	37.4	15.8	40.7
10.3	40.0	30.4	43.3	12.7	37.4	22.6	40.7
10.3	40.0	30.4	43.3	13.7	37.4	24.1	40.7
12.3	40.0	33.5	43.3	13.7	37.4	34.4	40.7
0.5	40.0	37.5	43.3	13.7	37.4	34.4	40.7
3.5	40.0	12.4	55.7	14.5	37.4	38.0	40.7
8.1	40.0	17.1	55.7	10.3	39.6	38.0	40.7
9.2	40.0	26.6	55.7	11.5	39.6	39.5	40.7
10.4	40.0	29.1	55.7	12.5	39.6	39.5	40.7
7.7	26.1	30.1	55.7	13.7	39.6	39.5	40.7
10.6	26.1	35.6	55.7	9.6	35.7	7.9	39.4
11.7	26.1	35.6	55.7	13.1	30.2	11.7	39.4
13.7	26.1	38.6	55.7	28.5	30.1	25.1	39.4
13.7	26.1	9.5	53.6	29.6	30.1	32.1	39.4
15.0	26.1	17.7	53.6	10.1	33.8	36.1	39.4
15.0	26.1	19.3	53.6	10.1	33.8	38.3	39.4
0.4	26.2	19.3	53.6	11.4	33.8	38.3	39.4
27.8	47.1	10.8	25.7	16.7	17.2	11.5	52.4
10.3	26.2	23.7	53.6	11.8	33.8		

APPENDIX E: HOPKINS STATISTIC DATA

APPENDIX E: HOPKINS STATISTIC DATA

Table 30. Hopkins statistics, suspended bead samples.

			Sample		
Field	A	B	C	D	Control
1	0.535	0.611	0.500	0.546	0.653
2	0.459	0.628	0.722	0.650	0.548
3	0.541	0.730	0.567	0.592	0.688
4	0.659	0.514	0.548	0.723	0.740
5	0.635	0.618	0.849	0.575	0.557
6	0.565	-	0.343	0.517	0.555
7	0.616	0.679	0.654	0.681	0.544
8	0.673	0.637	0.683	0.560	0.538
9	0.743	0.619	0.683	0.659	0.725
10	0.537	0.593	0.577	0.547	0.588
average	0.596	0.625	0.613	0.605	0.614
std.dev.	0.084	0.059	0.138	0.068	0.080

Note: Field B-6 was lost in the computer.

Sample A was taken 0.33 h after bead aggregation test was begun.
Sample B was taken 1.7 h after bead aggregation test was begun.
Sample C was taken 2.7 h after bead aggregation test was begun.
Sample D was taken 3.7 h after bead aggregation test was begun.
Control had beads not mixed with RotoTorque effluent.

Biofilm Samples

Beads were added to a mature biofilm.

1. 1.25 h after the end of bead addition: H = 0.96
2. 1.25 h after the end of bead addition: H = 0.98
3. 19 h after the end of bead addition: H = 0.93

APPENDIX F: CALCULATION OF A PARTICLE REYNOLDS NUMBER

APPENDIX F: CALCULATION OF A PARTICLE REYNOLDS NUMBER

The purpose of computing a particle Reynolds number is to see if viscous or inertial forces dominate particle movement in the bulk liquid of the RotoTorque. If inertial forces are large, momentum may cause particles to penetrate a biofilm.

Two methods will be used. The first computes a particle velocity based on a force balance, as in the derivation of Stoke's Law. The second computes particle velocity from diffusion and hydrodynamic turbulence.

DATA: T = 25°C

η = 0.0089 g cm-1 sec-1

ρ_w = 0.997 g cm^{-3}

v = 0.00893 cm^2 sec^{-1}

particles = latex spheres, diameter = 1 μm, specific gravity = 1.05

reactor = RotoTorque

diameter of inner cylinder = 10.1 cm

radius from central axis to outer wall = 5.85 cm

rotational speed = 200 rpm

(200 rev min^{-1})(2π rad rev^{-1})(1 min(60 sec)$^{-1}$) = 20.9 rad sec^{-1}

METHOD I. FORCE BALANCE

A_p = cross-sectional area of particle

V_p = volume of particle

C_D = drag coefficient

Drag = $C_D A_p \rho_w (v^* v/2)$

a = centripetal acceleration = $\omega^2 r$ = $(20.9 \text{ rad sec}^{-1})^2 (5.85 \text{ cm})$ = 2560 cm sec^{-2}

$\sum F = dv/dt = ma - C_D A_p \rho_w (v^* v/2)$

$v^2 = 2(1.05/0.997)(4/3)(0.5 \times 10^{-4} \text{ cm})(2560 \text{ cm sec}^{-2})(C_D)^{-1}$

C_D is a minimum of 0.4

$v^2 = 0.90 \text{ cm}^2 \text{ sec}^{-2}$, or $v = 0.95 \text{ cm sec}^{-1}$

$Re = (0.95 \text{ cm sec}^{-1})(1 \times 10^{-4} \text{ cm})(0.00893 \text{ cm}^2 \text{ sec}^{-1}) = 0.011$ -- in this range, $C_D = 24 \text{ Re}^{-1}$

$C_D = 24(0.011)^{-1} = 2260$

$v = 0.013 \text{ cm sec}^{-1}$, so Re = 0.0001

$C_D = 1.7 \times 10^{-5}$

$v = 0.0015 \text{ cm sec}^{-1}$, so $Re = 1.6 \times 10^{-5}$

$C_D = 1.5 \times 10^{6}$

$v = 0.00049 \text{ cm sec}^{-1}$

$Re = (0.00049 \text{ cm sec}^{-1})(1 \times 10^{-4} \text{ cm})(0.00893 \text{ cm}^2 \text{ sec}^{-1})^{-1} = \underline{\mathbf{5.5 \times 10^{-6}}}$

METHOD II. HYDRAULIC TURBULENCE (TURBULENT BURSTS)

The method is based on a paper by Beal (1970). Additional information is from Wang and Gerhar (1974) and was quoted by Gunawan (1991).

Needed for this calculation are the average bulk water velocity U and the friction factor f. The velocity distribution in an annular reactor is:

$$\frac{V-V_w}{V_*}=\frac{1}{\kappa}\ln\left[\frac{y/h}{2-y/h}\right] \quad (14)$$

- see Wang and Gerhar, p. 266, equation 9

$$V_{avg}=\frac{\int V dA}{\int dA} \quad (15)$$

Therefore,

$$V=\frac{V_*}{\kappa}\ln\left[\frac{y/h}{2-y/h}\right]+V_w \quad (16)$$

where: V_* = characteristic velocity =

$$\left(\frac{\tau_o}{\rho}\right)^{-1/2} \quad (17)$$

h = one-half of the distance between cylinders

V_w = one-half of the linear velocity of the edge of the rotating inner cylinder

κ = von Karman constant = 0.4

dA = Hdy where H = cylinder height

$$\int V dA = \int^{2h} \frac{V_*}{\kappa} \ln\left[\frac{y/h}{2-y/h}\right] H dy + \int^{2h} V_w H dy \qquad (18)$$

The first integral simplifies to:

$$\frac{V_* H}{\kappa} \left[\int^{2h} \ln(y/h)\, dy - \int^{2h} \ln(2 - y/h)\, dy\right] \qquad (19)$$

=

$$\frac{V_* H}{\kappa} \left[y \ln(y/h) + (2h-y) \ln(2-y/h)\right|^{2h}] \qquad (20)$$

$$= 0$$

Second integral = $$V_w H y\Big|^{2h} = 2 V_w H h \qquad (21)$$

Also,

$$\int dA = \int^{2h} H dy = H y\Big|^{2h} = 2 H h \qquad (22)$$

Therefore,

$$\frac{\int V dA}{\int dA} = \frac{2 V_w H h}{2 H h} = V_w \qquad (23)$$

The average velocity is one-half of the maximum velocity.

$V_w = v_{avg} = 0.5 \omega r_i = 0.5(20.9 \text{ rad sec}^{-1})(10.1/2 \text{ cm}) = 52.8 \text{ cm sec}^{-1}$

To get f, the graph reproduced in Gunawan's thesis (1991) on p. 25-26 was used. This assumes the f in this graph is the Fanning friction factor f used by Beal (1970).

$Re = (\omega d^2)(2\nu)^{-1}$

where: ω = angular velocity (rad sec^{-1})

d = diameter in inner cylinder (cm)

Re = (20.9 rad sec^{-1})(10.1 cm)^2 (2*0.00893 cm^2 sec^{-1})$^{-1}$ = 1.2x10^5

Assuming the biofilm surface is very rough, so ϵ is large, one may use d/ϵ = 87 from Figure 2 of Gunawan. This is a conservative assumption, because if d/ϵ is larger, f is smaller, and v_m is smaller, so Re_p becomes smaller. At Re = 120,000, f/2 = 0.008.

Using equation 27 from Beal:

$$v_m = \frac{U\sqrt{f/2}}{4}\left[v_m^+(d^+/2) + v_m^+(S^+)\right] \quad (24)$$

$d^+/2$ = dimensionless distance at d/2 = 0.5x10^{-4} cm.

$$y^+ = \left(\frac{yU\sqrt{f/2}}{\nu}\right) \quad (25)$$

Therefore,

$$\frac{d^+}{2} = \left(\frac{(0.5x10^{-4}\ cm)\ (52.8 cm\,sec^{-1})\ \sqrt{0.008}}{0.00893 cm^2\ sec^{-1}}\right) = 0.026 \quad (26)$$

Since this is less than 10, $v_m^+ = 0.05\ y^+ = 0.05(0.026) = 0.0013$

Next: for v_m^+ at $S^+ = y^+$,

$$S = \frac{0.05\,U d^2 \rho_p \sqrt{f/2}}{\mu} + \frac{d}{2} \quad (27)$$

from Beal, p. 11. D = particle diameter in this case.

$$S = \frac{0.05\ (52.8\ cm\,sec^{1})\ (1x10^{-4}\ cm)^2\ (1.05\ g\,cm^3)\ \sqrt{0.008}}{0.0089\ g\,cm^{-1}\,sec^{-1}} + 0.5x10^{-4}\ cm \quad (28)$$

S = 5.03x10^{-5} cm

$$S^+ = \frac{S\,U\sqrt{f/2}}{\nu} = \frac{(5.03x10^{-5}\ cm)\ (52.8\ cm\,sec^{-1})\ \sqrt{0.008}}{0.00893\ cm^2\ sec^{-1}} \quad (29)$$

$S^+ = 0.0266$ which is less than 10.

$V_m^+ = 0.05y^+ = 0.05(0.0266) = 0.0013$

$$v_m = \frac{U\sqrt{f/2}}{4}\left[v_m^+\left(\frac{d^+}{2}\right) + v_m^+(S^+)\right] = \frac{(52.8\,cm\,sec^{-1})\,(\sqrt{0.008})}{4}\,[0.0013 + 0.0013] \quad (30)$$

$v_m = 0.0031$ cm sec^{-1}

$$Re_p = \frac{v\,d}{\nu} = \frac{(0.0031\,cm\,sec^{-1})\,(1x10^{-4}\,cm)}{0.00893\,cm^2\,sec^{-1}} = 3.5x10^{-5} \quad (31)$$

SUMMARY: Method I gives a particle Reynolds number of $5.5X10^{-6}$.

Method II gives $3.5x10^{-5}$.

In both cases, viscous forces strongly dominate over inertial forces.

CONCLUSION: Penetration of biofilm by the latex beads due to momentum from bulk water turbulence is highly unlikely as their transport is greatly affected by viscous forces, as compared to inertial forces.

APPENDIX G: CALCULATION OF BIOFILM LIQUID VOLUME FRACTION

APPENDIX G: CALCULATION OF BIOFILM LIQUID VOLUME FRACTION

To compute ϵ_l, one needs the volume occupied by cells and the volume occupied by EPS. The volume of one cell is determined from image analysis data for average length to width ratio for the cells and the average cell area (Figure 30). EPS volume is determined from the areal concentration of EPS and an assumed EPS density. Bead volume is negligible. An example calculation, using realistic data, will be employed to describe the computation.

Equations: $A_{cell} = Ld + \pi R^2 = 2LR + \pi R^2$

$V_{cell} = \pi R^2 (L) + (4/3)\pi R^3$

$\epsilon_l = 1 - \epsilon_{cell} - \epsilon_{EPS}$

DATA:
$L_f = 30\ \mu m$
$X_f = 10^{12}\ m^{-2}$ (areal cell concentration)
$X_p = 0.2\ gC\ m^{-2}$
$L/d = 3$ therefore, $L = 6R$
$A_{cell} = 0.8\ \mu m^2$
$\rho_{EPS} = 110{,}000\ gC\ m^{-3}$ (assumes EPS has a specific gravity of 1.0)

1. Volume of cells

$A_{cell} = 2(6R)R + \pi R^2$

$0.8\ \mu m^2 = (12 + \pi)R^2$

$R = 0.23\ \mu m$

$V_{cell} = \pi R^2(6R) + (4/3)\pi R^3 = (22/3)\pi R^3 = (22/3)\pi(0.23)^3 = 0.28\ \mu m^3$

Volume of all cells = 0.28 μm^3 * 10^{12} m^{-2} * (30 $\mu m)^{-1}$ * (1 m^2 / 10^{12} μm^2)

= 0.01 m^3 cells / m^3 biofilm

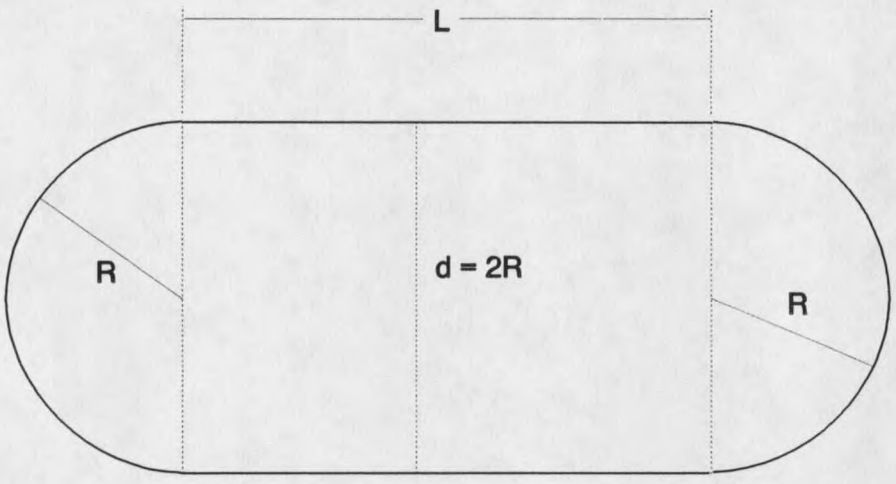

Figure 30. Sketch of a bacterial cell.

2. Volume of EPS

V_{EPS} = (0.2 gC m^{-2}) / (110000 gC m^{-3}) = 1.8 x 10^{-6} m^3 EPS / m^2 biofilm

1.8 x 10^{-6} m^3 EPS / m^2 biofilm * (30 $\mu m)^{-1}$ = 0.06 m^3 EPS / m^3 biofilm

3. ϵ_l = 1 - 0.01 - 0.06 = 0.93 m^3 liquid / m^3 biofilm

Averages for ϵ_l for mature biofilm were approximately 0.90.

APPENDIX H: CALCULATION OF THE LAMINAR BOUNDARY LAYER

APPENDIX H: CALCULATION OF THE LAMINAR BOUNDARY LAYER

Data:

$$v_* = \sqrt{\frac{\tau_o}{\rho}} \qquad (32)$$

where v_* = characteristic velocity ($L\ t^{-1}$)

τ_o = shear stress at wall ($M\ L^{-1}\ t^{-2}$)

ρ = density of water = 997 kg m^{-3} at 25°C

At 200 rpm, the shear stress is in the range of 1.4 N m^{-2} (B. Peyton, personal communication) to 1.9 N m^{-2} (Gunawan, 1991).

Also, ν = 0.897 x 10^{-6} m^2 s^{-1} at 25 °C

The boundaries of the transition zone between laminar and turbulent flow are $y^+ = 5$ and $y^+ = 26$ (Bird *et al.*, 1960). y^+ is a nondimensional distance.

Solution:

$$y^+ = \frac{y^* v_*}{\nu} \qquad (33)$$

Table 31. Boundaries of transition zone between laminar and turbulent flow in a RotoTorque.

y^+	τ_o	v_* (m s^{-1})	y (μm)
5	1.4	0.037	121
	1.9	0.044	103
26	1.4	0.037	630
	1.9	0.044	534

Summary: There is laminar flow from the RotoTorque surface to 103-121 μm away from the surface, transitional flow from 103-121 μm to 534-630 μm away from the surface, and fully turbulent flow at distances greater than 534-630 μm from the RotoTorque surface.

Mass Transfer Boundary Layer Thickness According to BIOSIM

The prediction of bulk liquid glucose concentrations by BIOSIM are sensitive to the "liquid boundary layer thickness." For the proper performance of the program, liquid boundary layer should mean mass transfer boundary layer. This raises the question of whether the laminar boundary layer is different from the mass transport boundary layer. On this subject, Fahien (1983) wrote:

> Unfortunately very few data are available on the variation of ... $Sc^{(t)}$ with position; but since the mechanisms of turbulent momentum, mass, and

> energy transport are essentially the same, it is common practice to assume that
> $Sc^{(t)} = 1.0$ or $D_{AB}^{(t)} = \nu^{(t)}$
>
> (Fundamentals of Transport Phenomena. p. 232)

Therefore, it will be assumed that the mass transfer boundary layer equals the laminar boundary layer.

Figure 31 presents BIOSIM predictions of bulk liquid glucose concentrations for various liquid boundary layer thicknesses between 1 and 100 μm (C. Ganzik, personal communication). For an accurate prediction of glucose concentrations, the liquid boundary layer thickness must be 1 μm. To match the growth rate derived from detachment data that is twice as high as the growth rate from the Monod equation (that is, bulk liquid glucose concentration = 1.0 to 1.2 gC m^{-3}; P. Stewart, personal communication), the liquid boundary layer thickness would have to be 20 to 30 μm. These thicknesses are much less than the laminar boundary layer thicknesses calculated above. The calculation assumes that the surface is smooth. Biofilm surface roughness may enhance mass transfer (Siegrist and Gujer, 1985). These results are consistent with this theory.

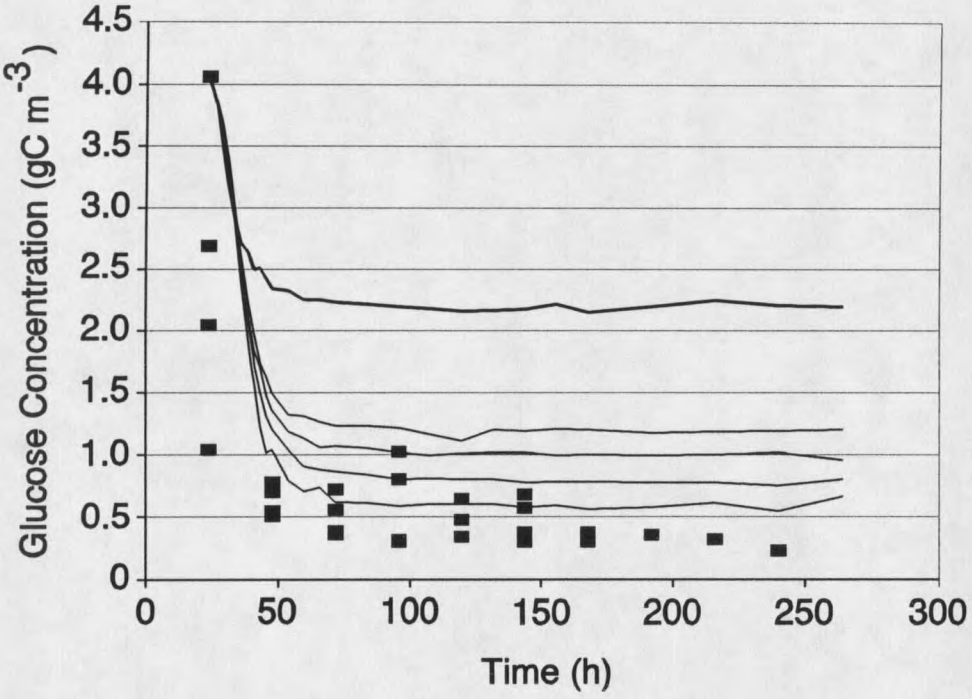

Figure 31. BIOSIM predictions for bulk liquid glucose concentrations for five mass transfer boundary layer thicknesses. The five boundary layer thicknesses tested were, from bottom to top, 1, 10, 20, 30, and 100 μm. The data (▪) indicates that the mass transfer boundary layer thickness is about 1 μm.

APPENDIX I: MODELLING THE MIXED POPULATION BIOFILM

APPENDIX I: MODELLING THE MIXED POPULATION BIOFILM

The undefined mixed population biofilm was simulated with BIOSIM. Coefficients used with the model are listed in Table 32. The value for μ_{max} was computed from batch growth experiments, using a homogenized biofilm sample taken at 168 h for the inoculum. K_S was assumed to be similar to that for *P. aeruginosa* (1.6 $gS_c\ m^{-3}$; Characklis, 1990b) because many microbes in laboratory water systems are pseudomonads (G. McFeters, personal communication). Another bacteral species has a similar K_S in the same medium; Siebel (1987) found the value to be 1.4 $gS_c\ m^{-3}$ for *Klebsiella pneumoniae*. The yield and polymer formation coefficients were determined from the steady state biofilm data. Model calibration was made to biofilm thickness by adjusting the detachment rate. While predicted bead concentrations were lower than the data (Figure 32), biofilm cell carbon (Figure 33) and EPS carbon (Figure 34) concentrations were modelled with good accuracy. Cell concentration predictions were consistently higher than the data, while simulation of EPS carbon concentrations were consistently lower. Apparently, there is an imbalance in the coefficients used that produces excess cells at the expense of EPS. Mixed population biofilms can be modelled as long as changes in microbial populations are not significant so that the coefficients used with the model are accurate throughout the simulation period. Also, the biofilm was modelled as if it contained a single

species; activity of phenotypes not modelled (sulfate reducing bacteria, for example) are ignored. Should such activity be deemed significant, a more complex model (multi-species) is required.

Table 32. Kinetic and yield coefficients for growth of an undefined mixed microbial population on glucose and oxygen.

Coefficient	Value
μ_{max}	0.49 h^{-1}
K_s	2.0 $gS_c\ m^{-3}$
$Y_{x/s}$	0.30 $gX_c(gS_c)^{-1}$
$Y_{p/s}$	0.32 $gP_c(gS_c)^{-1}$
$Y_{x/o}$	0.27 $gX_c(gO_2)^{-1}$
k_p	2.2 $gP_c(gX_c)^{-1}$
k_p'	4.0 $gP_c(gX_c)^{-1}d^{-1}$
ϵ_l	0.99
D_f/D	0.90
ρ_{cells}	118,000 $gC\ m^{-3}$
ρ_{EPS}	110,000 $gC\ m^{-3}$

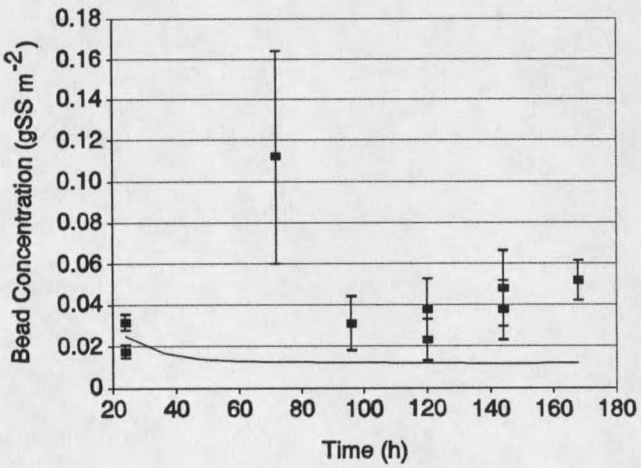

Figure 32. BIOSIM predictions and data for bead concentrations in the mixed population biofilm experiment. Error bars are one standard deviation in the bead counts.

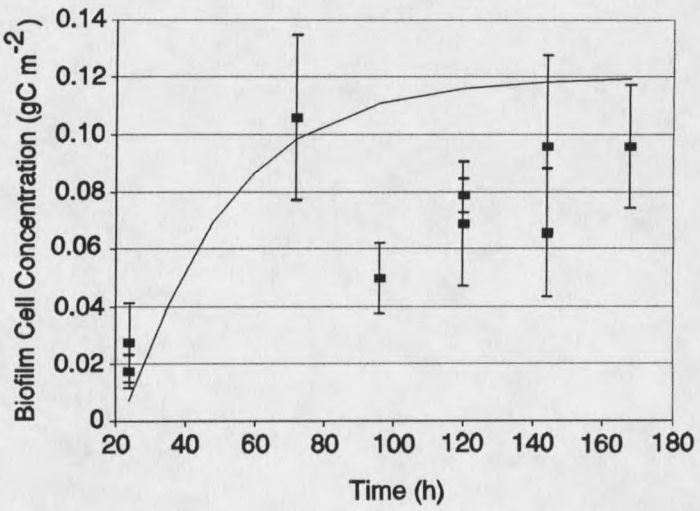

Figure 33. BIOSIM predictions and data for cell concentrations in the mixed population biofilm experiment. Error bars are one standard deviation in the counts of filtered cells.

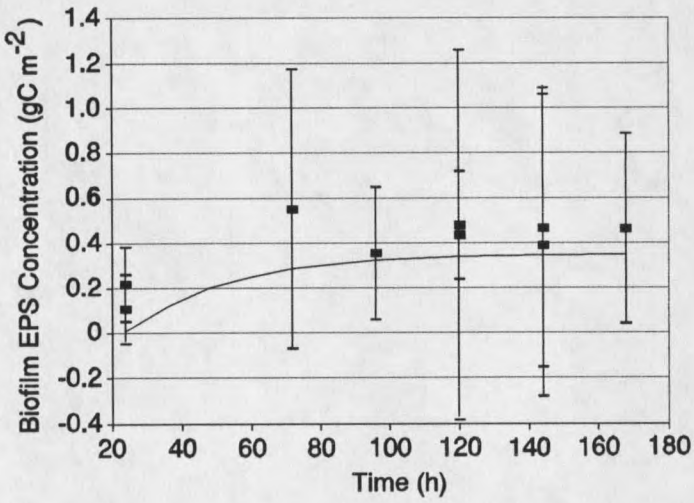

Figure 34. BIOSIM predictions and data for EPS concentrations in the mixed population biofilm experiment. Error bars are one standard deviation.

PART 1: MAXIMUM SPECIFIC GROWTH RATE

Table 33. Data for three batch growth cultures.

time (h)	#1 ABS	ln ABS	ABS	#2 ln ABS	ABS	#3 ln ABS
3.6				0.003		
4.6	0.009	-4.71053	0.003	-5.80914		
5.3	0.016	-4.13517	0.021	-3.86323	0.011	-4.50986
6.4	0.033	-3.41125	0.024	-3.7297	0.015	-4.19971
7.9	0.075	-2.59027	0.031	-3.47377	0.037	-3.29684
10.1	0.154	-1.8708	0.169	-1.77786	0.165	-1.80181
10.5	0.16	-1.83258	0.167	-1.78976	0.174	-1.7487
10.9	0.156	-1.8579	0.173	-1.75446	0.172	-1.76026

where: ABS = absorbance
ln ABS = natural log of absorbance

Regressing ln ABS against time produces:

flask 1 - (0.467 $\pm$0.054) h^{-1}
flask 2 - (0.435 $\pm$0.120) h^{-1}
flask 3 - (0.579 $\pm$0.055) h^{-1}

average = 0.494 $\pm$0.143 h^{-1}

Therefore, μ_{max} = 0.49 h^{-1}

PART 2: YIELD AND POLYMER FORMATION COEFFICIENTS

Four coefficients were computed from the mixed population biofilm data. They are the cell and polymer yield coefficients ($Y_{x/s}$ and $Y_{p/s}$) , and the polymer formation coefficients (k_p and k_p'). Methodology for these computations have been published (Siebel 1987). The polymer formation coefficients are computed from:

PART 1: MAXIMUM SPECIFIC GROWTH RATE

Table 33. Data for three batch growth cultures.

time (h)	#1 ABS	ln ABS	ABS	#2 ln ABS	ABS	#3 ln ABS
3.6				0.003		
4.6	0.009	-4.71053	0.003	-5.80914		
5.3	0.016	-4.13517	0.021	-3.86323	0.011	-4.50986
6.4	0.033	-3.41125	0.024	-3.7297	0.015	-4.19971
7.9	0.075	-2.59027	0.031	-3.47377	0.037	-3.29684
10.1	0.154	-1.8708	0.169	-1.77786	0.165	-1.80181
10.5	0.16	-1.83258	0.167	-1.78976	0.174	-1.7487
10.9	0.156	-1.8579	0.173	-1.75446	0.172	-1.76026

where: ABS = absorbance
ln ABS = natural log of absorbance

Regressing ln ABS against time produces:

flask 1 - (0.467 $\pm$0.054) h^{-1}
flask 2 - (0.435 $\pm$0.120) h^{-1}
flask 3 - (0.579 $\pm$0.055) h^{-1}

average = 0.494 $\pm$0.143 h^{-1}

Therefore, μ_{max} = 0.49 h^{-1}

PART 2: YIELD AND POLYMER FORMATION COEFFICIENTS

Four coefficients were computed from the mixed population biofilm data. They are the cell and polymer yield coefficients ($Y_{x/s}$ and $Y_{p/s}$) , and the polymer formation coefficients (k_p and k_p'). Methodology for these computations have been published (Siebel 1987). The polymer formation coefficients are computed from:

$$r_p = \mu * k_p + k_p' \qquad (34)$$

where: r_p = specific rate of polymer formation (t^{-1})

μ = cellular specific growth rate (t^{-1})

k_p = growth associated polymer formation coefficient (M M^{-1})

k_p' = non-growth associated polymer formation coefficient (M M^{-1} t^{-1})

Linear regression is performed, using r_p and μ from data, to get the unknown coefficients.

The yield coefficients are computed from:

$$r_s = \mu * [\frac{1}{Y_{x/s}} + \frac{k_p}{Y_{p/s}}] + \frac{k_p'}{Y_{p/s}} \qquad (35)$$

where: r_s = specific rate of substrate utilization (t^{-1})

$Y_{x/s}$ = cellular yield coefficient (M M^{-1})

$Y_{p/s}$ = cellular yield coefficient (M M^{-1})

Linear regression again supplies the unknown coefficients. The polymer formation coefficients must be computed first, because they are used in the regression of equation (35).

Steady state data was used in the computations. All data was time smoothed before the regressions were performed. Time smoothing was done by linear regression of steady state data, and then computing estimated data points using the slope and intercept from the regression.

DATA:

time(h)	P(gC m^{-3})	$\hat{P}$	R_p(gC d^{-1})	X(gC)	$\hat{X}$	$r_p = R_p X^{-1}$
72	1.66	1.569	0.0858		0.0105	8.2013
96		1.596	0.0873	0.0126	0.0124	7.0581
120	1.35	1.622	0.0887	0.0138	0.0143	6.2195
144	1.83	1.649	0.0902	0.0162	0.0162	5.5780

Note: $\hat{}$ = estimates from linear regression of the variable against time.

$R_p = P * Q$, where $q = 0.0547\ m^3\ d^{-1}$

time (h)	$X^{\wedge}$	$X_{eff}(gCm^{-3})$	$X_{eff}^{\wedge}$	$X_{eff}(gC\ d^{-1})$	ΔX	μ
72	0.0105					
96	0.0124		0.24	0.0131	0.0149	1.433
120	0.0143	0.20	0.20	0.0109	0.0128	1.035
144	0.0162	0.16	0.16	0.0088	0.0107	0.750

Note: ΔX = [increase in X from (time-24 h) to (time)] + X_{eff} (in gC d^{-1})

X_{eff} = cells in effluent, in gC d^{-1}; it is from $X_{eff}^{\wedge}$ * Q

μ = ΔX divided by X

Regressing r_s versus μ gives:

k_p = 2.162

k_p' = 3.965

MORE DATA:

time(h)	S (gCm^{-3})	$S^{\wedge}$	$D(S_i-S)$	$X^{\wedge}(gC\ m^{-2})$	r_s
72	0.12	0.147	580	0.0563	31.91
96		0.237	571	0.0665	26.61
120	0.41	0.326	563	0.0767	22.72
144	0.36	0.416	554	0.0869	19.75

Note: S_i = 6.19 gC m^{-3}, D = 4 h^{-1} = 96 d^{-1}

r_s = $D(S_i-S)$ * $(X*A\backslash V)^{-1}$ where A/V = surface area to volume ratio = 323 m^{-1}

Regression of r_s versus μ gives: r_s = 10.03μ + 12.26

$Y_{p/s}$ = $k_p'/12.26$ = 0.323

$(Y_{x/s})^{-1}$ = 10.03 - $(k_p/0.323)$ = 3.342

$Y_{x/s}$ = 0.2992

Standard Errors

Standard errors were estimated by a bootstrap method, where additional data sets are constructed by adding random deviations to the time-smoothed values from above. For example, the set of deviations for X consists of 6 deviations as follows: magnitude of deviation = absolute value($X - \hat{X}$) for times 96, 120 and 144 hours (which are the times used to get the estimates of X), and the deviaitons can be either positive or negative. Thus any bootstrap value of X gets the smoothed value of X from the original regression plus one of the 6 deviations. The deviation is picked by random sampling with replacement, so each of the 6 deviations is equally likely to occur at any point (W. Swanson, personal communication).

The bootstrap data are:

5 bootstrap samples of P

time	1	2	3	4	5
72	1.39	1.53	1.74	1.48	1.80
96					
120	1.38	1.84	1.71	1.38	1.39
144	1.53	1.47	1.30	1.80	1.83

5 bootstrap samples of X

time	1	2	3	4	5
72					
96	0.0126	0.0140	0.0156	0.0122	0.0144
120	0.0162	0.0126	0.0140	0.0162	0.0128
144	0.0140	0.0164	0.0128	0.0138	0.0164

5 bootstrap samples of S

time	1	2	3	4	5
72	0.18	0.39	0.50	0.12	0.25
96					
120	0.39	0.12	0.41	0.36	0.07
144	0.39	0.36	0.23	0.36	0.48

The $X_{effluent}$ data was used for all samples because bootstrap values could not be obtained from a data set with only 2 data points.

Computations of the coefficients from each set of bootstrap data produced the following coefficients:

coefficient	1	2	3	4	5
k_p	0.5986	1.9975	-1.1575	0.1019	2.2704
k_p'	5.0323	4.3154	6.6740	6.0594	4.2683
$Y_{x/s}$	0.2033	-4.7230	-0.0457	0.1355	-1.9536
$Y_{p/s}$	0.3009	0.2681	0.1631	0.3709	0.2737

Using these coefficients and the coefficients computed from the real data set, the following standard errors were obtained.

Standard error: the standard deviation is the estimated standard error of the estimated coefficient (M. Hamilton, personal communication).

$k_p = 1.410$ $k_p' = 1.068$

$Y_{x/s} = 2.123$ $Y_{p/s} = 0.0749$

APPENDIX J: MODELLING THE BINARY POPULATION BIOFILM

APPENDIX J: MODELLING THE BINARY POPULATION BIOFILM

The coefficients for *P. aeruginosa* are listed in Table 5. The biofilm characteristics (ϵ_f, liquid boundary layer thickness, and D_f/D) are as given in Table 5. The coefficients for *K. pneumoniae* are listed in Table 34. The raw data is in Appendix C.

Table 34. Kinetic and yield coefficients for growth of *Klebsiella pneumoniae* on glucose and oxygen (Siebel, 1987).

Coefficient	Value
μ_{max}	2.0 h^{-1}
K_S	1.43 $gS_c\ m^{-3}$
$Y_{x/s}$	0.08 $gX_c(gS_c)^{-1}$
$Y_{p/s}$	0.48 $gP_c(gS_c)^{-1}$
k_p	1.72 $gP_c(gX_c)^{-1}$
k_p'	4.80 $gP_c(gX_c)^{-1}d^{-1}$